Nedime KARAKULLUKCU

A Ph.D. Thesis

AGU 2024

PERCEPTION ESTIMATION AND TORQUE CONTROL FOR BIONIC HANDS USING EEG AND EMG SIGNALS

A THESIS
SUBMITTED TO THE DEPARTMENT OF ELECTRICAL AND COMPUTER ENGINEERING AND THE GRADUATE SCHOOL OF ENGINEERING AND SCIENCE OF ABDULLAH GUL UNIVERSITY
IN PARTIAL FULFILLMENT OF THE REQUIREMENTS
FOR THE DEGREE OF
Ph.D.

By
Nedime KARAKULLUKCU
March 2024

PERCEPTION ESTIMATION AND TORQUE CONTROL FOR BIONIC HANDS USING EEG AND EMG SIGNALS

A THESIS
SUBMITTED TO THE DEPARTMENT OF ELECTRICAL AND COMPUTER ENGINEERING AND THE GRADUATE SCHOOL OF ENGINEERING AND SCIENCE OF ABDULLAH GUL UNIVERSITY
IN PARTIAL FULFILLMENT OF THE REQUIREMENTS
FOR THE DEGREE OF
Ph.D.

By
Nedime KARAKULLUKCU
March 2024

SCIENTIFIC ETHICS COMPLIANCE

I hereby declare that all information in this document has been obtained in accordance with academic rules and ethical conduct. I also declare that, as required by these rules and conduct, I have fully cited and referenced all materials and results that are not original to this work.

Name-Surname: Nedime KARAKULLUKCU

Signature :

REGULATORY COMPLIANCE

Ph.D. thesis titled “PERCEPTION ESTIMATION AND TORQUE CONTROL FOR BIONIC HANDS USING EEG AND EMG SIGNALS” has been prepared in accordance with the Thesis Writing Guidelines of the Abdullah Gül University, Graduate School of Engineering & Science.

Prepared By	Advisor
Nedime KARAKULLUKCU	Prof. Bülent YILMAZ

Head of the Electrical and Computer Engineering Program

Assist. Prof. Samet GÜLER

ACCEPTANCE AND APPROVAL

Ph.D. thesis titled “PERCEPTION ESTIMATION AND TORQUE CONTROL FOR BIONIC HANDS USING EEG AND EMG SIGNALS” and prepared by Nedime KARAKULLUKCU has been accepted by the jury in the e Electrical and Computer Engineering Graduate Program at Abdullah Gül University, Graduate School of Engineering & Science.

28 / 03 / 2024
(Thesis Defense Exam Date)

JURY:

Advisor : Prof. Bülent YILMAZ

Member : Prof. Aydın AKAN

Member : Prof. Fatma LATİFOĞLU

Member : Assoc. Prof. Zeki ORALHAN

Member : Assist. Prof. Aykut EKEN

APPROVAL:

The acceptance of this Ph.D. thesis has been approved by the decision of the Abdullah Gül University, Graduate School of Engineering & Science, Executive Board dated ….. /….. / …….. and numbered ……..…… .

…….. /…….. / ……..

(Date)

Graduate School Dean
Prof. İrfan ALAN

ABSTRACT

PERCEPTION ESTIMATION AND TORQUE CONTROL FOR BIONIC HANDS USING EEG AND EMG SIGNALS

Nedime KARAKULLUKCU

Ph.D. in Electrical and Computer Engineering

Advisor: Prof. Bülent YILMAZ

March 2024

Upper extremity prostheses vary based on patients' articulation levels and movement methods. They can be cosmetic, operate mechanically with shoulder movement, or be controlled by myoelectronic and electroencephalography (EEG) signals. However, unnatural prosthesis control burdens users mentally. This thesis seeks to enhance bionic hand prosthesis control using EEG and electromyography (EMG) signals, coupled with users' visual weight perception, aiming to reduce physical and mental discomfort associated with mechanical prostheses. The prototype hand's preconditioning evaluates objects' weight visually, aiming to reduce shoulder force and mental load while holding an object. EEG and EMG signals from subjects were processed for real-time implementation. In the first stage, a study focused on operating the prosthesis using the motor intention waves of prosthesis users, and the machine learning approaches' classification success (detection of the intention to activate the prosthesis) was examined using EEG data from 30 healthy participants. The second stage recorded EEG and EMG signals from 31 participants during reaching, lifting, and placing an object, employing various classifications for object weight. In the real-time classification of multi-channel EEG signals from 20 healthy individuals using Fourier-based synchrosequeezing transform (FSST) and singular value decomposition (SVD) approaches, the system aimed to control the stiffness of the wrist part of the prosthesis. Consequently, the system could detect the weight of the object perceived by the user while using the prosthesis, allowing for the preconditioning of the prosthesis based on this weight when the user wants to hold and move the object.

Keywords: Brain-machine interface, Electroencephalography, Electromyography, Hand prosthesis, Weight perception

ÖZET

EL PROTEZLERİ İÇİN EEG VE EMG SİNYALLERİYLE ALGI KESTİRİMİ VE TORK KONTROLÜ

Nedime KARAKULLUKCU
Elektrik ve Bilgisayar Mühendisliği Anabilim Dalı Doktora
Tez Yöneticisi: Prof. Dr. Bülent YILMAZ
Mart-2024

Üst ekstremite protezleri, hastaların eklem düzeyleri ve hareket yöntemlerine bağlı olarak değişiklik gösterir. Protezlerin kozmetik, omuz hareketine bağlı çalışan, miyoelektronik ve elektroensefelografi (EEG) sinyalleriyle kontrol edilen türleri mevcuttur. Ancak, sezgisel ve doğal olmayan protez kontrolü kullanıcı üzerinde büyük bir mental yüke neden olmaktadır. Bu tez ile, EEG ve elektromiyografi (EMG) sinyalleri birlikte kullanılarak biyonik el protezinin kontrolünün kullanıcının görsel ağırlık algısından faydalanılarak daha iyi hale getirilmesini amaçlayan bir sistem geliştirilmeye çalışılmıştır. Bu sistem ile hastaların mekanik bir protezi kullanırken duyabilecekleri fiziksel ve mental yükü/rahatsızlığı azaltmak hedeflenmiştir. Bu amaçla öncelikle deneklerin EEG ve EMG sinyalleri gerçek zamanlı uygulama için işlendi. İlk aşamada, protez kullanıcılarının motor niyet dalgalarından yararlanılarak protezlerin çalıştırılmasını hedefleyen bir araştırma yapılmış ve 30 sağlıklı katılımcıdan EEG verileri alınarak makine öğrenmesi yaklaşımlarının sınıflandırma başarıları (protezi aktif hale getirme niyetlerinin tespiti) incelenmiştir. İkinci aşamada, 31 katılımcının nesneye uzanma, kaldırma ve yerleştirme hareketleri sırasında EEG ve EMG sinyalleri kaydedildi ve nesne ağırlığının tespiti için çeşitli sınıflandırmalar kullanıldı. 20 sağlıklı bireyin çok kanallı EEG sinyallerinin gerçek zamanlı sınıflandırmasında Fourier tabanlı senkrosıkıştırma dönüşümü (FSST) ve tekil değer ayrıştırma (SVD) yaklaşımları kullanılarak sistem, protezin bilek kısmının sertliğinin kontrolü sağlanmaya çalışılmıştır. Sonuç olarak, bireyler protezi kullanırken gördükleri cismin ağırlığının sistem tarafından algılanması ve o cismi kaldırmak istediklerinde protezin bu ağırlığa göre önkoşullandırılması mümkün olmaktadır.

Anahtar kelimeler: Beyin makine arayüzü, Elektroensefalografi, Elektromiyografi, El protezi, Ağırlık algısı

Acknowledgements

Firstly, I am profoundly grateful to my advisor, Prof. Bülent YILMAZ, for his consistent guidance, invaluable insights, and unwavering support. His mentorship significantly contributed to the development of this thesis and my academic progress.

I particularly want to express my heartfelt appreciation to my husband, Mustafa Serhat KARAKULLUKCU, for his unwavering support, understanding, and encouragement throughout this arduous journey. His love and belief in me were my pillars of strength.

I would also like to extend my gratitude to the members of my thesis committee, Prof. Aydın AKAN and Assoc. Prof. Zeki ORALHAN, for their valuable feedback and suggestions that significantly improved the quality of this research. Their expertise has been instrumental in shaping the direction of my work.

I would like to acknowledge the financial support provided by TÜBİTAK (Scientific and Technological Research Council of Turkey) under Project No.: 119E120. Additionally, Higher Education Council (HEC) of Turkey 100/2000 PhD Scholarship Program and 2211-A National PhD Scholarship Program made this research possible. Their investment in my work is deeply appreciated.

Last but not least, my friends and family have been a constant source of encouragement and emotional support. Their belief in me and their patience during my academic pursuits have meant the world to me.

Thank you all for being a part of this incredible journey.

TABLE OF CONTENTS

LIST OF FIGURES

LIST OF TABLES

LIST OF ABBREVIATIONS

AAC	Augmentative and Alternative Communication
ANN	Artificial Neural Network
ANOVA	Analysis of Variance
AR	Autoregressive
AUC	Area Under the Curve
BCI	Brain Computer Interface
BMI	Brain Machine Interface
CAR	Common Average Reference
CFC	Cross Frequency Couplings
CSP	Common Spatial Pattern
CWT	Continuous Wavelet Transform
DWT	Discrete Wavelet Transform
ECG	Electrocardiogram
ECoG	Electrocorticography
EEG	Electroencephalography
EMG	Electromyography
ERD	Event-Related Desynchronization
ERPs	Event-Related Potentials
ERS	Event-Related Synchronization
FDF	Frequency- Domain- Features
FFT	Fast Fourier- Transform
FN	False Negative
FP	False Positive
ICA	Independent Component Analysis
ITR	Information Transfer Rate
KNN	K-Nearest Neighbors
LDA	Linear Discriminant Analysis
MEG	Magnetoencephalography
MI	Motor Imagery
MRPs	Motor-Related Potentials
PSD	Power Spectral Density
RBF	Radial Basic Functions
RFE	Recursive Feature Elimination
RMS	Root Mean Square

ROC	Receiver Operating Characteristic
SCP	Slow Cortical Potentials
SFS	Sequential Forward Selection
SMR	Sensory-motor Rhythm
SST	Synchrosqueezing Transform
SSVEPs	Steady-State Visual Evoked Potentials
STFT	Short-Time Fourier Transform
SVM	Support Vector Machines
TDF	Time- Domain- Features
TN	True Negative
TP	True Positive
ZCR	Zero Crossing Rate

To all those who dare to dream and work tirelessly to make those dreams a reality

Chapter 1

Introduction

Individuals suffering from neural diseases, such as stroke, motor neuron disease, and locked-in syndrome, cannot produce voluntary muscle movements. They may be either totally unable or partially able to perform their daily activities or even express their wishes to caregivers [1]. To assist these patients, numerous researchers have been studying brain-computer interfaces (BCIs) that use brain waves to control external devices, including computers, speech synthesizers, assistive appliances, and neural prostheses [2]. Additionally, BCIs have recently been utilized in the rehabilitation and restoration of extremity movements and in video games [1]. The target audience of this area is divided into four groups: (1) Complete locked-in state (CLIS) patients, who have lost all voluntary movement [2], (2) locked-in state (LIS) patients, who are only able to move and blink their eyes, or twitch their lips [2], (3) physically disabled patients, who can speak and move their head, and (4) healthy individuals for entertainment.

The brain waves can be obtained using various neuroimaging methods [2], [3]. It is possible to categorize the methods as invasive and non-invasive. These methods can be categorized as either invasive or non-invasive. Invasive methods include electrocorticography (ECoG) and intracortical neuron recording, which allow for the collection of signals from within the brain, such as single-neuron action potentials (single units), multi-unit activity (MUA), and local field potentials (LFPs) [4], [5]. These signals are acquired using a single electrode or an electrode array placed either on the surface or inside the cortex [2]. The high-quality spatial and temporal features of these invasive methods contribute significantly to the successful decoding of the patient's intention [6], [7]. However, it's important to note that invasive techniques require surgery to implant microelectrode arrays onto the cortex.

An alternative method for recording brain activity is electroencephalography (EEG), along with functional magnetic resonance imaging (fMRI), magnetoencephalography (MEG), and near-infrared spectroscopy (NIRS), all of which

are non-invasive techniques. While fMRI offers higher spatial resolution, EEG is more commonly used due to its ease of use, cost-effectiveness, and portability [8].

1.1 General Perspective

EEG-based BCI systems receive the signal during a particular task such as thinking to move a cursor, or spelling words by looking at the specific area on the screen to control corresponding external devices. The acquired multi-channel waveforms are first pre-processed, and then time and/or frequency domain features are extracted from them. These features are used to generate commands for external devices either directly or through machine learning approaches. Hence, a precise protocol and paradigm must be selected for all stages of the experiment to apply the EEG-based BCI model to a specific implementation [8].

The paradigms in EEG-based BCI systems can be categorized in two groups as the visual and imagery. P300 is one of the visual paradigms [9], in which letters in a matrix flash one at a time, and the subject chooses a specific one by looking continually at it. Thus, the P300 potential appears over the parietal cortex as a positive peak ranging from 5 to 10 microvolts in size at about 300 ms [10]. Another visual paradigm is the steady-state visual evoked potentials (SSVEP). SSVEP detects the subject's gaze direction to a target character under the flickering stimuli. A light-emitting diode (LED) or a cathode ray tube (CRT) can generate the stimulus [8]. The response is observed on the visual cortex of the brain. For the imagery paradigm, motor imagery can be given as an example. It is a cognitive process in which the subject imagines performing a movement without motion and without even tensing the muscles. It requires conscious activation of the brain regions due to the fact that the subject prepares the execution of a movement [11].

Motor intention is defined as imagining a movement to execute a real movement [12]. Previous studies have demonstrated that imagining a movement activates the regions of the brain responsible for producing movement (the sensorimotor cortex) [13]. Alpha waves with 8-13 Hz frequency that occur in the sensorimotor cortex are called mu activity. A decrease in mu activity is observed in the sensorimotor cortex while imagining motor movement in the absence of movement. This reduction causes a desynchronization between 8–13 Hz mu and 14–25 Hz beta rhythms. This situation is called event-related desynchronization (ERD), and the power increase at a specific frequency is called event-

related synchronization (ERS) [14]. Changes in EEG signals in the mu and beta frequencies can be used to control prosthetic devices.

In summary, EEG-based BCIs can provide a communication means for the patients to control a computer cursor in at least three dimensions, to select letters for word-processing, to run computer-based programs, and to control external devices such as an electric wheelchair and neural prosthesis. The relationship between the recorded brain activity and biomechanics of the human body is one of the most challenging topics in BCI [8]. Therefore, in recent years, the research on the interactions between EEG signals and upper limb motion, both real and imagery (planning the movement), has become a hot topic [15], [16].

1.2 Literature Overview

Mental strategy (e.g., imagined movement, whole- body activities) is the center of the motor imagery (MI)-based BCI. The similarity in the cerebral activation of executed (i.e. motion) and imagined (i.e. motor intention, preparation to a movement) limb movement was proved by Lotze *et al.* in 1999 [17]. Hence, discrimination between different motor intentions (e.g., left versus right hand; hand versus foot) was investigated until today by numerous researchers [18], [19], [20], [21]. In the motor imagery paradigm, the user intention can be captured from the EEG signal before the motion occurs. By using motor imagery paradigm, simple motor actions were detectable from the EEG. Penny *et al.* [22] reported that cursor control can be accomplished employing EEG obtained from over sensorimotor cortex. In this study, subjects focused on the imagination of the movement of right or left hand. After processing the signal with autoregressive parameters and logistic regression, they trained their system by using a Bayesian evidence framework. As a result, they achieved a one-dimensional cursor movement. Pfurtscheller *et al.* [23] stressed the utility of the MI-based BCI with functional electric stimulation (FES) systems for assistive technology. They used the imagination of foot movement as a trigger for the FES. Once the trigger was generated, the subject with tetraplegia could grasp a glass of water. A similar study was made by Tan *et al.* [24] in which the goal was to make the stroke patients perform training of arm flexion and extension with the MI-based BCI-FES system. Bai *et al.* [25] used a combination of spatial and temporal filtering in order to discriminate the right and left-hand movement intention with 75% accuracy. López-Larraz *et al.* [26] studied with both healthy and spinal cord injury (SCI) patients

on seven self-initiated upper-limb movements, and showed that the studied movement could be decoded in both healthy subjects and patients with the same accuracy that ranged between 40 to 75%. Kim *et al.* [27] analysed the connectivity distinction between EEG and EMG signals during the movement of the upper limb in the same manner as the existence of the motion intention by implementing (linear) coherence and (non-linear) analysis of mutual information.

Thus far, however, the studies have primarily focused on the detection of the motor imagery tasks such as imagination of the right or left hand, foot, and tongue movements. On the other hand, detection of starting the movement intention is also important. In the movement intention paradigm, the user intention and resting state (task-negative state) can be distinguished from the EEG signal before the motion occurs. In the literature, there are a few studies about this paradigm. Ang *et al.* [28] emphasised robotic rehabilitation with MI-based BCIs and worked with 18 hemiparetic subjects whose EEG signals were acquired from 27 channels. This study consisted of the calibration and rehabilitation phases. They used filter bank common spatial pattern (FB-CSP) algorithm to extract features in order to discriminate the resting and motor imagery states. When the motor imagery was received but no motion was initiated, the user was supported by the robot with the purpose of moving the impaired limb. Muralidharan *et al.* [29] used the paradigm in order to distinguish the rest and attempted finger-extension for the purpose of opening or closing the hand. Four subjects with subcortical ischemic stroke were recruited in this study. They extracted features using power bands between 2Hz and 29Hz obtained from common-average referenced EEGs, and common spatial pattern (CSP) analysis. Another study of Bai *et al.* [30] was about the prediction of the movement intention before it occurred. The system recognised the movement of wrist extension in seven healthy users. They used spatial filtering (surface Laplacian derivation, SLD) and temporal filtering (Welch based power spectral density (PSD) estimation) as the feature extraction methods. In a different study by Rozado *et al.* [31] the aim was to monitor the subject's pupil diameter as an extra feature, and they investigated the discrimination of the motor intention from the resting state. The results proved that the performance of the classifier increased with that extra feature when compared with the traditional approach that used just the EEG derived features.

In a study conducted by recording EEG activity in the sensorimotor region, it was shown that movement execution, imagining the movement and preparing for movement

caused changes in the amplitudes of the signals received from the sensorimotor regions [32]. In this study, using this amplitude difference, patients were enabled to control the cursor of the computer. Leeb et al., obtained EEG signals with a sampling frequency of 512 Hz using the 16-channel g.USBamp system (Guger Technologies, Schiedleberg, Austria), and created power spectral density based feature vectors to be used in classification. They achieved an average accuracy of 70% as classification performance after user-specific feature selection using canonical variable analysis. In order to increase classification performance and ensure stable operation of the system, they applied for the 9-day training program. Eventually, it was seen that the average classification performance obtained from 9 people was 85%. In another study, the Radial Basic Functions (RBF) Artificial Neural Network (ANN) structure was created for the recognition of brain signals, and a 70% recognition rate was obtained by using NeuroSky EEG for the recognition of brain signals [33]. In sensory-motor-rhtythm (SMR) applications, Guger et al., used SMR to open and close a robotic hand with the imagination of right and left-hand movement [34]. Similarly, Sun, Fan [35], and Jia and Roy et al., [36] used motor intention to control the virtual upper limb. Moreover, SMR is also used in rehabilitation robots and hand orthoses [28], [37]. Basic level brain-controlled arm prosthesis design was carried out by Uyar et al. [38]. This study is a preliminary study to show that the prosthetic arm can be controlled with EEG signals. According to this study, the control of the designed hook prosthesis was carried out by transferring the data received from Emotiv and Emotiv software, EmoKey, to the microprocessor. However, EEG systems are not stable enough to control a prosthesis. For this reason, recent studies on the prosthesis control are on the use of EEG and EMG together. In a study carried out in this field, Leeb et al., showed that the fusion of EEG and EMG signals results in higher sensitivity than using both signals to generate neurofeedback alone [39]. Therefore, the hybrid BMA approach has a growing interest. However, there are few studies dealing with bionic applications. Existing studies have shown that combined multimodal data of EEG and EMG increase motion intention prediction rate with increased motion reliability [40]. In another study, EMG was used as a control mechanism, while EEG was used for right and left motor intention discrimination [41].

Based on the empirical studies, it can be seen that there is still a strong need for comprehensive research about the self-initiated EEG-based BCIs. Moreover, patients

with motor impairments are not able to start the operation of BCI systems and need caregivers' help. Initiating the BCI system by themselves without the need for someone else and any other supplementary systems such as a camera would highly help the patients feel more comfortable and independent. In the literature, there are limited number of studies focusing on the discrimination of resting, motor imagery, and motion states. The transition between these states may be used as a trigger for the external devices in real-time using EEG signals. Furthermore, in the studies reviewed above, the number of subjects included in the experiments was not high enough for a good generalization. Due to the characteristics of the EEG, it is proven that the small sample size can cause discrepant findings in the literature [42].

1.3 Research Question/Problem Statement and Hypothesis

Prostheses that have been developed to facilitate the daily lives of individuals who have lost one or more limbs due to accidents or diseases have been used for years. The prostheses used especially for the upper extremity differ according to the level of amputation, just as the methods used to move the prosthesis. In some prosthesis types, only cosmetic use is prominent, while in others, the hand is opened and closed by the individual's own power, for example by moving the shoulder. Another type of prosthesis is called a myoelectric prosthesis. In this type, arm and hand movements are performed with the muscle signals received from the electromyography (EMG) electrodes placed in the appropriate places (on the skin) of the amputated limb. Recently, efforts have been made to use electroencephalography (EEG) signals in upper extremity prostheses. A key problem in the prostheses is that nonintuitive and unnatural prosthesis control causes a great mental burden on the user.

The central question that this thesis asks, then, is: Can the mental and physical burden/discomfort experienced by individuals while using the prosthesis be reduced?

In this study, it is planned to create a brain machine interface (BMI) system that uses EEG and EMG signals together and to control the bionic hand using this system. Preconditioning of the prototype hand prosthesis to be produced by evaluating the weight of the objects seen by the patients to the extent that the brain perceives them visually will be provided. In this way, the force applied by the patient from the shoulder while holding

the object will be reduced. If the object that the patient wants to hold is heavy, a command signal will be sent to the prototype hand prosthesis, and it will then be able to lift most of the weight. Thus, the load on the patient's muscles will be reduced. As a result, patients using the prosthesis, which will be designed as EEG and EMG controlled, will be made to accept the prosthesis as their own limb and the patient's motivation will be increased. Additionally, the weight upon their body will be significantly reduced when handling more challenging objects. To realize this hypothesis, EEG and EMG, which is a non-invasive method, will be received as brain and muscle signals from the subjects, and these signals will be first processed in a laptop computer environment, and then the real-time application will be developed.

The main purpose of the thesis work is to produce a brain and muscle-controlled bionic hand for the use of people who have lost one or two upper extremities. It also aims to overcome the physical and mental load that patients can feel while using a mechanical prosthesis. The purpose of this study is twofold: (1) To produce a prototype of an electromechanical hand prosthesis by applying real-time signal processing approaches to the signals received from a multi-channel commercial EEG and EMG device, and (2) to test them on subjects.

This thesis is divided into four main parts. Chapter 2 presents the first part, which investigates self-initiated EEG-based BCI to assess the feasibility of employing portable and wireless EEG systems for identifying movement intentions in individuals with motor impairments. In Chapter 3, the second part of the thesis delves into the study of weight perception using EEG signals, employing both conventional machine learning and transfer learning methods. The third part, covered in Chapter 4, explores weight perception from EMG signals, employing conventional machine learning techniques. Finally, the last part, discussed in Chapter 5, focuses on real-time prosthesis control using EEG signals.

Chapter 2

Fundamentals

2.1 Introduction to Brain-Computer Interfaces

A Brain-Computer Interface (BCI), also known as a Brain-Machine Interface (BMI), is a technology that enables direct communication between the human brain and external devices, such as computers or prosthetic limbs. BCIs translate brain signals into commands that can be used to control these devices or to convey information from the brain to the external world. The basic principle working a EEG-based BCI system is illustrated in Figure 2.1. BCIs typically work by recording electrical activity in the brain using various methods, such as electroencephalography (EEG), electrocorticography (ECoG), or intracortical electrodes. These brain signals are then processed by a computer, which decodes them and performs specific actions based on the user's intent. There are several applications for BCIs, including:

- Assistive Technology: BCIs can help individuals with severe motor disabilities regain communication and control over their environment. For example, people with locked-in syndrome or spinal cord injuries can use BCIs to operate a computer, control a robotic arm, or communicate through text or speech synthesis.
- Neuroprosthetics: BCIs can be used to control artificial limbs, exoskeletons, or other assistive devices, allowing people with limb loss or paralysis to regain mobility and independence.
- Communication: BCIs can be used for augmentative and alternative communication (AAC) for individuals with communication disorders. They can assist in spelling, typing, or generating speech through brain signals.
- Neurofeedback and Cognitive Enhancement: BCIs are also used in research and clinical settings to provide neurofeedback training, which can help individuals enhance their cognitive abilities, manage stress, or improve focus and attention.

- Research and Brain Mapping: BCIs are valuable tools for studying the brain's function and understanding neural activity patterns, which can aid in the development of new treatments for neurological conditions.

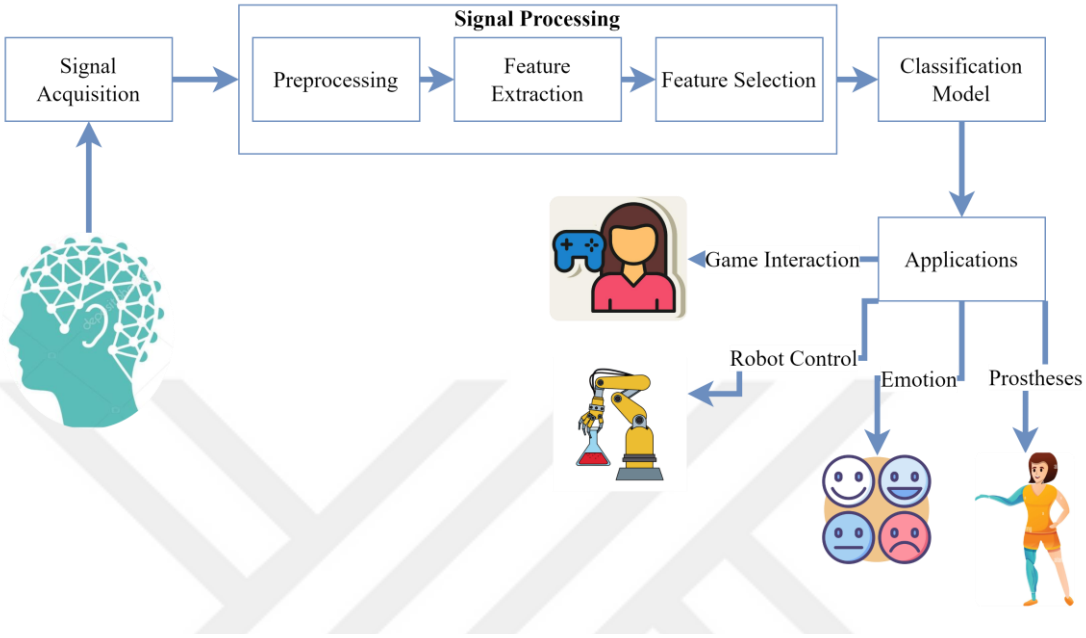

Figure 2.1 BCI structure

BCI technology continues to advance, and researchers are exploring various methods to improve its accuracy, ease of use, and applications. As a result, BCIs hold the potential to significantly enhance the quality of life for people with disabilities and provide valuable insights into the workings of the human brain.

The concept of Brain-Computer Interfaces (BCIs) started to take form during the 1960s and 1970s, with early ideas revolving around the utilization of brain signals for communication and control. Pioneering work conducted by researchers such as José Delgado delved into the use of brain implants and electrical stimulation for controlling animal behavior [43]. In the 1970s, researchers like Vidal and Wolpaw started using electroencephalography (EEG) to detect brain signals and explore their use for communication [44]. In the 1980s and 1990s, significant progress was made in using EEG to develop simple BCIs, primarily for individuals with disabilities. Early applications included spelling and cursor control. In the 1990s, research into invasive BCIs began to gain traction [45]. These systems involved implanting electrodes directly into the brain to improve signal quality. The development of BrainGate in the early 2000s marked a

milestone, allowing individuals with severe paralysis to control computer cursors and robotic arms using implanted electrodes [46]. Moreover, BCIs continued to advance, leading to a wider range of applications. These included assistive technologies for communication, neuroprosthetics, and even artistic and gaming applications [47]. Research efforts have also focused on non-invasive BCIs, such as functional near-infrared spectroscopy (fNIRS) and magnetoencephalography (MEG), to provide additional options for users. BCIs have also been used in research settings to study brain function, cognitive enhancement, and neurofeedback [48]. In recent years, commercial BCIs and consumer-grade EEG headsets have become available, enabling applications in areas like gaming and relaxation [49]. Companies like Neuralink, founded by Elon Musk, have garnered significant attention for their efforts to develop high-bandwidth BCIs for a wide range of applications, including medical and non-medical uses [50].

2.2 Signal Acquisition

Brain-Computer Interfaces (BCIs) use various methods to acquire signals from the brain. These methods are designed to record and measure the electrical activity produced by neural processes. The choice of signal acquisition method depends on factors such as the specific application, the user's needs, and the level of invasiveness or non-invasiveness required. Here are some common signal acquisition methods for BCIs:

- Electroencephalography (EEG):
    - EEG is a non-invasive technique that involves placing electrodes on the scalp to record the electrical activity of the brain.
    - It is widely used for BCIs due to its ease of use, portability, and relatively low cost.
    - EEG signals are primarily used for non-invasive BCIs, such as those for communication or control of external devices.
- Electrocorticography (ECoG):
    - ECoG involves placing electrodes directly on the surface of the brain, typically by placing a grid of electrodes over the exposed cortex during neurosurgery.

- ECoG provides high-quality signals with better spatial resolution compared to EEG, making it suitable for advanced BCI applications.
- ECoG BCIs are often used for research and clinical applications.

- Intracortical Electrodes:
  - Intracortical electrodes, such as microelectrode arrays or single-unit recording electrodes, are implanted directly into the brain tissue.
  - These electrodes offer high spatial and temporal resolution, making them suitable for precise control of prosthetic limbs and advanced research applications.
  - The invasiveness of this method is higher, and it is typically used for individuals who have electrode implants for medical reasons.

- Functional Magnetic Resonance Imaging (fMRI):
  - fMRI measures changes in blood flow and oxygenation in the brain, indirectly indicating neural activity.
  - It provides detailed spatial information about brain activity but has limitations in terms of temporal resolution and accessibility.
  - fMRI is mainly used in research settings to study brain function and connectivity.

- Near-Infrared Spectroscopy (NIRS):
  - NIRS measures changes in blood oxygenation in the brain by shining near-infrared light through the skull and detecting the transmitted or reflected light.
  - It offers a balance between spatial and temporal resolution, making it suitable for some BCI applications.
  - NIRS is non-invasive and can be used for brain-computer communication and neurofeedback.

- Magnetoencephalography (MEG):
  - MEG records the magnetic fields generated by neural activity.

- It provides excellent temporal and spatial resolution but is relatively expensive and less common in BCI applications.

The choice of signal acquisition method depends on the specific requirements of the BCI system, including the desired balance between spatial and temporal resolution, invasiveness, and user comfort. Each method has its advantages and limitations, and researchers continue to explore new technologies and techniques to improve BCI signal acquisition and usability. In this thesis, signal acquisition was conducted using EEG due to its portability, ease of application (non-surgical), and popularity as a recording method. In the Figure 2.2, electrode placements for EEG, ECoG and intracortical recordings is illustrated.

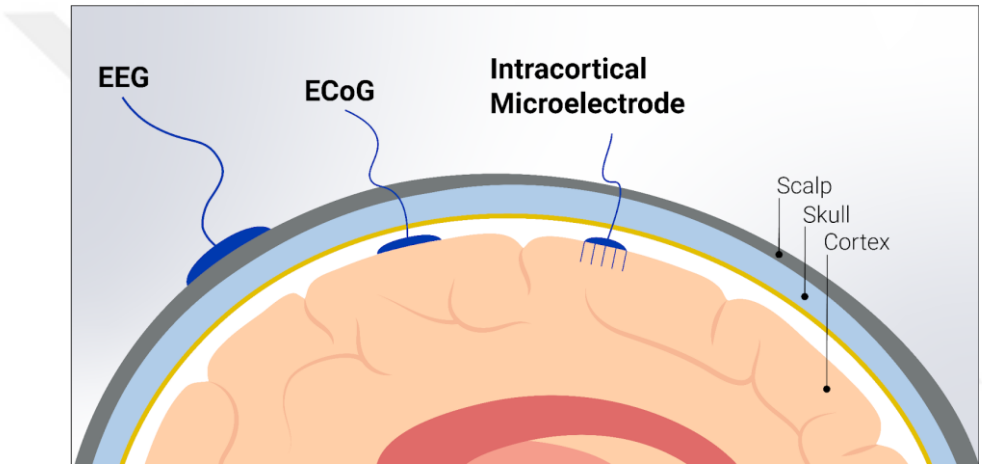

Figure 2.2 Neural signal recording methods: EEG, ECoG, and intracortical electrodes [51].

2.2.1 Electroencephalogram

An EEG is a non-invasive neurophysiological test that measures and records the electrical activity of the brain. It is a valuable tool for diagnosing various neurological conditions, monitoring brain function during surgery, and conducting research on brain activity. Small, flat metal discs called electrodes are attached to the patient's scalp using a special conductive paste or gel. The number of electrodes used can vary, but a standard EEG often involves 19 to 25 electrodes placed at specific locations on the scalp. The locations are defined by the International 10-20 System, a standardized method for electrode placement. In the Figure 2.3, electrode placement follows the 10-20 international system is illustrated. The system designates electrode sites with specific

combinations of letters and numbers, with the letters indicating the brain region and the numbers representing the hemisphere and the specific electrode's position within that region. Odd numbers signify electrodes on the left side of the head, while even numbers indicate electrodes on the right side. Capital letters denote specific cortical region: frontal (F), central (C), parietal (P), temporal (T), and occipital (O). Fp and A represent the frontal pole and auricular. Two key reference points are the nasion (the midpoint between the forehead's bridge and the top of the nose) and the inion (the bony prominence at the base of the skull). The 10-20 System divides the distance between the nasion and inion into equal parts, with 10% and 20% increments. And Electrodes are positioned on the scalp according to these percentages.

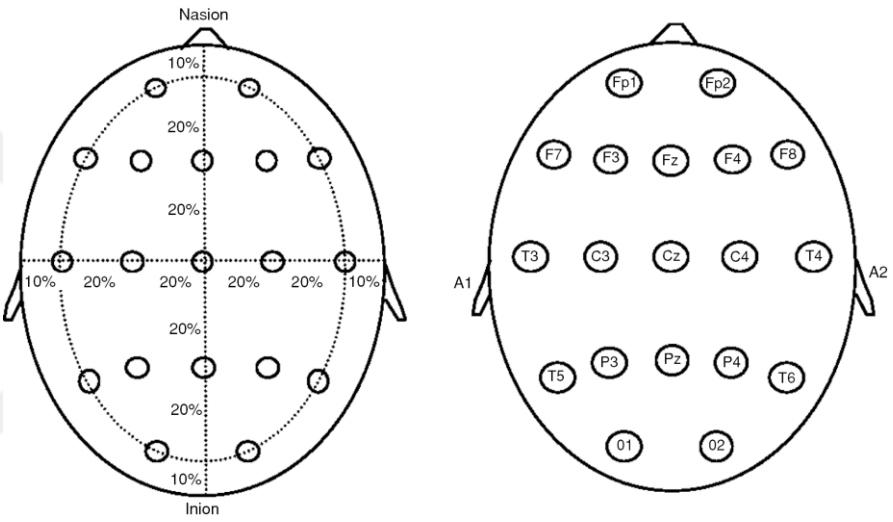

Figure 2.3 The standardized 10-20 electrode placement [52].

EEG is a valuable tool for studying the electrical activity of neurons in the brain and provides insights into the timing, synchronization, and information processing within different brain regions. Understanding the structure and functioning of neurons is crucial for interpreting EEG data and relating it to specific cognitive processes and brain functions. The neurons are the essential units of the nervous system, responsible for transmitting electrical and chemical signals. They have a complex structure, including the cell body, dendrites for receiving signals, an axon for transmitting signals, and myelin sheaths that speed up signal propagation. Neurons generate action potentials, which are all-or-nothing electrical signals, and transmit them along the axon to communicate with other neurons at synapses. The strength and frequency of action potentials convey information. Understanding neuron structure and function is crucial for studying brain function and neurological disorders. The electrical signals detected by the electrodes are

very weak, so they need to be amplified for accurate measurement. EEG machines contain amplifiers that increase the strength of these signals. The amplified signals are recorded by the EEG machine and displayed on a computer monitor or paper printout. The resulting output is a visual representation of the brain's electrical activity, known as an EEG recording. A neurologist or EEG technician interprets the EEG recording, looking for abnormal patterns, such as spikes, sharp waves, and slow waves, which can provide valuable information about brain function and potential neurological disorders.

EEG measurements are used in various clinical and research applications, such as diagnosing epilepsy, assessing the effects of anesthesia, studying sleep disorders, and investigating cognitive processes. The test is painless and safe, making it an essential tool in the field of BCI.

However, artifacts can significantly impact the quality and interpretation of EEG recordings. Artifacts in EEG refer to unwanted signals or interference that are not a direct result of neural electrical activity but can obscure or distort the true brain signals. These artifacts can arise from various sources, and they can complicate the analysis and interpretation of EEG data. Here are some common artifacts and their effects on EEG:

- **Physiological Artifacts:**
    - **Eye Movements and Blinks:** Rapid eye movements or eye blinks can introduce voltage changes in EEG recordings. These artifacts often manifest as sharp and transient signals in the EEG, which can make it challenging to distinguish from neural activity.
    - **Muscle Activity (Electromyographic Artifacts):** Muscle contractions, even subtle ones, can contaminate EEG recordings. These artifacts are often characterized by low-frequency noise and can interfere with the analysis of EEG rhythms.
    - **Cardiac Activity (Electrocardiographic Artifacts):** Electrical activity generated by the heart can be detected in EEG signals. These artifacts are

typically rhythmic and can resemble brain oscillations, leading to misinterpretation.

- **Nonphysiologically Artifacts:**

  - **Power Line Noise:** Electrical noise from power lines (at 50 Hz or 60 Hz, depending on the region) can introduce a regular, periodic interference into EEG recordings. It can obscure underlying brain signals, particularly in the lower-frequency bands.

  - **Amplifier Noise:** Noise generated by the EEG amplifier or recording equipment can distort the EEG signal. It may appear as random fluctuations and affect the overall signal quality.

  - **Electrode Artifacts:** Sudden changes in the properties of the electrode-scalp interface, such as electrode movement or impedance changes, can lead to brief artifacts in EEG recordings.

The effects of these artifacts on EEG data include reduced signal quality, making it difficult to accurately assess brain activity. Artifacts can mimic neural patterns, making it challenging to distinguish true EEG features from interference. Therefore, artifact removal and filtering procedures are essential in EEG data processing to minimize the impact of these unwanted signals.

Various techniques, such as filtering, artifact rejection, and independent component analysis (ICA), are used to mitigate the effects of artifacts. These methods help enhance the reliability and interpretability of EEG data, allowing researchers and clinicians to focus on the genuine neural activity of interest.

2.2.2 Event-Related Potentials (ERPs) in EEG: Understanding Cognitive Processing in the Brain

Event-Related Potential (ERP) is a type of electrophysiological measurement that involves recording the brain's electrical activity in response to specific events or stimuli. ERPs are time-locked to the presentation of a stimulus, and they provide valuable insights into the brain's processing of sensory, cognitive, and motor information [42]. ERPs, represent a unique category of electrical brain responses evoked by specific events or

stimuli. These events may encompass visual, auditory, somatosensory, or cognitive stimuli, giving rise to characteristic ERP waveforms marked by specific components such as the P300 or N400, each indicative of distinct cognitive processes. Importantly, ERPs are time-locked to the onset of the event or stimulus under investigation. This temporal alignment allows researchers to capture the brain's electrical activity at precise moments following the event, and by averaging EEG or MEG signals across multiple trials, the ERP response can be extracted from background noise [53].

ERPs offer critical insights into the timing and sequence of cognitive processes associated with the perception, processing, and response to stimuli. For instance, the P300 component is linked to attention and memory functions, while the N400 component is associated with language comprehension and semantic processing [54]. These versatile neurophysiological measures find applications in both research and clinical domains. In research, ERPs are invaluable tools for the investigation of various cognitive functions, including attention, memory, language, and perception. In clinical settings, they play a crucial role in the diagnosis and monitoring of neurological and psychiatric conditions such as epilepsy, autism, and cognitive disorders. To elicit and study ERPs, researchers design specific experimental paradigms. For instance, in the context of language processing research, participants may be presented with words or sentences, and their brain responses (ERPs) are recorded as they read or hear the stimuli.

ERPs are commonly recorded through EEG (Electroencephalography), although MEG (Magnetoencephalography) can also be employed for this purpose. Electrodes are strategically placed on the scalp following standardized systems like the International 10-20 system to ensure accurate measurement and analysis.

2.2.3 Types of Neurophysiological Signals in BCI Systems

P300

The P300, also known as the P3, is a positive deflection observed in the EEG, a recording of brain electrical activity. It typically appears approximately 300 milliseconds (hence the name) after the presentation of a rare or surprising, task-relevant stimulus. The P300 is considered a cognitive ERP that reflects processes related to attention, memory, and decision-making. To elicit the P300, subjects are asked to observe a sequence of two types of stimuli. One stimulus type, referred to as the oddball or target stimulus, appears

infrequently in the sequence. The other stimulus type, the normal or nontarget stimulus, appears more frequently. Whenever the target stimulus occurs, a P300 component can be observed in the EEG [9].

The P300 has been widely used in various cognitive and neuroscience studies to investigate processes related to stimulus evaluation, memory updating, and context processing. In the context of Brain-Computer Interfaces (BCIs), the P300 has been harnessed for communication purposes, allowing users to make selections from a matrix of symbols or options displayed on a screen by attending to the desired target. This approach is known as the "P300 speller" [55].

Steady-State Visual Evoked Potentials

Steady-State Visual Evoked Potentials (SSVEPs) are a type of neural response in the brain that occurs in response to repetitive visual stimulation [56]. When visual stimuli, such as flashing lights or patterns, are presented to an individual at specific frequencies, the brain exhibits oscillatory electrical activity at those same frequencies and their harmonics or subharmonics. This phenomenon can be measured using electroencephalography (EEG) or other neuroimaging techniques. In the context of Brain-Computer Interfaces (BCIs), SSVEPs are harnessed to enable users to make selections or control devices. BCI systems typically display multiple visual stimuli, each flickering at a different frequency [57]. When a user focuses their attention on one of these stimuli, the corresponding frequency band in the EEG exhibits increased amplitude, indicating their choice. SSVEP-based BCIs have found applications in various domains, including communication and assistive technologies [58].

Slow Cortical Potentials

Slow Cortical Potentials (SCPs) are a category of neurophysiological signals that provide insights into slow electrical activity in the human brain [59]. These signals are characterized by their gradual changes in voltage over an extended period, typically ranging from seconds to minutes. SCPs primarily originate from the cortex and are associated with processes like attention, learning, and self-regulation. Unlike rapid ERPs or oscillatory brain rhythms, SCPs unfold slowly and can be consciously modulated. This unique feature makes SCPs valuable in the context of BCIs and neurofeedback applications, where individuals can learn to control their SCPs to achieve desired

cognitive or behavioral states [60]. SCP-based BCIs have been explored for various applications, including the management of attention disorders, relaxation training, and improving cognitive performance. These applications leverage the ability to regulate SCPs as a means to influence cognitive and physiological states, demonstrating the potential of SCPs in neuroscientific research and practical interventions.

Motor-Related Potentials

Motor-Related Potentials (MRPs) are a category of electrophysiological signals that are independent of sensory perception or cognitive processing [14]. They are directly linked to the preparation or imagination of motor movements. MRPs manifest as slow negative potentials in the brain, typically observed over the sensorimotor cortex. What makes MRPs particularly intriguing is their somatotopic organization, which means that the location of the greatest MRP amplitude can indicate which body part is being prepared for movement or imagined in the process. This property enables researchers and clinicians to infer the intended movement or motor imagery based on the specific area of the sensorimotor cortex that exhibits the strongest MRP activity [62]. MRPs have been utilized in Brain-Computer Interface (BCI) systems, particularly in those focusing on motor imagery tasks, to enable users to control external devices or applications through the power of thought, without the need for actual physical movement [63], [64]. The MRPs can be connected to the concept of the homunculus, specifically the motor homunculus, which is a representation of the body within the brain, with the relative sizes of body parts corresponding to the amount of neural representation in the somatotopic motor cortex as illustrated in Figure 2.4 [65].

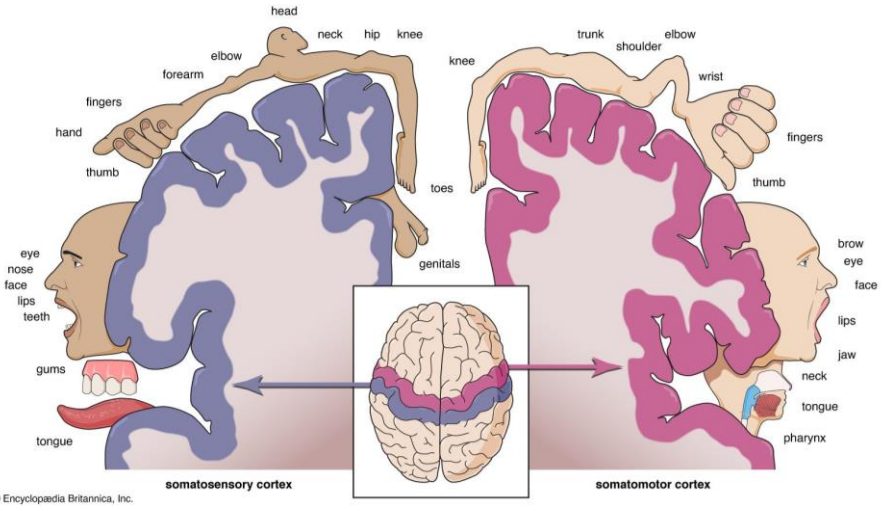

Figure 2.4 The somatosensory homunculus and the motor homunculus [61].

When discussing MRPs, it's important to note that these potentials are observed over the sensorimotor cortex and are linked to the preparation and imagination of motor movements. Given the somatotopic organization of the sensorimotor cortex, MRPs can provide insights into which specific body part is being prepared for movement or imagined [66]. The connection to the motor homunculus can be made by considering that MRPs essentially offer a way to "read" or interpret the neural activity associated with specific body parts in the motor cortex. For example, if there is an increase in MRP activity in the area of the sensorimotor cortex corresponding to the hand, it suggests that the individual is preparing to move or is imagining movement in the hand. In this way, MRPs serve as a bridge between the neural representation of motor control in the brain (as depicted in the motor homunculus) and the actual execution or imagination of movements [67]. It's a practical application of the somatotopic organization of the motor cortex, allowing for the inference of user intentions related to specific body parts. This connection highlights the role of MRPs in translating the neural representation of movement into actionable information in applications like Brain-Computer Interfaces.

Oscillatory Brain Activity

EEG frequency bands represent distinct ranges of frequencies that are observed in EEG recordings. These frequency bands reflect the rhythmic and oscillatory patterns of electrical activity in the brain [68]. These bands are essential for characterizing different brain states, cognitive processes, and neural activities. Each band corresponds to a specific range of frequencies [69]. The primary EEG frequency bands include Delta (0.5-4 Hz), which is associated with deep sleep and unconscious states, and Theta (4-8 Hz), often observed during drowsiness and relaxation, as well as in memory-related processes and meditation. Alpha (8-13 Hz) waves dominate in relaxed, non-attentive states and are linked to improved focus and inhibition of extraneous brain processes. Beta (13-30 Hz) waves are prominent during active, alert, and engaged mental states, such as problem-solving and cognitive tasks. Gamma (30-100+ Hz) waves, the fastest EEG waves, are associated with high-level cognitive functions and sensory perception. The Mu band (8-13 Hz), a subset of alpha waves, is observed primarily over the sensorimotor cortex and plays a role in motor planning and execution. Sigma waves consist of two sub-bands, one related to sleep spindles (12-16 Hz) and the other to rapid eye movement (REM) sleep (16-31 Hz), contributing to sleep regulation and cognitive processes during sleep.

Event-Related Desynchronization/ Synchronization

Event-Related Desynchronization (ERD) is a neurophysiological phenomenon that involves a decrease in the power of brain oscillations, particularly in specific frequency bands, in response to an event or a cognitive task. ERD is often observed in EEG or MEG recordings when individuals engage in cognitive activities, such as motor planning and execution [70]. During motor preparation and execution, there is a decrease in the power of the mu or beta frequency bands (typically 8-30 Hz) in the sensorimotor cortex. This decrease in power is referred to as ERD and is thought to reflect increased neuronal activation and desynchronization of neural oscillations in the motor-related areas of the brain. ERD is often used as a marker for understanding and quantifying motor-related brain activity, making it valuable in applications like brain-computer interfaces (BCIs) and motor imagery tasks [71]. In essence, ERD provides a window into the dynamic changes in brain activity associated with motor planning and execution, shedding light on the neural mechanisms underlying motor control and cognitive processing [72].

Conversely, event-related synchronization (ERS) refers to an increase in the power or synchronization of neural oscillations and is typically time-locked to the presentation of a stimulus or the occurrence of an event. ERS can signify enhanced neural engagement in response to specific cognitive demands. It is often associated with cognitive processes such as attention, perception, and memory. For example, during a task requiring heightened attention, ERS can be observed in regions related to attentional processing, indicating increased neural resources allocated to the task [72].

2.3 Signal Pre-processing

Proper signal pre-processing and artifact removal are crucial for accurate EEG analysis, particularly in tasks like event-related potential (ERP) studies or functional connectivity analysis. These steps help researchers extract meaningful neural information while minimizing noise and artifacts, ensuring the reliability of EEG findings [73]. Below, a detailed explanation of signal pre-processing and artifact removal in EEG data analysis is provided.

2.3.1 Filtering

Low-Pass Filter

This filter is used to allow only low-frequency components to pass through and attenuate high-frequency noise. Common settings for low-pass filters in EEG analysis are around 30 Hz or lower. It helps smooth out the EEG signal and remove high-frequency noise introduced by sources such as muscle activity and electrode artifacts [74].

High-Pass Filter

High-pass filters remove slow changes in the EEG signal, often referred to as baseline drift. This drift can be caused by factors like electrode impedance or physiological processes. High-pass filters are typically set at frequencies around 0.1 Hz to 1 Hz to remove DC drift and low-frequency artifacts caused by electrode impedance changes or physiological sources [75], [76], [77].

Notch Filtering

Notch filters are designed to eliminate specific frequencies known to introduce noise into the EEG signal, such as electrical interference at 50 Hz (in Europe) or 60 Hz (in the United States). Removing these line noise frequencies is crucial for clean EEG recordings [78], [79], [80].

2.3.2 Artifact Removal

Artifacts can arise from various sources, including eye blinks, which can cause large, sharp spikes in the EEG, muscle activity (EMG), and electrocardiogram (ECG) interference. Automated algorithms, visual inspection, and statistical techniques can be used to detect and mark segments contaminated by artifacts [81], [82]. Once artifacts are detected, various methods can be applied to remove or minimize their impact [83], [84], [85], [86], [87], [88]:

Independent Component Analysis (ICA)

ICA is a powerful technique for separating the EEG signal into independent components, some of which may represent artifacts (e.g., eye blinks). These artifact components can be removed or corrected.

Regression-Based Techniques

Specific artifacts, such as ECG or EMG, can be regressed out of the EEG data using recorded signals from these sources. This approach helps remove the influence of these artifacts.

Data Interpolation

Missing data points caused by artifact removal can be interpolated using various methods such as spline interpolation to maintain a continuous data stream.

Riemannian Geometry

Artifact handling with Riemannian modification is an approach used in EEG data analysis to address artifacts and enhance the quality of EEG signals. This technique is particularly useful when dealing with non-stationary artifacts or when traditional methods like ICA or regression-based approaches are not sufficient [89]. Artifact handling with Riemannian modification is an advanced approach employed in the analysis of EEG data to effectively address non-stationary artifacts that pose challenges to traditional artifact removal methods. This technique leverages the principles of Riemannian geometry, a mathematical framework used to manipulate covariance matrices representing EEG signal properties [90]. In this method, the identification of artifacts within EEG data is a critical initial step, often achieved through sophisticated artifact detection procedures. Once identified, Riemannian modification aims to improve data quality by adjusting the covariance matrices associated with segments containing artifacts. These adjustments typically involve the alteration of eigenvalues and eigenvectors to minimize the influence of artifacts while retaining essential EEG information [91].

Riemannian modification strategies can vary in their specifics but share the goal of enhancing the reliability of EEG data. Common approaches include eigenvalue adjustments and eigenvector rotations, each designed to disentangle artifact-related components from EEG-related components. After application, the technique is evaluated

to quantify the degree of artifact reduction and improvement in EEG data quality [89]. This method finds application in EEG research areas, such as brain-computer interfaces, neurofeedback, and clinical EEG analysis, where the need for robust data quality is paramount. Implementing Riemannian modification requires a deep understanding of mathematical concepts and EEG data analysis, and careful selection of modification strategies and parameters to achieve effective artifact handling [92], [93], [94], [95].

2.3.3 Additional Pre-processing Techniques for Ensuring Data Reliability

In addition to the methods mentioned above, various other techniques, including spatial filtering, baseline correction, data segmentation, artifact rejection, montage selection, resampling, and quality control, are also employed in the preprocessing of data to ensure its reliability. The techniques are summarized below:

Spatial Filtering

Techniques such as common average reference (CAR) or Laplacian referencing are applied to improve spatial resolution and minimize the effects of volume conduction, where electrical activity from one part of the brain is detected at multiple electrodes [57], [96], [97], [98], [99].

Baseline Correction

EEG data are often baseline-corrected to set a particular time point (e.g., the onset of a stimulus) as the reference [100]. This correction helps remove the influence of baseline shifts, making it easier to analyse changes relative to a consistent reference point. This is particularly useful for ERPs and other cognitive studies [101].

Data Segmentation

EEG data is typically divided into epochs or segments aligned with specific events of interest (e.g., stimulus presentation). These epochs can be further filtered or baseline-corrected individually, allowing for focused analysis.

Artifact Rejection

In cases where artifact removal is not feasible or leads to significant data loss, segments with severe artifacts may be rejected, ensuring that only clean data is used for analysis.

Montage Selection

The choice of EEG montage, which specifies electrode combinations for signal recording and referencing, can impact the quality of the recorded signals. The selection of an appropriate montage is essential for accurate EEG analysis.

Resampling

In some cases, EEG data may be resampled to a different sampling rate, depending on the analysis requirements or to reduce computational load [102].

Quality Control

Regular quality control checks and visual inspection of the pre-processed data are performed to ensure data quality and identify any residual artifacts that may require further correction.

2.4 Feature Extraction

In the previous section, the techniques for pre-processing EEG data have been discussed. Signal pre-processing has ensured the quality and reliability of EEG data. The next crucial step is feature extraction to identify key patterns, characteristics, and relevant information within the EEG data. Features refer to distinctive attributes or characteristics that are extracted from the EEG data. These features are numerical representations of specific aspects of the EEG signal that carry information relevant to the analysis or classification of brain activity. Common types of features extracted from EEG signals include measures of signal amplitude, frequency, spectral power, coherence, and various statistical parameters. These features are used to describe and quantify specific aspects of the brain's electrical activity. They are subsequently utilized in tasks such as BCI classification, event detection, or cognitive state assessment [103], [104], [105]. The choice of features depends on the research or application objectives, and various feature extraction methods are employed to capture the most informative aspects of the EEG data

for a particular analysis. The extracted features are then used as input to machine learning algorithms or other analytical techniques to derive meaningful insights from EEG recordings [106]. The methods for extracting features can be categorized into four groups: time-domain, frequency domain, time and frequency domain, spatial methods [107], [108], [109].

2.4.1 Time Domain Features

Time domain features in EEG signal processing are quantitative measurements that capture characteristics of brain electrical activity over time. These features are computed based on the amplitude and timing information of the EEG signal, offering insights into the temporal aspects of neural activity. By analyzing the EEG signal in the time domain, valuable information about the brain's response dynamics can be obtained [110]. Mean amplitude, also referred to as the average amplitude, computes the average magnitude of the EEG signal within a defined time window, serving as an indicator of signal intensity during that period. This facilitates comparisons between cognitive states or tasks [111], [112]. In contrast, Root Mean Square (RMS) quantifies signal energy by calculating the square root of the average of squared amplitudes within a specific time frame, making it a valuable tool for assessing signal variations and activity intensity [113]. The Zero Crossing Rate (ZCR) feature assesses the rate of signal oscillations by quantifying how often the EEG signal crosses the zero level in a given time segment, aiding in the detection of changes in signal frequency or pattern. On the other hand, standard deviation characterizes amplitude variability within a defined time window, with a high standard deviation indicating significant signal variations. Skewness and Kurtosis provide insights into the shape of the amplitude distribution and the peakedness of the signal, aiding in the description of signal characteristics [114], [115]. The Hurst exponent is a measure of long-range dependence or self-similarity, aiding in the understanding of patterns or trends over time. Additionally, Entropy measures assess unpredictability and complexity, with higher entropy values signifying greater unpredictability [116], [117]. Signal Slope is useful for identifying rapid changes or trends in brain activity, as it measures the rate of change in amplitude over time. Zero-lag correlation helps determine the synchrony or coherence of neural activity by quantifying the correlation between EEG channels within the same time window.

2.4.2 Frequency Domain Features

Frequency domain features in EEG signal processing pertain to characteristics that are extracted from the spectral content of the EEG signal. These features offer insights into the frequency distribution and oscillatory patterns within the brain's electrical activity [103]. Power Spectral Density (PSD) characterizes the distribution of signal power across diverse frequencies. Computed through methods like the Fast Fourier Transform (FFT), it quantifies the signal's power within specific frequency bands. Utilizing PSD analysis enables the identification of dominant frequency components in the EEG signal, thereby aiding in the recognition of frequency patterns associated with cognitive states or disorders [118]. Relative Power, on the other hand, examines the contribution of particular frequency bands to the total power of the EEG signal, typically categorized as delta, theta, alpha, beta, and gamma. This allows researchers to assess alterations in power distribution and track cognitive states or neurological conditions. Moving to spectral entropy, this metric gauges the complexity of the frequency spectrum of the EEG signal, providing insights into the uniformity of power distribution across different frequency components [119], [120]. Applied in tasks like cognitive workload assessment and sleep analysis, high spectral entropy values indicate broad power distribution, while low values signify concentration within specific frequency ranges. Coherence measures the synchronization between EEG signals from distinct electrode locations, evaluating phase and magnitude similarity in specific frequency bands [121], [122], [123]. It is instrumental in studying functional connectivity within the brain, unveiling relationships between brain regions during diverse tasks or conditions. Cross-frequency couplings (CFC) explores interactions between different frequency bands, examining how the amplitude of low-frequency oscillations modulates the phase of high-frequency oscillations [124], [125], [126], [127], [128]. This feature is crucial for understanding complex brain dynamics, such as memory processes and information integration. Lastly, frequency band ratios involve comparing power or amplitude between different frequency bands, such as the theta/beta ratio [129]. Common in clinical EEG, these ratios provide insight into conditions like attention deficit hyperactivity disorder (ADHD) by assessing the balance between slow and fast wave activity. Each of these frequency analysis techniques contributes to a comprehensive understanding of EEG signals and their implications in various applications.

2.4.3 Time-Frequency Domain Features

Time-Frequency domain features in EEG signal processing offer a dynamic perspective, capturing changes in brain activity over both time and frequency. These features are crucial for understanding how neural oscillations evolve during different cognitive tasks or states. One prominent example is the Short-Time Fourier Transform (STFT), which reveals how the frequency content of the EEG signal changes over short time intervals [130], [131]. This is achieved by applying the Fourier transform to successive overlapping windows of the signal, enabling the tracking of frequency changes over time. Additionally, the Wavelet transform is employed, decomposing the EEG signal into different frequency components with varying temporal resolutions [132], [133], [134], [135]. This allows for the identification of specific frequency bands associated with distinct cognitive processes. Another notable feature is spectrogram, a visual representation of the STFT, providing a time-frequency map of the signal's energy distribution [136], [137]. This graphical tool aids in identifying patterns and changes in neural activity over time and frequency. Morlet Wavelet transform for time-frequency analysis can also be used, as it allows for precise localization of oscillatory components in both time and frequency domains. Moreover, the Continuous Wavelet Transform (CWT) is utilized to capture non-stationary signals by employing wavelets of varying scales. An advanced technique, the Synchrosqueezing Transform (SST), has gained attention. SST enhances the precision of time-frequency analysis by reshaping the traditional spectrogram, providing improved localization of oscillatory events [104], [138], [139], [140], [141], [142], [143]. This makes SST particularly valuable for extracting detailed information from EEG signals with complex frequency dynamics.

2.4.4 Spatial Features

Spatial features play a crucial role BCI applications, where the spatial distribution of electrical activity is leveraged for various tasks. One significant spatial feature in BCI is spatial filtering, a technique that enhances relevant spatial information and suppresses noise or unwanted sources. Methods such as Common Spatial Patterns (CSP) play a crucial role in enhancing relevant spatial information while mitigating noise and unwanted sources [75], [144], [145], [146], [147], [148], [149], [150], [151], [152]. CSP optimizes the spatial filters to maximize the variance of one class while minimizing the variance of another, making it particularly effective in distinguishing different mental

states [153]. Another essential spatial feature is Independent Component Analysis (ICA), a powerful method for separating mixed signals into statistically independent components [154]. In the context of BCIs, ICA helps identify distinct sources of neural activity, contributing to more accurate decoding. By extracting spatially independent components, ICA allows BCIs to focus on specific brain regions, improving the precision of control commands. Another essential spatial feature is channel selection is a spatial feature employed to optimize BCI performance by selecting the most informative EEG channels [155], [156], [157]. Techniques like recursive channel elimination aid in identifying channels that contribute significantly to the BCI task. Source localization is another spatial feature that involves estimating the cortical regions generating EEG signals [158], [159], [160], [161], [162]. Advanced methods such as beamforming enhance source localization accuracy, contributing to the development of high-resolution BCIs. These spatial features are integral to BCI systems, enhancing their reliability and effectiveness in translating neural activity into actionable commands.

2.5 Channel and Feature Selection

Selecting the appropriate EEG channels is essential for focusing on regions that are most informative for the specific BCI task [155], [157], [162], [163]. Techniques such as Spatial Filtering, which includes methods like Common Spatial Patterns (CSP), aim to identify the channels that exhibit the most discriminative information for a given task. Another approach involves considering anatomical regions, selecting channels from specific brain regions relevant to the task at hand.

Once relevant channels are identified, extracting informative features is crucial [164], [165], [166]. It involves choosing the most relevant features from the available set of features extracted from EEG signals, aiming to enhance the system's performance, reduce computational load, and mitigate the risk of overfitting. Univariate feature selection methods, exemplified by Analysis of Variance (ANOVA), assess individual features independently, prioritizing those exhibiting significant differences in means between different classes [167]. Recursive Feature Elimination (RFE) employs an iterative approach, systematically eliminating the least relevant features until an optimal subset is attained [168]. An illustration of RFE in action is provided by Support Vector Machine Recursive Feature Elimination (SVM-RFE), which synergizes SVM classification with recursive elimination to pinpoint the most informative features [169].

Filter methods, such as mutual information, evaluate feature relevance without considering the classifier, relying on statistical or information-theoretic metrics to identify features with high mutual information scores [170]. Wrapper methods, like Sequential Forward Selection (SFS), gauge feature subsets based on the performance of a designated classifier, progressively adding the most discriminative features [171], [172]. Embedded Methods, such as L1-Regularization (Lasso), seamlessly integrate feature selection into the training process of the classifier itself, encouraging sparsity and automatic feature selection [173]. Hybrid Approaches, typified by combining ANOVA with Recursive Feature Elimination (RFE-ANOVA), leverage the strengths of multiple selection methods for a more comprehensive and refined feature subset.

2.6 Classification

Classification is a pivotal component of Brain-Computer Interface (BCI) systems, responsible for translating extracted features from EEG signals into meaningful control commands. The process involves assigning EEG patterns to predefined classes or categories, allowing users to convey intentions through their brain activity [174], [175], [176], [177].

Linear classifiers, such as Linear Discriminant Analysis (LDA), form the foundational layer of BCI classification [178]. LDA seeks to maximize the distance between the means of different classes while minimizing the spread within each class. This technique is particularly effective when the underlying data exhibits a linear separability pattern. Support Vector Machines (SVM), on the other hand, are versatile classifiers capable of handling both linear and non-linear relationships [169], [179], [180], [181]. SVM constructs hyperplanes in high-dimensional spaces, providing an effective means of distinguishing between different classes.

Non-linear classifiers introduce a layer of complexity to accommodate the intricate nature of EEG signals. Random Forests, an ensemble learning method, comprise multiple decision trees, each contributing to the final classification [182], [183]. Neural Networks, inspired by the structure of the human brain, consist of interconnected nodes that learn hierarchical representations, making them adept at capturing non-linear relationships in data [33], [111], [182], [184], [185]. K-Nearest Neighbors (KNN) is a proximity-based

classifier that assigns a class label based on the majority class among its nearest neighbors in the feature space [186], [187], [188].

Ensemble classifiers enhance the robustness of BCI systems by combining predictions from multiple classifiers [189]. Voting classifiers aggregate decisions from diverse classifiers and assign the class label that receives the majority of votes. Bagging (Bootstrap Aggregating) involves training multiple instances of the same classifier on different subsets of the training data and averaging their predictions. Boosting, a sequential training method, focuses on refining the mistakes of previous learners, progressively improving the overall classification performance [190]. One notable ensemble classifier is XGBoost (Extreme Gradient Boosting), which has gained prominence for its exceptional speed, efficiency, and regularization capabilities [191].

XGBoost, in particular, has become a stalwart in the BCI landscape. It operates as an optimized gradient boosting library, building a series of weak learners, typically decision trees, and combining their predictions to create a robust final model [192]. With features like regularization, cross-validation, and parallelization, XGBoost navigates complex relationships within EEG data efficiently. Its adaptability and accuracy have made it a popular choice in BCI applications, especially in scenarios where rapid decision-making is crucial.

The choice between linear, non-linear, and ensemble classifiers depends on the nature of the EEG signals and the specific requirements of the BCI application. Linear classifiers may suffice for scenarios with straightforward separability, while non-linear classifiers and ensemble methods shine in situations where the relationships are intricate and dynamic. As BCI technology continues to advance, the interplay of these classifiers contributes to the development of increasingly sophisticated and adaptive systems, enabling users to harness the power of their thoughts for effective control and communication.

2.7 Performance Evaluation

After classification, evaluating the performance of the classifiers is an important step in assessing their effectiveness in decoding EEG signals. Various metrics and methodologies are employed to quantify the diverse aspects of classifier performance such as accuracy, precision, recall, kappa, information transfer rate (ITR) [193].

Accuracy

Accuracy, a fundamental metric, measures the overall correctness of the classifier [177]. The equation for accuracy is given by:

$$Accuracy = \frac{TP + TN}{TP + TN + FP + FN} \tag{2.1}$$

where TP and TN represent true positives and true negatives, FP and FN stand for false positives and false negatives.

Precision, Recall, and F-measure

Precision, recall, and f-measure are vital metrics focusing on the classifier's ability to correctly identify positive instances. F-measure is the weighted harmonic mean of the precision and recall [194]. Precision is computed using equation 2.2. It focuses on the accuracy of positive predictions. Recall is a measure of sensitivity and yields how many of the actual positives are predicted by the model as positive (equation 2.3). The equations are as follows:

$$Precision = \frac{TP}{TP + FP} \tag{2.2}$$

$$Recall = \frac{TP}{TP + FN} \tag{2.3}$$

$$f\text{-}measure = 2 \times \frac{precision \times recall}{precision + recall} \tag{2.4}$$

Area Under the Curve

The Area Under the Curve (AUC) is a metric commonly used to evaluate the performance of binary classification models, including those in BCI applications. It is particularly associated with the Receiver Operating Characteristic (ROC) curve [195]. The ROC curve is a graphical representation of a classifier's performance across different discrimination thresholds. It plots the true positive rate (sensitivity) against the false positive rate (1 - specificity) at various threshold settings. The curve illustrates the trade-off between sensitivity and specificity, allowing for the identification of an optimal threshold based on the application's requirements [196]. The AUC is the area under the ROC curve. It quantifies the classifier's ability to distinguish between positive and negative instances [197]. A perfect classifier would have an AUC of 1, indicating a curve that reaches the top-left corner of the plot. A random classifier would have an AUC of 0.5, representing a diagonal line from the bottom-left to the top-right.

Cohen's Kappa

Cohen's Kappa is a statistic that measures inter-rater agreement for categorical items. In the context of BCI, Cohen's Kappa is often used to assess the agreement between the predicted and actual class labels produced by a classifier [198], [199]. It calculates with equation 2.5.

$$Kappa = \frac{Observed\ Agreement - Expected\ Agreement}{1 - Expected\ Agreement} \tag{2.5}$$

where Observed Agreement is the proportion of instances where the classifier and true labels agree, and Expected Agreement is the proportion of instances where agreement is expected by chance. Cohen's Kappa ranges from -1 to 1. A value of 1 indicates perfect agreement, 0 indicates agreement equal to chance, and negative values suggest agreement worse than chance. Kappa adjusts for the possibility of chance agreement, making it a robust metric for imbalanced datasets. It provides a more nuanced understanding of classification performance, especially when classes are unevenly distributed [200].

Information Transfer Rate

Information Transfer Rate (ITR) is a metric that quantifies the speed at which information is transmitted in a BCI system. It is particularly relevant when assessing the real-time performance of a system, as it considers both accuracy and speed of operation [201], [202], [203].

$$ITR = \frac{log_2(N) + P\log_2(P)}{T} \tag{2.6}$$

where N is the number of classes, P is the classification accuracy, T is the time taken to make a decision. The term $log_2(N)$ represents the uncertainty in the system before making a decision. $P.log_2(P)$ accounts for the information gained by making a correct decision.

Chapter 3

Detection of Movement Intention in EEG-Based Brain-Computer Interfaces using Fourier-Based Synchrosqueezing Transform

In this chapter, our primary objective is to discern the purpose behind the movement for asynchronous Brain-Computer Interface (BCI) applications, with a focus on aiding individuals with motor impairments. The chapter, derived from a published article by the author [143]. We have introduced the Fourier synchrosqueezing transform (FSST) as a novel approach for feature extraction and employed singular value decomposition (SVD) as the method for feature selection/reduction. Additionally, our investigation encompassed determining the most effective features and channels for discriminating between resting and imagery states in Motor Imagery (MI)-based BCIs. Furthermore, we conducted a comparative analysis, pitting the FSST approach against a combination of statistical, time-, time-frequency-, and frequency-domain approaches, as well as established methods like common spatial patterns (CSP) and sub-band CSP (SBCSP). Lastly, we explored the use of both clean and tolerable Electroencephalogram (EEG) signals, both independently and in conjunction, for training and testing data, aiming to assess the resilience of our feature extraction and classification methods.

3.1 Introduction

Individuals suffering from neural diseases like stroke, motor neuron disease and locked-in syndrome cannot produce voluntary muscle movements. They are totally unable or partially able to do their daily work, or even express their wishes to the caregivers [1], [204]. In order to help these patients many researchers have been studying on the brain-computer interfaces (BCI), in which the brain waves are used to control

external devices such as computers, speech synthesizers, assistive appliances, and neural prostheses, and neurorehabilitation. [57], [163], [205], [206], [207], [208], [209], [210], [211], [212], [213], [214]. The brain waves can be obtained using various non-invasive neuroimaging methods such as electroencephalography (EEG), functional magnetic resonance imaging (fMRI), magnetoencephalography (MEG), and near-infrared spectroscopy (NIRS). Although fMRI has higher spatial resolution, EEG is more popular in BCI applications because it is an easy to use, low cost, and portable system [8].

Some degrees of similarity in the cerebral activation of executed (i.e., motion) and imagined (i.e., motor intention or imagery, preparation to a movement) limb movement was proven by Lotze et al. in 1999 [17]. In the motor imagery (MI) paradigm, the user intention can be captured from the multichannel EEG signals before the motion occurs [215]. By using MI paradigm, simple motor actions become detectable from the signals. López-Larraz et al., [216] studied with both healthy and spinal cord injury (SCI) patients on seven self-initiated upper-limb movements and showed that the studied movement could be decoded in both healthy subjects and patients with the same accuracy that ranged between 40 to 75%. Kim et al. [27] analyzed the connectivity distinction between EEG and EMG signals during the movement of the upper limb in the same manner as the existence of the motion intention by implementing (linear) coherence and (non-linear) analysis of mutual information. Zapała et al. [217] reported that cursor control can be accomplished by employing EEG signals obtained from the electrodes placed over sensorimotor cortex. Thus far, however, the studies have primarily focused on the detection of the motor imagery tasks such as imagination of the right or left hand, foot, and tongue movements. On the other hand, detecting initiation of the movement intention is also important. In the movement intention paradigm, the user intention and resting state (task-negative state) can be distinguished from the EEG signals before the motion occurs [8]. Ang et al. [28] emphasized robotic rehabilitation with MI-based BCIs, and worked with 18 hemiparetic subjects whose EEG signals were acquired from 27 channels. They used filter bank common spatial pattern (FB-CSP) algorithm to extract features in order to discriminate the resting and motor imagery states. Muralidharan et al. [29] used the paradigm in order to distinguish the rest and attempted finger-extension for the purpose of opening or closing the hand. Only 4 subjects with subcortical ischemic stroke were recruited in this study. They extracted features using common spatial pattern (CSP) analysis. In another study by Bai et al., [30] they focused on the recognition of the wrist

extension in 7 healthy users, and used spatial (surface Laplacian derivation) and temporal filtering (Welch based power spectral density estimation) as the feature extraction methods. In a different study by Rozado et al., [31] the aim was to monitor the subject's pupil diameter as an extra feature, and they investigated the discrimination of the motor intention from the resting state.

For discriminating cognitive states using EEG signals many features extraction approaches have been investigated so far. One of the methodologies used in this context is the short-time Fourier transform (STFT) in which is EEG signals are divided into windows to model them as stationary signals even though they are non-stationary [218]. On the other hand, the synchrosqueezing transform (SST) is an appropriate method to make localized time-frequency (TF) representation of non-stationary signals. It is introduced in the context of many applications like audio signal analysis [219], seismic data analysis, fault diagnosis of a wind turbine, detection for earthquake-damaged structure [140], detecting and quantifying damage in smart highrise building structures [220], [221], [222] and biomedical signal processing applications such as emotion recognition from EEG [104], [223], discover breathing dynamics from ECG [224], and heart beat classification from ECG [225].

Although there are various studies on motor imagery-based BCI in the literature, the SST algorithm, whose compatibility with EEG signals has been proven, has not been investigated on this paradigm. In this study, it is aimed to contribute to the literature by using the Fourier-based SST algorithm (FSST) to distinguish resting and imagery states to be used in the self-initiated EEG-based BCIs. The transition between these states might be used as a trigger for the external devices in real-time using EEG signals.

Based on these empirical studies, it can be seen that there is still a strong need for a comprehensive research in this field. Currently, the classification accuracy levels attained in the abovementioned studies are not sufficient to control external devices outside the laboratory [47]. Furthermore, in the studies reviewed above, the number of subjects included in the experiments was not high enough for a good generalization. Due to the characteristics of the EEG, it is proven that the small sample size can cause discrepant findings in the literature [42].

The main goal of this study is to identify the intention of the movement for asynchronous BCI applications in order to assist people with motor impairments. If detectable, this motor-planning activity may be used in real-time to activate (wake-up from the sleep mode) external devices like wheelchair, arm/hand prosthesis, and/or computer application.

In this study, the main contributions to the motor imagery literature are as follows: (i) We introduced the usability of the Fourier synchrosqueezing transform (FSST) as the feature extraction approach, which has recently been proposed, and singular value decomposition (SVD) as the feature selection/reduction method, (ii) we investigated the most effective features and channels for the discrimination of the resting and imagery states in the MI-based BCI, (iii) we compared the FSST approach with a combination of statistical, time-, time-frequency- and frequency-domain approaches and well-known methods such as common spatial patterns (CSP) and sub-band CSP (SBCSP), and (iv) we examined the use of clean and tolerable EEG signals alone and together as the training and test data to investigate the robustness of our feature extraction and classification methods.

The rest of this paper is organized as follows; the custom-built EEG dataset used in our study is presented in Sections 3.2.1 and 3.2.2. The analysis of the EEG signals and proposed FSST and SVD feature sets are introduced in Section 3.2.3. The classifiers, performance evaluation metrics, along with statistical analysis of the data are presented in Section 3.2.4. Experimental results are dedicated in Section 3.3. The discussion of the results is given in Section 3.4 and the conclusions are depicted in Section 3.5.

3.2 Materials and Methods

3.2.1 Experimental Setup

The multichannel EEG signals from 28 right-handed subjects were collected while they were seated in a chair approximately 60 cm away from a monitor that delivered visual and auditory cue. All the subjects (mean age 23, age range 20-34) were healthy, and were asked to remain relaxed during the recordings. Except for eye blinks, they were asked to avoid eye movements, body adjustments, throat clearing, and other movements. The research was approved by the Erciyes University Ethics Committee (January 9, 2019, 2019/32), Kayseri, Turkey. In the experiments g.tec (Schiedleberg, Austria) products and

MATLAB based software were used. The active dry electrode (g.Sahara) cap and the wireless EEG signal amplification system (g.Nautilus), were employed in order to record 16 channels located at Cz, FP2, F3, Fz, F4, T7, C3, FP1, C4, T8, P3, Pz, P4, PO7, PO8, and Oz electrode positions according to the 10-20 international system [226]. The reference electrodes were attached to antitragus (behind the ear). The sampling rate of the signal acquisition system was 500 Hz. In the system, the signals were filtered using a hardware bandpass (2-30 Hz) and a notch (50 Hz) filter.

3.2.2 Experimental Protocol

During the experiments each subject carried out three mental tasks. Each subject performed at least two sessions; each session was 6–7 min, and was followed by a 5–10 min break. A session consisted of 30 trials each of which included 13 seconds of recording. Each trial began with the preparation (2 s), and was followed by the resting (1 s), motor intention (3.8 s), and the motion states (2.8 s), respectively. The pictorial explanation of the experimental paradigm can be seen in Figure 3.1. Briefly, at the beginning of each trial, the background of the screen was grey corresponding to the preparation time. The preparation time corresponds to lay the groundwork mentally for the following states in the trial. A beep sound was heard after the preparation, and a relatively large plus sign was displayed in the middle of the screen, meaning that the resting state has begun. The participants were instructed to keep relaxed during this state. A red arrow appeared on the right or left side of the plus sign after the resting state was over (on the third second), and lasted only one second. For the next 3.8 s, they were asked to imagine the movement of their respective hand (opening and closing the right hand for example when the arrow was pointing to the right), but not to perform the motion. The condition is referred to as the preparation to movement. At the 7.8 s instant, the second arrow appeared on the plus sign for 1 s, which corresponded to the motion of the respective hand (opening and closing the hand). Motor execution is the name given to this condition. As a result, we had a total of 30 repetitions (15 right and 15 left hand) of each mental task for each session for each subject.

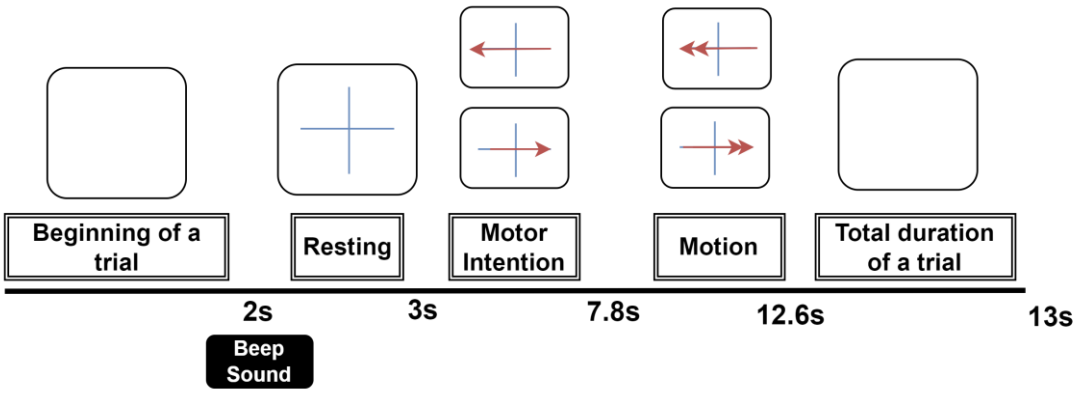

Figure 3.1 The experimental paradigm.

3.2.3 Data Selection and Feature Extraction

Data Selection

Once the experiments were over, our dataset was ready to be pre-processed manually using a custom-built MATLAB (R2019a, Mathworks®) code. First, we checked the EEG signals from each channel, and found that the signals coming from the FP1 and FP2 channels on the forehead were highly corrupted due to the muscle movement, and thus did not carry any information about the underlying brain activity. Therefore, we decided to eliminate these channels from the study, and only 14 channels were used for further steps. In addition, in order to determine the channels and states (resting, motor imagery, and motion) to be included in the analysis we checked the signals visually, and selected clean and tolerable trials. For this reason, we considered noisy portion duration on the whole signal in each trial and its amplitude. For a signal to be tolerable, its amplitude should be greater than 100 μV and the duration of the noisy portion should be longer than 10% of the whole trial duration (13 sec). Otherwise, we labelled the signal as clean. Besides, the trials that included high amplitude and long duration noisy signals were labelled as noisy and discarded from the experiment. There were 30 trials for each run, 2, 3 or 4 runs for each subject, and a total of 78 runs. Therefore, the number of trials was 7020 (78 runs x 3 states x 30 trials). However, 5643 trials were labelled as workable/clean and 1014 trials were labelled as tolerable. Both were included in the data set for further steps. Examples of clean and tolerable trials can be seen in Figure 3.2. By this way we were left with 14-channel EEG data from 28 participants. The number of trials from each state differed from participant to participant.

A)

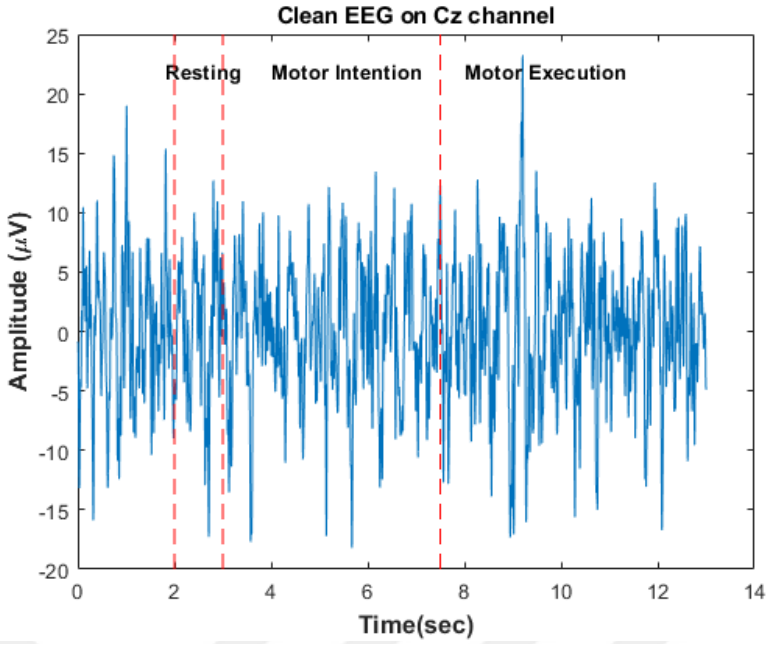

B)

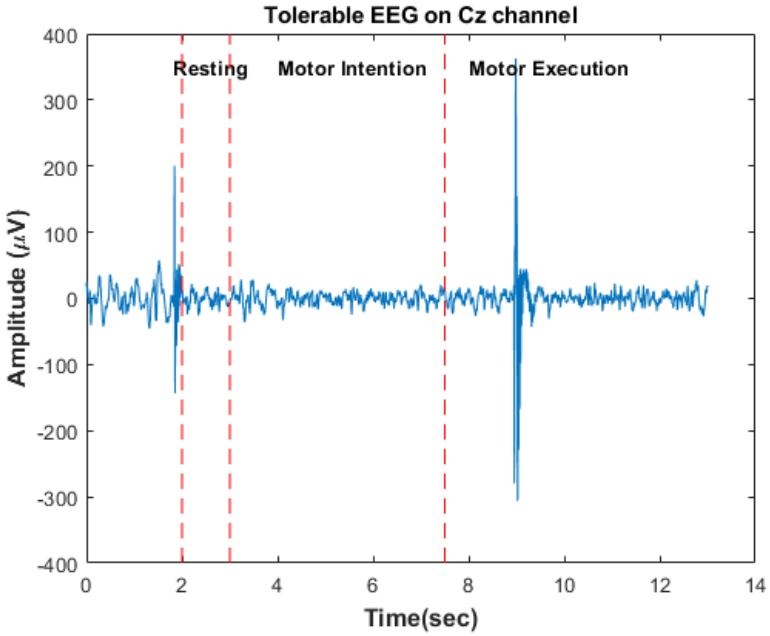

Figure 3.2 A. An example of a clean raw data and its intervals of resting (R), motor intention (I), and motor execution (M) can be seen. B. An example of a tolerable raw data and its intervals.

Feature Extraction

In this study, the second phase consisted of the investigation of the feasibility of statistical methods, time-domain, frequency-domain, and time-frequency domain features in the MI-based BCI. In order to determine the best features twelve methods were used: (1) Statistical features such as the skewness, log energy entropy, Shannon entropy, kurtosis, and energy, (2) as the time-domain methods, autoregressive (AR) modelling

(order was empirically selected as 4), (3) as the frequency-domain approaches power spectral density (PSD) using the Welch method with a Hamming window (50% overlap), mu (8-12.5 Hz) and beta (13-30 Hz) powers, and their ratio (mu power/beta power) (4) as the time-frequency domain feature, discrete wavelet transform (DWT) with Daubechies 4 wavelet function and the Fourier-based synchrosqueezing transform (FSST). In further steps, we will refer these methods except for the FSST as "S-T-F-TF." The methods were applied to each channel separately.

In this study, our main focus was to discriminate resting and motor intention states from the multichannel EEG signals. To achieve this goal, FSST provides a powerful tool for time-frequency representation. It is based on the short-time Fourier transform and focuses on the spectrogram's energy. Unlike conventional transform, FSST offers sharpened time-frequency representation [140]. We refer to [218], [227] for the basis and theoretical aspects of SST. We summarize the process of FSST relevant to this study as follows: (1) FSST was applied to each EEG channel and coefficients were obtained as complex numbers. While computing the coefficients a Kaiser window of length 128 was used to provide adequate frequency resolution and a 65x501 matrix was obtained for each channel. (2) A series of frequencies over the frequency range from 2 Hz to 30 Hz was extracted and the dimension of the matrix became 7x501. (3) Absolute values of the coefficients obtained from each channel were calculated and then the values were normalized by subtracting mean and dividing by the standard deviation (z-score). In the scope of this work, 7 frequencies of interest for each channel were determined as the FSST coefficients and a 98x501 matrix was obtained from 14 channels. (4) For dimension reduction and extract significant features from the FSST coefficients the singular value decomposition (SVD) algorithm was used to make the analysis more effective and simpler because of its stability [228].

$$A = U \times S \times V' \tag{3.1}$$

where A is the FSST coefficient matrix, U is the left singular vectors in 501x501 orthogonal matrix and V is the right singular vectors in 7x7 orthogonal matrix. S is diagonal with the singular vectors in 501x7. When extra rows of zeros in S are excluded for the economy-size decomposition, S becomes the singular vectors in 7x7. In this work, the diagonal values were taken into consideration as the features with matrix dimension of 1x98 for 14 channels on a trial.

Besides, performance comparison of S-T-F-TF with well-known feature extraction methods in motor imagery such as common spatial patterns (CSP) and sub-band CSP (SBCSP) was also investigated. CSP method extracts spatial information which is needed in multichannel EEG recordings. CSP maximizes the variance of one class and minimizes of other class using spatial filter pairs [29]. In this study, odd numbers from 1 to 14 spatial filter pairs were conducted on the data, and 9 spatial filter pairs were found to be the optimal filter pairs. The SBCSP method comprises multiple bandpass filters using zero-phase Butterworth filters, spatial filters using the CSP algorithm. There were no feature selection algorithms, so all CSP features were used to classify two states. The sub-band frequencies were: 2-6 Hz, 6-10 Hz, 10-14 Hz, 14-18 Hz, 18-22 Hz, 22-26 Hz, and 26-30 Hz.

3.2.4 Classification

In this work, we focused on the discrimination of resting and motor imagery states. We split our data into two subsets using a subject-based approach: testing data and training data. Additionally, we fitted our model on the training data, in order to make predictions on the testing data. Moreover, to determine the best performing classifier as the method of choice for the test phase of the classification and to avoid overfitting, we created validation data from the training data leave-one-out in which we did not use data from the same subject in both training and validation sets. In the test set each of 28 participants considered as test data in different iterations. To prevent any bias, we did not use any data coming from the test subject in the training and validation phases. Moreover, for S-T-F-TF 154 features (11 features x 14 channels) and for FSST 98 (7 features x 14 channels) served as the feature set for the training and validation.

On the other hand, for the sake of investigating the robustness of the model, we included tolerable data as the test set. In this stage, clean trials (3100 trials) were used for training of the model.

The classification methods we investigated were the k-nearest neighbors (k-NN, k=10, distance metric was Euclidean), linear discriminant analysis (LDA), fine tree (maximum number of splits = 100, split criterion was based on Gini's diversity index), Naive Bayes (kernel type was Gaussian), and the support vector machines (SVM) with fine Gaussian kernel and quadratic kernel [229], [230]. A statistical comparison using

Kruskal-Wallis test (KWT) on test subjects' classifier accuracies was performed for each feature extraction method. The null hypothesis was that the medians of all classification accuracies were equal, and the alternative hypothesis was that at least one median of one classifier was different from the median of at least one other classifier. The p-values obtained for tolerable and clean and tolerable data combined cases were less than 0.05, rejecting the null hypothesis. A multiple comparison test following KWT demonstrated that only SVM with fine Gaussian kernel was statistically different from and significantly lower than the other classifiers. This result showed that well performing classifiers did not have statistically significant accuracy differences. In conclusion, the best performing classifier in terms of accuracy, SVM with quadratic kernel, was selected as the method of choice in the test phase of this part oof the study. The c parameter of the SVM method with quadratic kernel was 1, and the gamma parameter was determined automatically by the classification learner application of MATLAB [231].

Performance Metrics

In this study we evaluated the performance of the classification methodologies using accuracy, area under curve (AUC) and f-measure metrics. Accuracy is the percentage of correctly predicted classes [230] and is computed using the following equation:

$$Accuracy = \frac{TP + TN}{TP + TN + FP + FN} \tag{3.2}$$

where TP and TN represent true positives and true negatives, FP and FN stand for false positives and false negatives. f-measure is the weighted harmonic mean of the precision and recall [194]. Precision is computed using equation 3.3. Recall is a measure of sensitivity and yields how many of the actual positives are predicted by the model as positive (equation 3.4). In our study, precision and recall have the same weights, and thus, we calculated f-measure using equation 3.5.

$$Precision = \frac{TP}{TP + FP} \tag{3.3}$$

$$Recall = \frac{TP}{TP + FN} \tag{3.4}$$

$$fmeasure = 2 \times \frac{precision \times recall}{precision + recall} \tag{3.5}$$

Statistical Analysis

IBM SPSS Statistics 25.0 software package was used to analyze the data and the results statistically. To determine the most discriminative (of resting and motor imagery states) electrode-feature combinations, we explored whether each electrode-feature combination was statistically significantly different. In the comparison of resting and motor imagery states, we took one of the features (say skewness) obtained using one electrode (say T7) during the resting state, and compared them with the values obtained using the same electrode during the motor imagery state. Our null hypothesis was that the distribution of these features had equal means or medians according to the normality of the distribution of the samples. When we had significant evidence against the null hypothesis (p<0.05) we claimed that this specific electrode-feature combination (T7-skewness) would be a good choice for the discrimination of these two states. In the statistical comparisons, we initially checked the normality of the data (features in the second phase) based on Kolmogorov-Smirnov approach with the Lilliefors significance correction, and observed that the data were not normally distributed. Hence, we used the Mann-Whitney U test as the non-parametric method. Additionally, a statistical comparison was performed between the classifiers with the accuracies obtained for each feature method. Since the sample size for each group less than 30, we used Kruskal-Wallis test for multiple group comparison.

3.3 Results

The classification methods were compared to determine the best performing classifier according to accuracy, area under curve (AUC) and f-measure metrics. Figure 3.3 illustrates the classification performances on the test data for the resting and motor imagery states. As depicted by the results in Figure 3.3A, Fine Tree, SVM Quadratic and Medium KNN had the highest accuracy level on S-T-F-TF.

On the other hand, SVM Fine Gaussian and LDA yielded better classification performances using SBCSP and CSP methods respectively. Nevertheless, except for the Fine Tree method all approaches resulted in 100% accuracy with FSST features. Figure 3.3B shows the comparison of methods when only clean trials were used as the training set. Accuracy levels ranged between 91% and 99% when S-T-F-TF was considered, whereas the accuracies were between 99% and 100% when FSST was used as the feature extraction method. Moreover, the maximum accuracy was 77.69% when CSP features

were used for the classification using LDA. Additionally, when LDA was used to classify SBCSP features, the maximum accuracy attained was 96.84%. Although the SBCSP has given better results than the CSP, it has fallen behind the classification performances when the features came from FSST and S-T-F-TF. We chose the SVM method with quadratic kernel over the other classification approaches for further analysis because it produced more robust accuracy results in the test phases of the analysis. This paragraph summarizes the results of the validation phase of the classification process. The goal here was to determine the best method to be used in the test phase whose results are reported in the following paragraph.

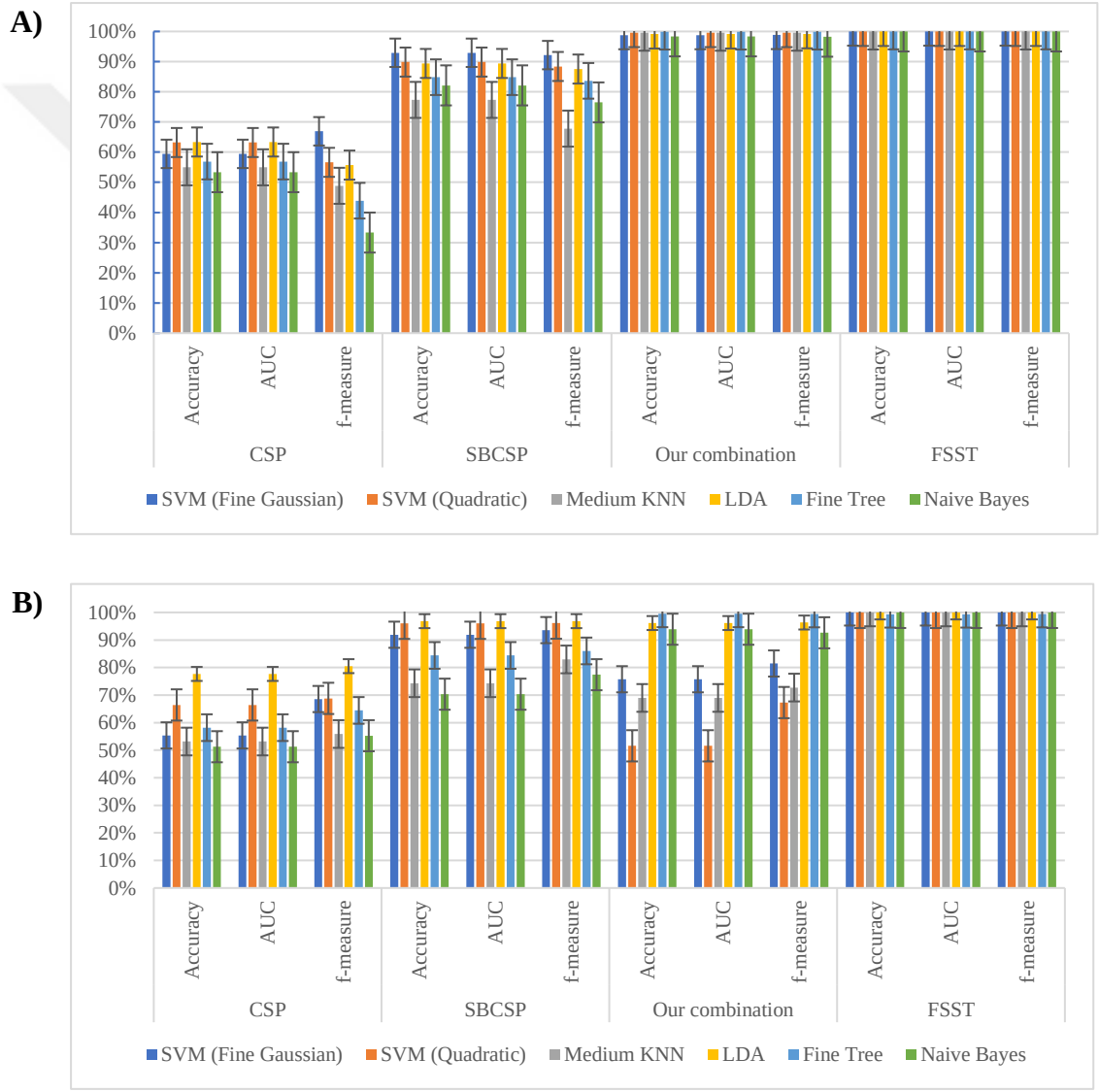

Figure 3.3 The classification accuracies, area under curve and f-measure values on the testing data using different classification methods. A) When clean and tolerable trials were used together as training set. B) When only clean trials were used as the training set.

We summarize the mean, maximum and minimum of subject's accuracies when clean and tolerable trials were used together in Figure 3.4A. According to the results, the classification accuracy levels in S-T-F-TF were above 97% for all test subjects whereas FSST have provided 100% accuracy for all test subjects. On the other hand, using CSP and SBCSP methods, the results of the classification performances were significantly lower than S-T-F-TF and FSST.

The mean, maximum and minimum accuracies when only tolerable trials were used as the test set are presented in Figure 3.4B. According to our results, the classification accuracy levels in S-T-F-TF were above 66.8% whereas FSST provided 100% accuracy

A)

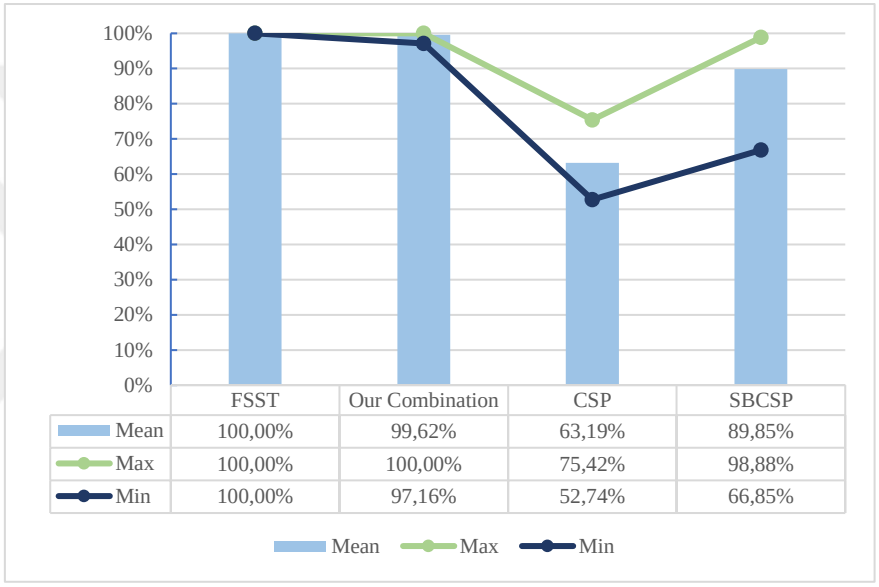

	FSST	Our Combination	CSP	SBCSP
Mean	100,00%	99,62%	63,19%	89,85%
Max	100,00%	100,00%	75,42%	98,88%
Min	100,00%	97,16%	52,74%	66,85%

B)

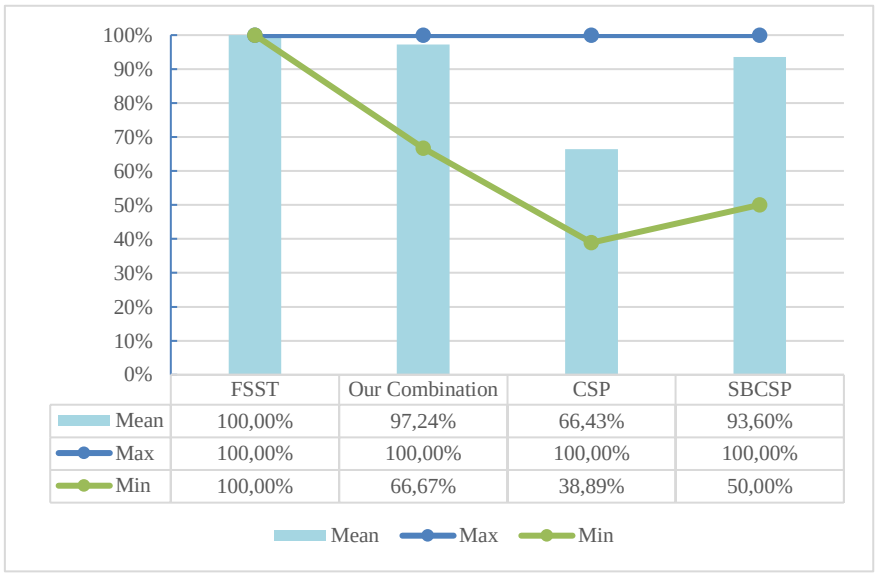

	FSST	Our Combination	CSP	SBCSP
Mean	100,00%	97,24%	66,43%	93,60%
Max	100,00%	100,00%	100,00%	100,00%
Min	100,00%	66,67%	38,89%	50,00%

Figure 3.4 The average, maximum and minimum classification accuracies. A) When clean and tolerable trials were used together. B) When only tolerable trials were used as the test set.

for all test subjects. The maximum and minimum accuracies for features extracted with CSP were 100% and 38.89% respectively. On the contrary, accuracies for SBCSP changed between 50% and 100%.

In the second phase of the study whose aim was to determine the most discriminative channel-feature combination for the classification of two states, we performed comparisons on the data with clean trials and the data with combination of clean and tolerable trials. For this reason, we performed feature extraction on the data within each trial. In the classification of resting and motor imagery states both on clean trials and on the clean and tolerable trials combined, over the feature set which belongs to S-T-F-TF the electrode-feature combinations were investigated. For each dataset, the Mann-Whitney U test ($p<0.05$) indicated that the prominent channels and features were F4, Fz, C3, Cz, C4, and Pz, and relative power, DWT, kurtosis, Shannon entropy, log energy entropy, and energy. On the other hand, PSD and AR did not have statistically significant difference between classes for any of the channels. Besides, FSST features on each dataset were statistically significant for all channels. The channel-feature combinations that do not have any statistically significant difference between resting and imagery states have been highlighted in Table 3.1, and the remaining cells (without highlight) mark the prominent channel-feature combinations. We should note that the significance values were adjusted by the Bonferroni correction for multiple testing.

Computation cost analysis was also necessary to evaluate the speed of our model. The execution durations for processing one-second signal with 14 channels are shown in Table 3.2 for different feature extraction methods and SVM Quadratic as the classification method. The values indicate the averages of ten repeated computations. For S-T-F-TF, the computation times are also presented according to each feature extraction approach in order that the impact of each method in the combination could be examined. The results showed that the minimum computation cost belonged to AR with 53.2 milliseconds whereas the maximum cost referred to DWT with 427 milliseconds. Moreover, S-T-F-TF was analyzed, and it is found that its computation cost is about 1 second while the combined duration of FSST based feature extraction and SVD based feature selection was 0.24 seconds.

Table 3.1 P value as a result of Mann- Whitney U test for each algorithm and channel combination.

Feature \ Channel	PO8	Oz	PO7	P4	Pz	P3	T8	C4	Cz	C3	T7	F4	Fz	F3
Mu Band Power	0.001	0.01	**0.055**	**0.087**	0.005	**0.063**	**0.143**	**0.181**	**0.842**	**0.639**	0.014	**0.3**	**0.056**	0.036
Beta Band Power	**0.214**	**0.126**	**0.094**	0.019	0.001	0.002	**0.428**	<.001	<.001	0.012	<.001	<.001	<.001	<.001
Ratio Band Power	<.001	<.001	0.006	0.007	<.001	0.004	**0.11**	0.004	<.001	**0.184**	0.046	0.002	0.038	<.001
AR	**0.482**	**0.444**	**0.626**	**0.981**	**0.868**	**0.984**	**0.933**	**0.367**	**0.346**	**0.861**	**0.699**	**0.606**	**0.663**	**0.938**
PSD	**0.285**	**0.364**	**0.512**	**0.757**	**0.926**	**0.592**	**0.896**	**0.417**	**0.065**	**0.29**	**0.674**	**0.951**	**0.907**	**0.681**
DWT	<.001	<.001	<.001	<.001	<.001	<.001	<.001	<.001	<.001	<.001	<.001	<.001	<.001	<.001
Kurtosis	<.001	<.001	<.001	<.001	<.001	<.001	<.001	<.001	<.001	<.001	<.001	<.001	<.001	<.001
Skewness	**0.986**	**0.207**	**0.617**	**0.534**	**0.813**	**0.509**	**0.847**	0.03	**0.14**	**0.495**	0.006	0.008	**0.515**	**0.39**
Shannon Entropy	<.001	<.001	<.001	<.001	<.001	<.001	<.001	<.001	<.001	<.001	<.001	<.001	<.001	<.001
Log Energy Entropy	<.001	<.001	<.001	<.001	<.001	<.001	<.001	<.001	<.001	<.001	<.001	<.001	<.001	<.001
Energy	<.001	<.001	<.001	<.001	<.001	<.001	<.001	<.001	<.001	<.001	<.001	<.001	<.001	<.001
FSST and SVD	<.001	<.001	<.001	<.001	<.001	<.001	<.001	<.001	<.001	<.001	<.001	<.001	<.001	<.001

Table 3.2 Computation cost for different feature extraction approaches.

Algorithm		Time (sec)	
FSST and SVD		0.24	
CSP		0.075*	
SBCSP		6.330*	
S-T-F-TF	PSD	0.081	Total: 1.063
	Mu Band Power	0.081	
	Beta Band Power	0.081	
	Ratio Band Power	0.163	
	AR	0.053	
	DWT	0.427	
	Kurtosis	0.092	
	Skewness	0.079	
	Shannon Entropy	0.193	
	Log Energy Entropy	0.088	
	Energy	0.058	

*For computation CSP needs 2 classes. That is why the values are valid for a signal with 14 channels whose duration was 4.8 seconds (2400 samples = 500 samples corresponding to resting state and 1900 samples for motor intention state).

3.4 Discussion

In this paper, we introduce FSST and SVD approaches for the discrimination and classification of resting and motor imagery states with high accuracy. Our goal in this study was to identify and characterize the movement intention using multichannel EEG signals to be used as a means to initiate a BCI system without an extra accessory/methodology. In our work, we performed experiments in which 28 participants were asked to stay at rest with no movement and imagination of the movement of their limbs, or to imagine the opening and closing of their hands (motor imagery), and to realize that movement. For each state we obtained more than 1500 trials in total. We recorded EEG signals from 28 participants while imagining opening and closing their hands in order to overcome the limitation of previous studies in the literature [163], [232], [233], [234], [235], [236], [237], [238].

We employed 14 EEG channels spread over the scalp, and extracted time-frequency features using FSST. Moreover, we propose SVD for feature selection. In our proposed method, the FSST and SVD were investigated for the first time in the motor imagery literature. The performance of the FSST and SVD is compared with several popular feature extraction approaches such as CSP, SCSP, DWT, AR and nine more approaches.

In addition, for each classification scheme, we investigated the most discriminative electrode-feature combinations. Especially, our focus in this research was to suggest the best electrode-feature combination and the classification methodology to distinguish the resting and motor imagery states. We believe that this can pave the way for the use of a self-initiated, portable, and wireless EEG based BCI system used by the patients. This classification scheme is important, because the preparation for the movement may be used to turn on the external devices in real-time, which is currently a significant issue in BCI applications.

We have proven in this study that although the classification accuracy of S-T-F-TF (methods that comprise S-T-F-TF have commonly been used in the literature separately but not in a combined manner as we have done here) is as good as FSST, the performance of FSST is the best in terms of accuracy with between 99% and 100%, computation time 0.24 seconds with SVD and robustness to noise.

As illustrated in Table 3.2, although SBCSP was more effective than CSP in the classification of motor imagery tasks, it was not as good as the combination of 11 features that we introduced in this study. Collectively, our results indicate that the intention of the movement in people with motor impairments can be identified with high classification accuracy. Overall, our study was the one that obtained the best classification performances. Additionally, use of FSST and SVD makes a great contribution to motor imagery based self-initiated BCIs.

In the literature, there are many studies about motor imagery that use different features. Niazi et al. [232] detected the movement-related cortical potential (MRCP) from EEG signals in 8 healthy subjects in real-time. They used an optimized spatial filter (OSF) method to create template of the initial negative phase of MRCPs. They obtained true positive rate (TPR) of $67.15 \pm 7.87\%$ for the motor imagery (MI) task. Another study was about the detection of the readiness potential (RP, cortical potential). [239] In their study, they implemented constrained blind source extraction (CBSE) algorithm for detecting RP with 3 healthy subjects. Pre-movement trials were used for true positive rate evaluation. Furthermore, Jochumsen et al. [234] used 15 healthy subjects with 5 stroke patients. They investigated the possibility of recognizing MRCPs from a single EEG channel during palmar grasping tasks. Their aim was to detect movement intention from executed and imaginary grasps. They extracted features by using the following 4 methods: (i) peak of

maximum negativity, (ii) mean amplitude, (iii) slope of a linear regression fitted to the data window, and (iv) the average power in the interval from 0–5 Hz. They performed the SVM classifier to compare motor execution, motor imagery, and attempted motor execution (for stroke patients). They detected about 75% of the movements correctly ~100 ms before the onset of the movement. A similar study about the capture of voluntary motor intentions from EEG was demonstrated in [235]. They detected the MRCPs by using Locality Preserving Projection methods, and classified using the linear discriminant analysis. Nine healthy subjects were used in this study. To discriminate execution and imagery tasks, they performed classification with 79 ± 11% true positive rate (TPR). Aliakbaryhosseinabadi et al. [236] investigated the effect of random and non-random cue paradigms on the detection of MRCP. In the experiment, the researchers used a template-matching algorithm in 8 healthy subjects. They showed that the TPR of detection of movement intention were 63.5 ± 5.9% for random cue, and 75.3 ± 5.5% for the non-random cue. Several other studies have been carried out to investigate the feasibility of different approaches [28], [29], [30], [31]. In these studies, the number of electrodes used ranged between 27-32, and the feature extraction approaches were filter bank or regular common spatial pattern, band powers, and surface Laplacian derivation.

Our results, just like other studies in the literature, confirm that the imagination of movement manifests a significant effect on brain signals. Despite all this, the prediction accuracy of the movement intention is lower than that of our proposed study. In [25], for the prediction accuracy of the movement intention was 75%. Additionally, in [240], the researchers used the MRCPs to detect motor execution and imagination, worked with 15 subjects, and demonstrated an optimized spatial filtering method to obtain high TPR (82.5 ± 7.8%). Another study [241] was about the detection of gait initiation by using MRCP. Although they used ICA as the pre-processing method, the TPR of detection was 76.9 ± 8.97%. On the other hand, in [242], authors used FSST of EEG signals for classifying focal and non-focal classes by using 2D-convolutional neural network (CNN) with 100% accuracy rate.

The FSST based methods allow analyzing nonstationary signals, like EEG, in time-frequency (TF) domain. Unlike the STFT, FSST has the ability to obtain a high-resolution TF representation by minimizing the unnecessary information of nonstationary signals. Therefore, we introduced the classification accuracy of the FSST for classifying resting and motor intention states that showed high success rates by using machine learning

approaches. However, the FSST suffers from the limitation that it requires feature selection to extract representative features from TF coefficient matrix when it is used with machine learning algorithms.

Although the highest possible accuracy values were obtained, our study suffers from some limitations due to offline analysis. Furthermore, we collected EEG data not from patients with motor disabilities but from healthy subjects although our goal was to identify and characterize the movement intention in people with motor impairments. From a previous study [234], we know that the data recorded from the patient with motor impairments can affect the classification accuracy in a negative way. In the future, this limitation will be addressed by developing online classification approaches with high accuracy and robustness using the data collected from the patients with motor impairments.

As part of our future research agenda, we plan to investigate the feasibility of novel classification approaches such as Neural Dynamic Classification algorithm [243], Dynamic Ensemble Learning Algorithm [182], Finite Element Machine for fast learning [244], and Deep Support Vector Neural Networks [184], [245], [246].

3.5 Conclusions

This study provided a detailed analysis of the combination of popular feature extraction techniques used for EEG-based resting and motor imagery task discrimination. Among the feature extraction approaches the Fourier-based Synchrosqueezing Transform (FSST) (singular value decomposition was also used to reduce the number of features) were found to have the best discrimination performance. This study is the first showing the feasibility of this approach in motor intention paradigm in BCIs. Moreover, this study also investigated the use of tolerable data, which contain certain amount of noise but not dominating the information carried in the EEG signals in addition to the clean counterparts. Furthermore, the statistical analysis of EEG channels with the best discrimination (of resting and motor imagery states) characteristics demonstrated that the frontal and central electrodes were the most effective ones.

To conclude, the resting state has a role in the idle state (baseline) of the participants whereas the motor intention state represents the intention required to start a BCI. Our approach proposes the use of FSST-SVD features coming from the EEG channels, and if

the outcome of the classification method indicates motor intention state the BCI system will be initiated. We propose here that the signal acquisition, preprocessing, feature extraction/selection and classification will be performed continuously until such an intention is detection. Once the system is started MI-based EEG signal decoding will be in place for other specific operations. If no further motion intention were detected in a certain time period the system will be switched to the idle state and will wait for another detection of intention to restart the system.

Chapter 4

EEG-Based Preconditioning for Object Weight Estimation in Upper-Limb Prostheses: Enhancing Functionality and Usability

In this chapter, we aim to explore the estimation of object weight using EEG signals in the context of upper-limb prostheses. By leveraging neuroimaging techniques, we seek to develop a neurofeedback system that enables individuals to estimate the weight of objects grasped by their prosthetic limbs. This research has the potential to enhance the functionality and usability of upper-limb prostheses, empowering individuals with more natural and intuitive control over their interactions with the environment. For this purpose, widely used feature extraction algorithms in the literature have been applied to EEG signals to classify objects' weights into light, medium, and heavy categories. Part of this section is excerpted from the author's accepted article.

4.1 Introduction

Accurate perception of the weight of objects is crucial for individuals utilizing upper-limb prostheses to interact with the environment effectively. The prostheses used especially for the upper extremity differ according to the level of amputation, just as the methods used to move the prosthesis. In some prosthesis types, only cosmetic use is prominent, while in others, the hand is opened and closed by the individual's own power, for example by moving the shoulder. Another type of prosthesis is called a myoelectric prosthesis. In this type, arm and hand movements are performed with the muscle signals received from the electromyography (EMG) electrodes placed in the appropriate places (on the skin) of the amputated limb [247], [248]. Recently, efforts have been made to use electroencephalography (EEG) signals in upper extremity prostheses.

While traditional prosthetic devices offer remarkable functionality, they often lack the ability to provide real-time feedback on the weight of grasped objects. Consequently, individuals with upper-limb prostheses may struggle to regulate their grip force and adequately adapt their movements to different object weights.

Recent advancements in neuroimaging techniques, such as EEG, present an innovative approach to address this challenge. EEG allows for the analysis of brain activity patterns associated with object weight perception, providing an opportunity to develop a neurofeedback system that enables individuals to estimate the weight of objects grasped by their prosthetic limbs.

Previous research has demonstrated the potential of EEG in decoding various aspects of motor control and perception, including studies on motor imagery [62], [174], [209], [249], [250], [251], emotion recognition [252], sleep stage classification [253], tactile perception [254]. However, the application of EEG to estimate the weight of objects to be carrying specifically in the context of upper-limb prostheses remains largely unexplored. Investigating the neural correlates of weight perception in individuals using prosthetic limbs can offer valuable insights into the underlying mechanisms and inform the development of neurofeedback-based strategies for weight estimation. The primary objective of this study is to investigate the feasibility and accuracy of estimating the weight of objects using EEG signals in individuals.

The effectiveness of classifying EEG signals relies directly on the discriminative capability of a combination of chosen features and the machine learning classifier employed. Numerous approaches for extracting features have been explored thus far to differentiate cognitive states using EEG signals. A methodology commonly employed in the field of EEG analysis is Common Spatial Pattern (CSP) [181], [255]. It is specifically employed in the context of motor imagery-based brain-computer interfaces (BCIs). CSP aims to enhance the discriminative power of EEG signals by transforming them into spatial patterns that highlight the differences between different cognitive states or tasks. The conventional Common Spatial Pattern (CSP) approach in the time domain can sometimes struggle to preserve the distinguishing characteristics between different classes. To address this limitation, various enhanced CSP algorithms have been suggested. Examples of these improved approaches include sub-band common spatial pattern (SBCSP) in which SBCSP analyzed the EEG data on different sub-bands [149],

filter bank common spatial pattern (FBCSP) that chose features extracted from various frequency sub-bands according to the maximal mutual information criterion [103], and deep CSP (DCSP) [256]. Nanxi Yu et al. [256] proposed DCSP model with optimal objective function to improve classification accuracy. Another alternative approach to CSP is a method based on Online Recursive Independent Component Analysis (ORICA)-CSP [181]. Antony et al. demonstrated that ORICA-CSP yielded more reliable motor imagery feature extraction compared to conventional CSP and Wavelet-CSP methods. This superiority can be attributed to ORICA-CSP's ability to provide additional information about the interactions among different cortical areas during mental activities.

On the other hand, various methods for extracting features from EEG signals to distinguish between different cognitive states have been explored extensively. In this context, one of the methods employed is the short-time Fourier transform (STFT). STFT is commonly used in the EEG signal processing community. STFT method divides EEG signals into segments/windows to analyze them as if they were stationary signals. In [131], two deep learning pipelines utilizing Convolutional Neural Networks (CNN) and Long Short-Term Memory (LSTM) are used for the classification of motor imagery tasks. Frequency domain representations from EEG signals are extracted with STFT and fed into pipelines for training the models. Feature selection from STFT covariances are proposed to extract spatial, time and frequency features concurrently in [130]. Since EEG signals inherently exhibit non-stationary characteristics, synchrosqueezing transform (SST) provides a better time-frequency representation for the feature extraction as compared to STFT [141], [143], [228], [257], [258]. SSF is suitable for generating a localized time-frequency (TF) representation of nonstationary signals. In [228], a novel approach is introduced for emotion classification using EEG signals. This approach incorporates singular value decomposition (SVD) and multivariate SST. In another study, emotion recognition methodology that relies on multivariate SST analysis on multichannel EEG data [104]. Precise TF localization of SST is also convenient for the epileptic seizure detection as reported in [258]. In EEG based BCI framework, time-frequency coherence using STFT and SST methods are found between electrophysiological signals.

The successful development of an EEG-based weight estimation system for upper-limb prostheses carries several potential benefits. Firstly, it can enhance individuals' ability to interact with objects in their environment by providing them with accurate real-

time weight information. This, in turn, can improve their ability to regulate grip force and adapt their movements, accordingly, resulting in more natural and efficient interactions. Additionally, this research can contribute to advancements in prosthesis design and neurofeedback technologies, further enhancing the functionality and usability of upper-limb prostheses.

4.2 Materials and Methods

4.2.1 Experimental Setup and Dataset

In this work, two experimental setups were used for the analysis. Thirty-one healthy volunteers enrolled in the study, with a mean age of 22 years and an age range of 19–35. The research received approval from the Erciyes University Ethics Committee on January 9, 2019 (Approval No: 2019/32), Kayseri, Turkey. The experiments utilized g.tec products (Schiedleberg, Austria) and MATLAB-based software. The active dry electrode cap (g.Sahara) and the wireless EEG signal amplification system (g.Nautilus) recorded 16 channels located at Cz, FP2, F3, Fz, F4, T7, C3, FP1, C4, T8, P3, Pz, P4, PO7, PO8, and Oz electrode positions according to the 10-20 international system [226]. Reference electrodes were attached to the antitragus (behind the ear). The signal acquisition system had a sampling rate of 500 Hz. The signals were filtered using a hardware bandpass (2-200 Hz) and a notch (50 Hz) filter in the system.

Subjects performed actual movement and imagery sessions in a different sequence with 30 repetitions. Trials for the actual movement session comprised five phases: the rest phase, holding phase, lifting phase, replacement phase, and relaxation phase. In the rest phase, a red circle was presented in the middle of the plus sign for 2.5 seconds, and subjects fixed their eyes on the circle. During the holding phase, three visual cues representing objects with different weights were displayed for 0.5 seconds to aid subjects in grasping the weight for 1 second. In the lifting phase, the up-arrow icon was presented for 2 seconds to guide subjects in lifting the object. In the replacement phase, subjects returned the object to its initial position after the appearance of the down-arrow icon. In the relaxation phase, subjects relaxed and mentally prepared for the next trial. Each of the three weights was performed 10 times.

In the imagery session, trials consisted of three phases: the rest phase, imagination phase, and relaxation phase. In the rest phase, a red circle icon was displayed in the middle

of the plus sign, instructing subjects to stay relaxed. A visual cue representing one of the three objects with different weights appeared for 0.5 seconds, and the plus sign was presented for three seconds to guide subjects in imagining the weight of the object. The relaxation phase was performed similarly to the actual movement session. The experimental paradigm is shown in Figure 4.1.

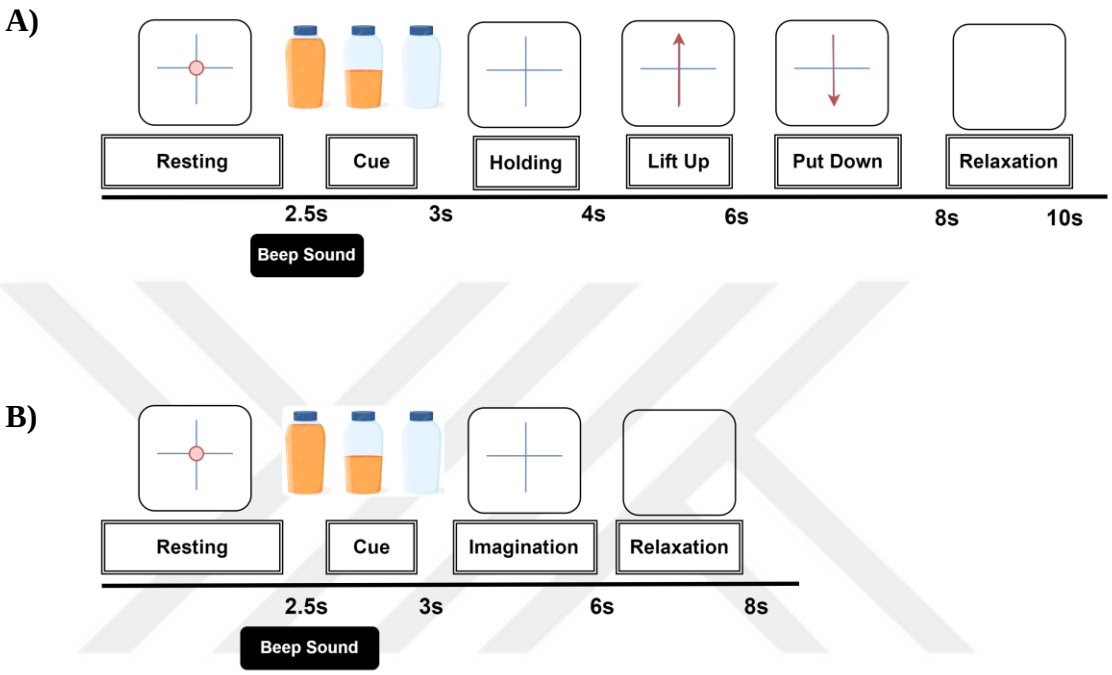

Figure 4.1 The experimental paradigm. (A) Actual movement session. (B) Imagery session.

In both the actual movement and imagery sessions, subjects were asked to carry out the requested task immediately after the execution cue appeared. Each of the three different weights of the objects in any given epoch was randomly selected. All subjects were healthy with no history of neurological disease and were instructed to remain relaxed during the recordings. Apart from eye blinks, they were asked to avoid eye movements, body adjustments, throat clearing, and other movements. After the actual movement session, the imagery session was performed since performing real movements first would make it easier to perform the imagined movement [259]. Between the actual movement and imagery sessions, we set up a minimum 15-minute break to minimize fatigue.

The data for each subject in one session consist of a total of 30 trial data, with each trial representing either one actual movement or one MI task, belonging to one of three

weight classes: 10 trials of light weight (25g empty bottle), 10 trials of medium weight (523g half-full bottle of water), and 10 trials of heavy weight (1037g full bottle of water). Thus, there are a total of 60 trials (30 actual movement, 30 MI) per subject in the dataset. The grand total of trials from all subjects is 924 trials for the actual movement session and 924 trials for the motor imagery session.

4.2.2 Preprocessing

EEGLab toolkit (version eeglab2021.0) of MATLAB (R2019a) software was used to pre-process the collected data. We applied independent component analysis (ICA) to remove eye-movement and blinking artifacts from single channel EEG signal. Additionally, the pre-processing includes filtering with an 8-30 Hz Butterworth band-pass filter to eliminate physiological-, movement-, and equipment-related artifacts in EEG.

We use time domain, frequency domain, time-frequency domain methods for feature extraction in MATLAB (2019a). In this study, we first conducted feature extraction to the signals from 2.5s - 5.5s (visual cue and imagination phase) of imagery session. Afterwards, to explore the effect of actual movement session on the predicting of the weight perception, we employed a new method that includes the data from the 4s - 6s (lifting phase) of the actual movement session.

4.2.3 Statistical and Time Domain Features

In order to investigate the feasibility of statistical methods, the skewness, log energy entropy, Shannon entropy, kurtosis, and energy were used.

Skewness is a measure of the asymmetry of the corresponding probability distribution [114], [260]. In the context of analyzing EEG (Electroencephalogram) signals, skewness can be used as a feature to describe the shape of the signal's amplitude distribution [260]. Equation (4.1) use to calculate skewness:

$$S = \left[\frac{\sum(x_i - \mu)^3}{N\sigma^3}\right] \tag{4.1}$$

where S is the measure of skewness for the EEG data, x represents the data point i in the EEG data, μ is the mean of the EEG signal, N is the total number of data points in the EEG signal, σ is the standard deviation of the EEG signal.

Entropy is about how much information a signal carry. Entropy can be used to describe the complexity or irregularity of the brain activity [215]. The study conducted two different types of entropy measures: Shannon entropy (ShanEn) and log energy entropy (LogEn). Shannon entropy measures the uncertainty or information content in a dataset, whereas log energy entropy measures the distribution of energy across different frequency bands. The formulas for ShanEn and LogEn can be introduce with equation (4.2) and (4.3), respectively [116].

$$ShanEn(x) = -\sum_{i=0}^{N-1} \left(p_i(x)\right)^2 (log_2(p_i(x)))^2 \tag{4.2}$$

$$LogEn(x) = -\sum_{1=0}^{N-1} (log_2(p_i(x)))^2 \tag{4.3}$$

where p_i represents the probability distribution function, and i indicates one of the discrete states.

Kurtosis is a measure of the difference between the highest value of the probability distribution and the highest value of the normal distribution of a random variable with real values, and it can be used to describe the peakedness or flatness of the distribution of amplitudes in analyzing EEG signals [115]. The equation 4.4 to calculate kurtosis is as follows:

$$\boldsymbol{Kurtosis} = \left[\frac{\sum(\boldsymbol{x_i} - \boldsymbol{\mu})^4}{\boldsymbol{N\sigma^4}}\right] \tag{4.4}$$

where x_i represents each data point in the EEG signal, μ is the mean of the EEG signal, N is the total number of data points in the EEG signal, σ is the standard deviation of the EEG signal.

In the context of EEG signal processing, energy is often computed to measure the total energy or power in a specific frequency band or across the entire signal. The formula for calculating energy in an EEG signal depends on the specific context and the desired frequency range. In a time-domain EEG signal to calculate the total energy, square each data point in the EEG signal and then sum up all the squared values [261].

AR modelling was adapted to EEG data as a time domain feature, and the means of the AR coefficients from each channel were extracted as features. In this approach, the best AR order, 4, was selected by trial and error [262].

All the features were calculated with MATLAB built-in functions. These features were applied separately for each of the 16 channels. Therefore, 6 features were extracted from each channel.

4.2.4 Frequency Domain Features

Another feature extraction method used for MI-based BCI was the power spectral density (PSD) in which the Welch method with a Hamming window (50% overlap) was employed. The state was divided into eight segments, and all segments were averaged to obtain a smoothed estimation. Additionally, this method was preferred to estimate the power at chosen frequency bands, the range between 8-12.5 Hz (mu band) and 13-30 Hz (beta band). Moreover, the band power ratios of the mu and beta activity served as the additional features. The methods were applied to each channel separately. In further steps, we will refer these methods mentioned above section 4.2.3 and section 4.2.4 as “S-T-F-TF”.

4.2.5 Time-Frequency Domain Features

Different EEG signal frequency bands contain different information about the MI. In order to decompose a signal in multiresolution frequency and time, discrete wavelet transform (DWT) and Fourier-based synchrosqueezing transform (FSST) was used in this study. In DWT, Daubechies 4 was the wavelet function, and the wavelet decomposition level was determined automatically using MATLAB.

EEG is a non-stationary signal whose spectral characteristics change with time. The short-time Fourier transform (STFT) and continuous wavelet transforms (CWT) have a deficiency in linear projection for non-stationary signals [141]. On the other hand, FSST is effective for a sharpened time-frequency representation. We previously demonstrated the contribution of FSST in the detection of motor intention [257]. We recommend consulting References [218] and [227] for the fundamental principles and theoretical aspects of FSST. Additionally, the singular value decomposition (SVD) algorithm was performed after applying FSST to reduce the dimensionality of the output of FSST and to extract significant features from the FSST coefficients. The process is also summarized in the algorithm provided in Table 4.1. According to the algorithm, FSST was applied to individual EEG channels, generating complex number coefficients. To compute these

coefficients, a Kaiser window of 256 units in length was employed to ensure accurate frequency resolution, resulting in a 128x500 matrix for each channel. After that, since the frequency range of interest was 8-30 Hz, the size of the matrix obtained from the FSST, which represents 128 frequencies, was reduced to 11x500 by selecting only the frequencies within the range of interest. Then, the absolute values of the coefficients for each channel were calculated and then normalized these values. Next, to reduce dimensionality and extract important features from the FSST coefficients, we utilized the Singular Value Decomposition (SVD) algorithm for a more effective and streamlined analysis due to its stability. The SVD formula was introduced with equation (4.5).

$$A = U \times S \times V' \tag{4.5}$$

where A represents the coefficient matrix, U signifies the left singular vectors, V denotes the right singular vectors, and S takes the form of a diagonal matrix with singular vectors in a 500x11 configuration. Excluding extra rows of zeros in S for a more efficient

Table 4.1 The algorithm to calculate the FSST coefficients with the SVD as a dimension reduction method.

Algorithm 1: *FSST-SVD*	
Input*: Processed EEG signals* ***Window:*** *Kaiser* ***Window Length:*** *256* ***Selected Frequency:*** *8-30Hz*	**Output**
1. *Apply FSST to each channel*	*128x500 complex*
2. *Select interested frequencies*	*11x500 complex*
3. *Calculate absolute values of the coefficients*	*11x500 double*
4. *Apply SVD to each channel.*	*A: 11x500* *U: 500x500* *V: 11x11* *S: 500x11*
5. *Exclude extra rows of zeros in S for the economy-size decomposition*	*S:11x11*
6. *Select the diagonal values of S*	*S: 1x11*
7. *Gather the 16 channels features*	*s: 1x176 (11x16)*

decomposition yields singular vectors in a 11x11 configuration. In our study, we regarded the diagonal values as features, creating a 1x176 matrix for each of the 16 channels in a single trial. The visualized FSST coefficient matrix, created by taking the average of trials for each weight, is shown in Figure 4.2.

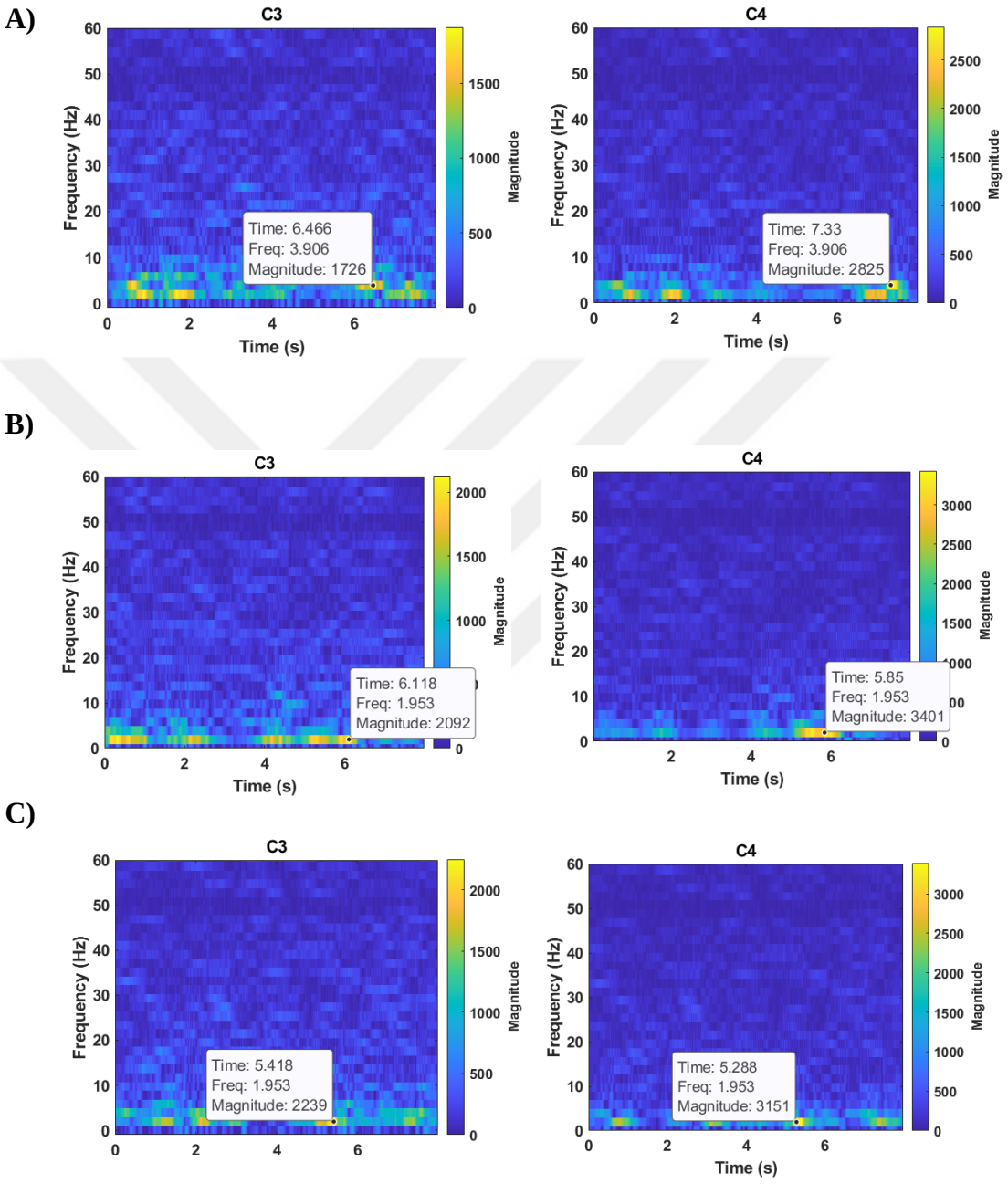

Figure 4.2 The time-frequency representation created using FSST for the weights (first 2.5 seconds for the rest phase and the intention phases between 3 and 6 seconds). A) Average of trials for light weight object. B) Average of trials for medium-weight object. C) Average of trials for heavy object.

Gray Level Co-Occurrence Matrix

Gray level co-occurrence matrix (GLCM), commonly used for texture classification, is also employed to extract features from signals with time-frequency domain representations [263]. GLCM provides information about the relationships between pixel intensities, indicating how often neighbouring pixels repeat in horizontal, vertical, and diagonal directions [264]. Therefore, the co-occurrence matrix carries information about the angle (θ), distance (d), and frequency. The angle value varies in 45-degree increments, creating matrices at θ = 0°, 45°, 90°, and 135° angles. Due to computational simplicity, d is often chosen as 1.

The co-occurrence matrix holds spatial distribution information about the gray levels in the image [265]. M. Haralick defined 14 texture features, including homogeneity, entropy, energy, and contrast, providing information about the image [266]. In this study, GLCM is utilized to extract second-order statistical features, namely contrast, correlation, energy, and homogeneity, from the FSST image. The steps to create feature matrix from the GLCM image is shown in Figure 4.3.

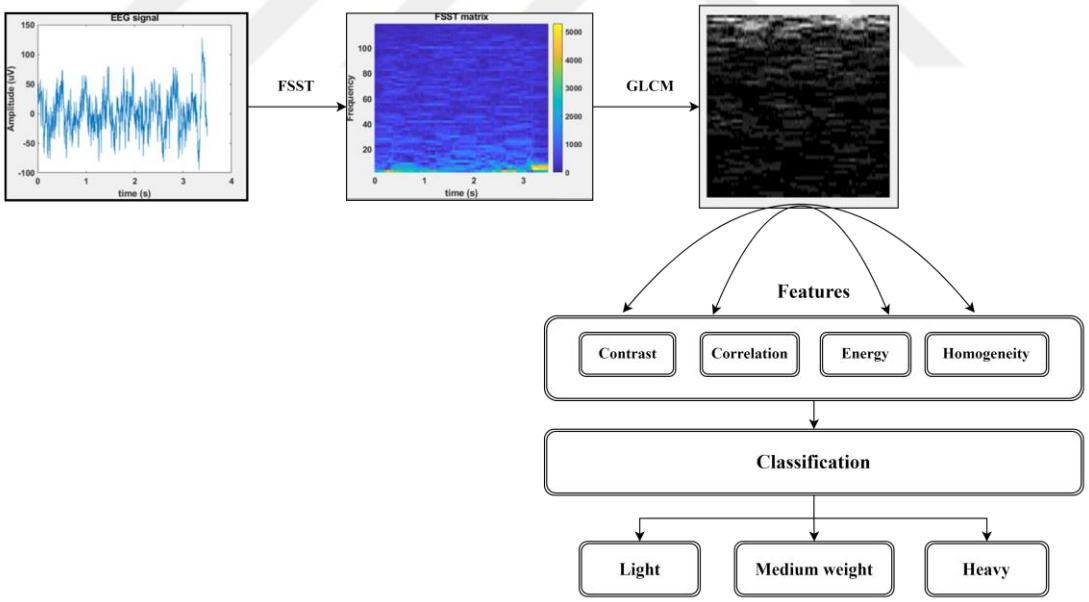

Figure 4.3 The method used for representing FSST coefficient matrix with GLCM image**.**

4.2.6 Relative band power

Another commonly used method for analyzing EEG signals is to focus on relative band powers [267]. After averaging band power signals in different sub-frequency bands (2-4 Hz Delta; 4-7 Hz Theta; 8-12 Hz Alpha; 13-30 Hz Beta, 31-120 Hz Gamma), power spectral densities (PSD) are obtained. This yields a single number summarizing the contribution of a frequency band to the total power of the signal [174]. This number is calculated using the equation 4.6.

$$P_{ort} = \frac{PSDi}{PSDtoplam} \tag{4.6}$$

Equation 4.6 represents the average power of P_{ort} for frequency bands, denoted by i. Figure 4.4 illustrates the calculated average band powers for each weight. Here, the average band powers of signals obtained from the intention phase, including the visual stimulus portion of the signal recorded during the imagination phase, are calculated.

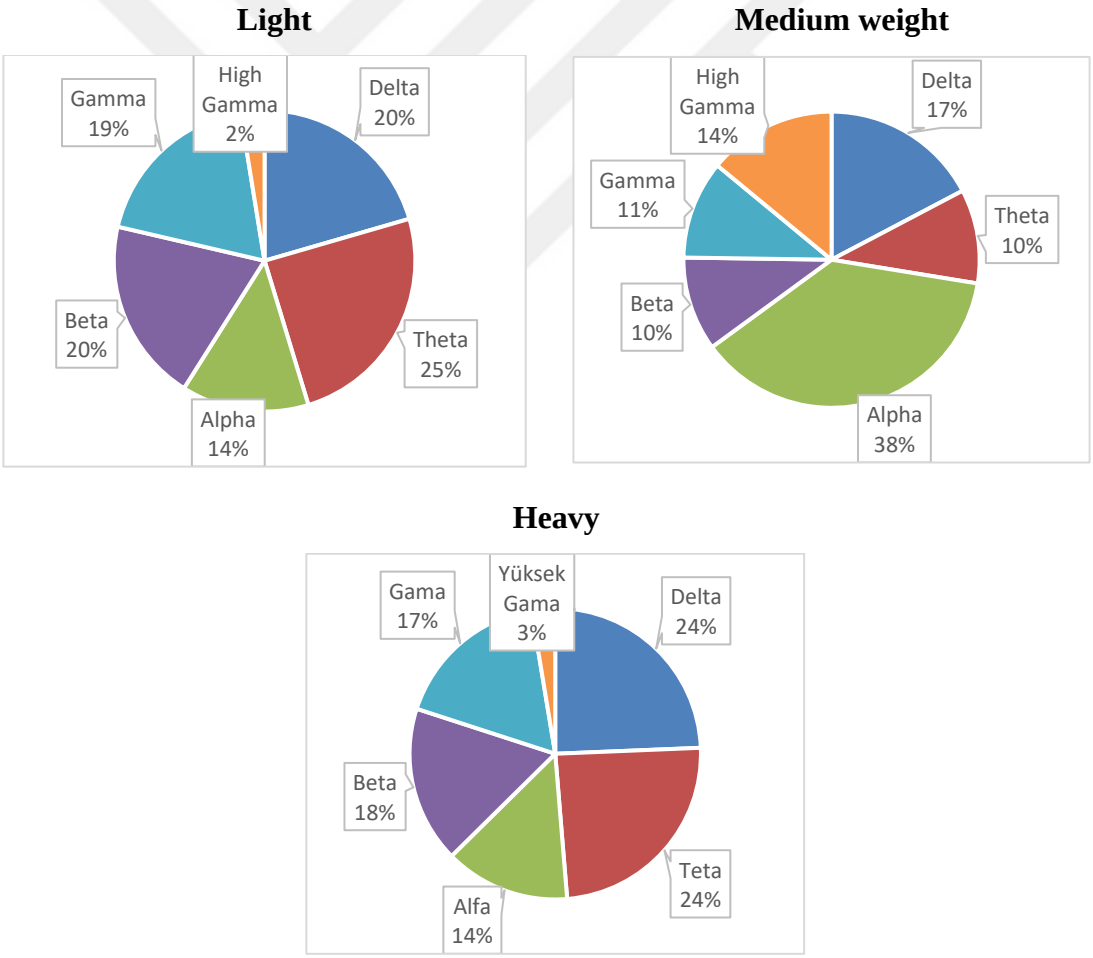

Figure 4.4 The average band powers obtained from Participant 1.

For relative band power, calculations were made using signals recorded during the rest (R) and intention phases in the imagination phase. The ratio of the average band

power in the intention phase (MI) to the average band power in the rest phase provides the relative band power. The following equation 4.7 was used to obtain relative band power.

$$PB_i = 100 \times \frac{PMI_i - PR_i}{PR_i} \tag{4.7}$$

Equation 4.7 represents PB as the relative band power, PMI as the band power during the motor intention phase, and PR as the band power during the rest phase. Here, i is used as a representation for each band (alpha, beta, gamma, theta, delta). The values of relative band powers are reported in Table 4.2. Negative results imply that the band power during the rest phase is greater than the band power during the motor intention phase.

Table 4.2 Relative band powers for Participant 1

Class / Band	Light	Medium-weight	Heavy
Delta	-37	4.3	-9.2
Theta	-5.5	9.5	-20.4
Alpha	-25.7	-0.09	-16.1
Beta	-6.3	-20.8	-12.2
Gamma	-2.5	-0.4	-1.9
High gamma	3.1	1.2	-12.6

4.2.7 Convolutional Neural Network

Obtained data from the mentioned methods have been used as input to the classifier for machine learning. In addition to these methods, deep learning applications are widely used today to enhance classification performance. In BMI applications, deep learning is utilized in various domains such as speech recognition, computer vision with natural language processing, and classification of activities performed from brain frequency bands [268]. To investigate whether different weights have a meaningful effect on brain signals, Convolutional Neural Network (CNN) is a powerful architecture for time-frequency-based image input. A CNN is a deep learning algorithm that can take an input image, calculate pixel values in the image, and analyze the relationship between pixels, consisting of layers as shown in Figure 4.5.

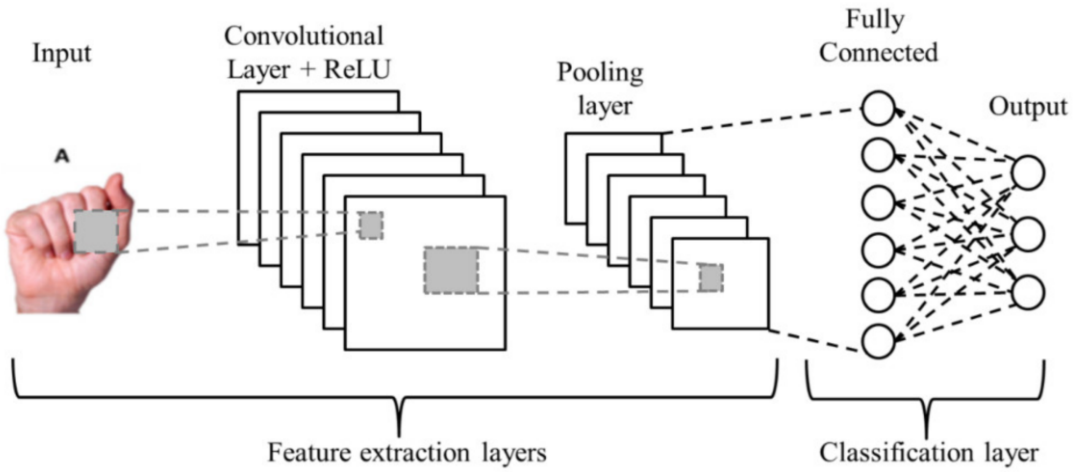

Figure 4.5 CNN layers [269].

In this study, two methods were applied using CNN architecture. These can be categorized as classifying time series using wavelet analysis and being a continuous convolutional neural network (CCNN) with three-dimensional input.

Wavelet Analysis and Deep Learning

Continuous wavelets transform (CWT) was utilized to generate time-frequency spectrogram images used as input in the CNN architecture to classify time series [135]. A spectrogram is calculated as the absolute value of CWT coefficients, representing frequency-time energy density [270]. Figure 4.6a and b respectively display the raw EEG signal and its spectrogram. Signals in the imagination phase of carrying the specified object were transformed into images, and three classes were classified based on the object's weight: light, medium, and heavy. When converting EEG signals to images, a separate image was created for each channel (Figure 4.6c), and these channel images were stacked on top of each other to cluster, preserving channel information before being input into the deep learning algorithm. The clustered image is shown in Figure 4.6d. The GoogLeNet neural network, a pre-trained neural network, was used for model training, and hence, input dimensions were fixed at 224x224x3. To avoid overfitting due to an excess of deep learning parameters, a dropout was recommended [156] and applied in this study. The dropout layer sets input elements to zero randomly with a probability of 0.6. Training a neural network is an iterative process involving minimizing a loss function. A gradient descent algorithm was employed to minimize the loss function. In each iteration, the gradient of the loss function was evaluated, and the descent algorithm updated the weights.

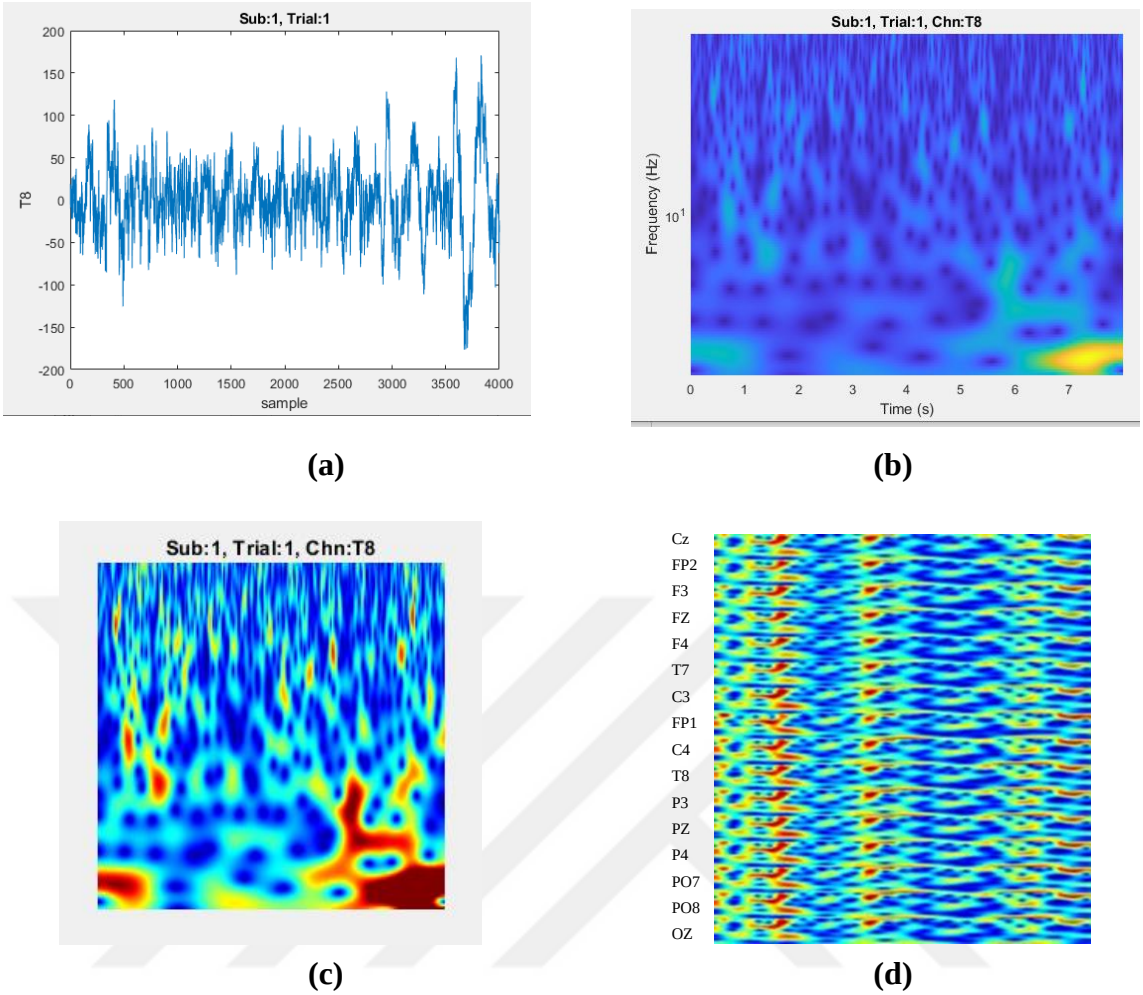

Figure 4.6 a) EEG signal in the time domain, b) time-frequency representation of the signal (spectrogram), c) RGB image of the spectrogram, d) clustered 16-channel EEG spectrogram image (sub: participant, trial: trial number, chn: EEG channel)

Continuous Convolutional Neural Network with 3D Input (CCNN)

Yang et al., used a continuous convolutional neural network (CCNN) to recognize emotions with a 3D EEG signal as input [271]. The 3D input integrates multiple frequency bands while preserving spatial information between electrodes. In this method, signals from the imagination phase of carrying the specified object were used. Additionally, signals filtered with bandpass filters (with lower bands) were used to obtain EEG waves: 2-4 Hz (delta), 4-8 Hz (theta), 8-12 Hz (alpha), and 12-30 Hz (beta). Furthermore, an equivalent matrix was created using the EEG electrode map to form a two-dimensional plane. The EEG electrode map and the equivalent matrix are shown in Figure 4.7.

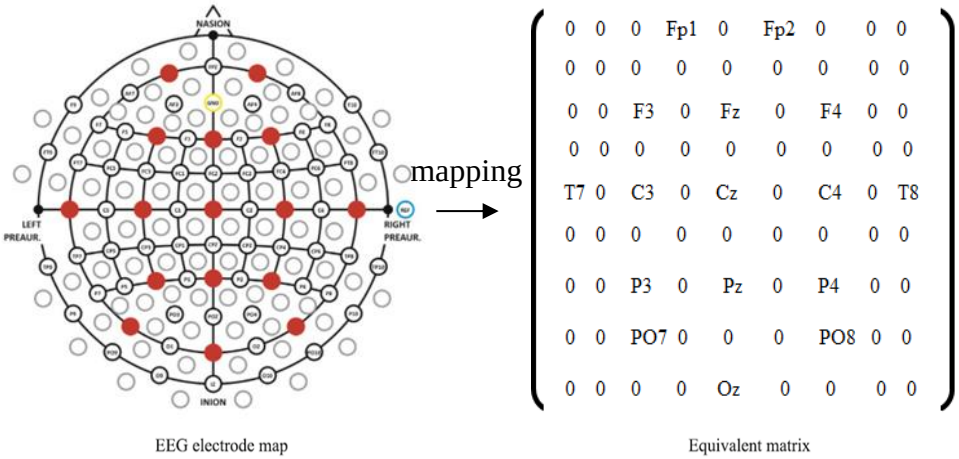

Figure 4.7 Creating an equivalent two-dimensional matrix using EEG electrode mapping [271].

During the mapping process, the energy of the channels was computed, and these energy feature values were utilized within the 3D matrix. The steps of creating the 2D matrix and the 3D cube are discussed in Figure 4.8.

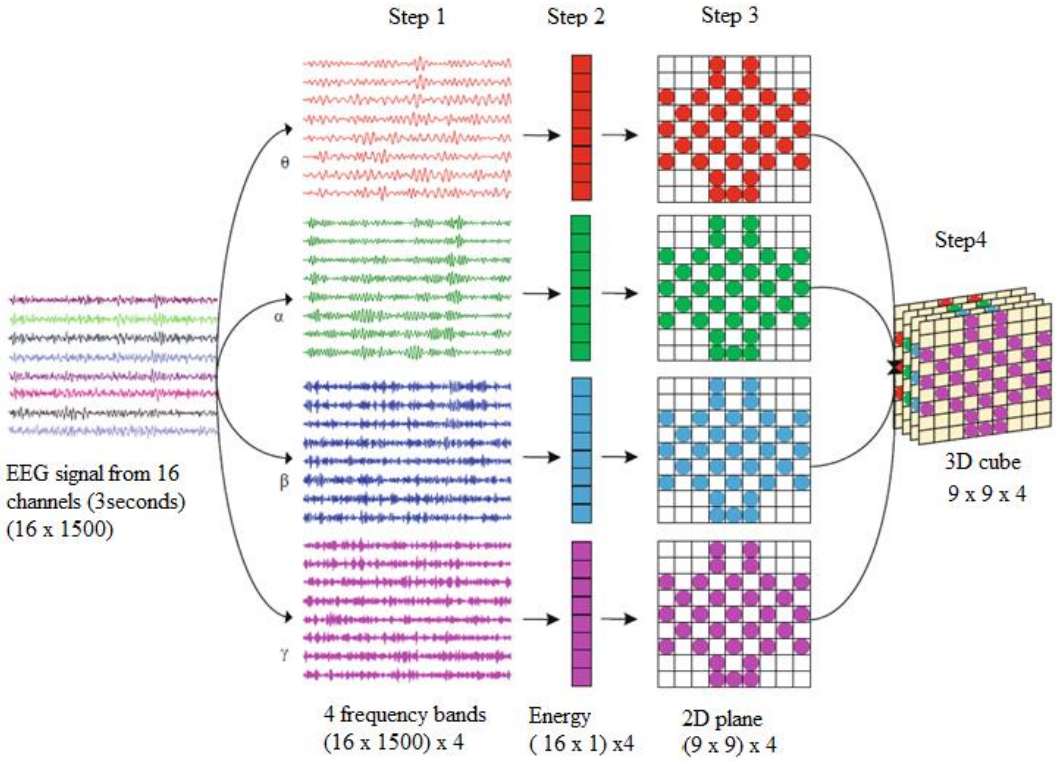

Figure 4.8 Creating the stages of a 3D cube [271].

Yang et al., suggested that the 3D cube generated by this method can be considered as an image [271]. Therefore, this cube has been used as an input to the CNN. Four convolutional layers were used to construct the CCNN architecture. While the filter sizes of the first three layers are 4x4, the filter size of the last convolutional layer is selected as 1x1 for computational simplicity. The values of the feature maps for these four layers are 64, 128, 256, and 64, respectively. Following the convolutional layer, a rectified linear unit layer (ReLU) was added for the activation process. A fully connected layer (FC) with a dropout was used to transform the image's pattern-related features into a one-dimensional feature vector. Finally, a softmax layer was used as the classification layer to compute the probability distribution of the classes. The reason for naming this architecture as CCNN is the absence of a pooling layer between the two convolutional layers, providing dimension reduction. Due to the spatial features containing channel information of the 3D cube, a pooling layer was not used. Figure 4.9 represents the CCNN architecture.

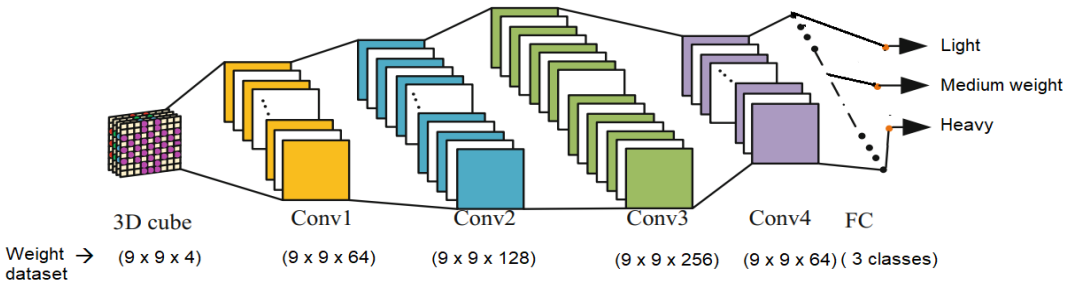

Figure 4.9 Continuous convolutional neural network (CCNN) architecture [271].

4.2.8 Classification

The aim was to predict weight perception from EEG. Thus, we used two sessions paradigm which allows decoding weight perception from both actual movement and imagery sessions.

First, we used only imagination phase signals of imagery session for the interested signal area. For the binary class classification problem, each subject has 20 trials. After calculating the features such as S-T-F-TF, FSST-SVD, we created the test dataset from four trials of one subject by dividing the trails into five folds whereas the remaining 16 trials of the subject and 600 trials recorded from the other 30 subjects were employed for

the training dataset. By taking the average accuracy of all folds, we computed the classification performance for the subject. This technique was applied to all subjects using the subject-based "leave-one-subject-out" approach.

On the other hand, we proposed a new method that originally constructs the training dataset and test dataset of each subject to investigate the effect of the actual movement on the evaluation of the classification performance in the weight perception problem. For this purpose, the trials from the imagination phase of the imagery session of one subject were divided into five-folds and one-fold was used for the test dataset. The remaining four folds (16 trials) of the subject and the 20 trials from lifting phases of the actual movement session of the subject were used in the training dataset. This procedure was repeated for each subject. The proposed methodology is illustrated in Figure 4.10.

MATLAB (2019a) was used for classification. We investigated k-nearest neighbors (k-NN, k=10, distance metric was Euclidean), linear discriminant analysis (LDA), fine tree (maximum number of splits = 100, split criterion was based on Gini's diversity index), Naive Bayes (kernel type was Gaussian), and the support vector machines (SVM) with fine Gaussian kernel and quadratic kernel [230].

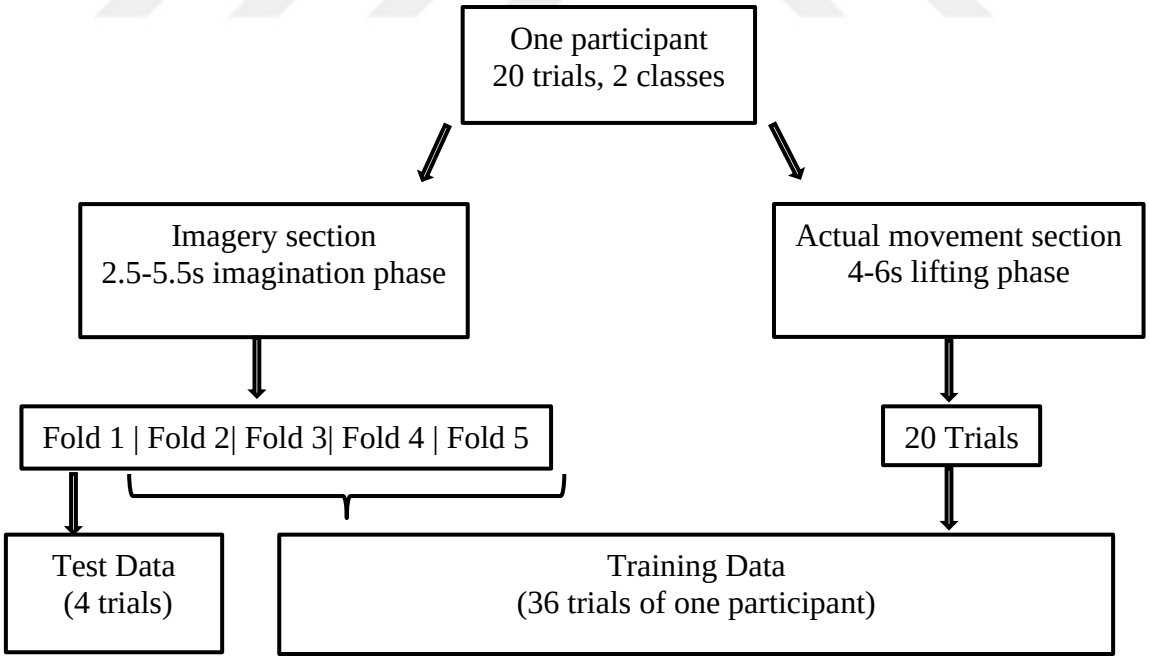

Figure 4.10 The procedure of the proposed methodology.

4.2.9 Real-time Processing of EEG Signals

A model design was created using the MATLAB/SIMULINK program with the aim of obtaining and extracting features from EEG signals in real-time. Real-time EEG data, obtained using 1-second samples, were stacked, and feature extraction processes were applied to these samples. FSST approach, a time-frequency domain analysis method, was employed to obtain the feature matrix. FSST facilitates a clearer representation in the time-frequency axis by separating components of linear and non-stationary signals.

In this study, FSST was applied to each channel, and coefficients for the time-frequency space were obtained as complex numbers. For coefficient calculations, a Kaiser window of length 256 was used to ensure sufficient frequency resolution, resulting in a matrix of size 65x500 for each channel. The frequency range of interest is 8-30 Hz, and accordingly, 11 frequencies of interest were determined for each channel, resulting in an 11x500 matrix for each channel. The absolute values of the coefficients obtained from each channel were calculated, standardized by subtracting the mean and dividing by the standard deviation (z-score). The SVD algorithm was used for dimensionality reduction and to extract significant features from the FSST coefficients. Consequently, diagonal values were considered as features with a matrix size of 16x11 for 16 channels in one trial.

The calculated features were classified using SVM. There are two classes: heavy and medium-heavy. The light class was used to indicate the prosthetic hand in the default (zero) position. The classification was applied to the grasping phase. The block produces a "2" value for other phases, which was randomly selected and used for signals not in the area of interest. Signals in the area of interest (grasping phase) were classified to produce output as 0 or 1. The outputs from the classification block were sent as commands to Arduino; if the output is 0 or 1, it is sent as a command, and if the output is 2, it is only displayed on the screen. This way, only the classification output from the area of interest is sent as input to Arduino.

Commands from the decision-making block are sent to Arduino. Arduino is connected to the computer via USB for serial communication. The generated commands are sent to digital pin 13 of Arduino, and the required input data for the motor is read from this pin.

In this context, a new model supporting the mentioned algorithm was created when constructing the SIMULINK model. The blocks used in SIMULINK are shown in Table 4.3, and their names and functions are detailed Figure 4. 11.

Table 4.3 Blocks used in modeling and their functions

	Block name	**Function**
1.	g.Nautilus	Transfers real-time EEG signals to Matlab/SIMULINK.
2.	Preprocessing block	Suppresses powerline noise in signals.
3.	Subsystem	Subsystem is a sub-model in which features are calculated from 1-second signals using FSST and SVD methods.
4.	Classification	The signals coming from the holding phase are classified to produce 0 or 1 output.
5.	Decision Making	Classification output is sent to Arduino as input.
6.	Arduino IO support blocks	Incoming commands are detected and sent to Arduino.
7.	To workspace	Saves raw EEG signals, extracted features and predicted labels to MATLAB workspace.
8.	Paradigm	This block is where we set the duration of the simulation and the visuals in the experiment setup. The experimental setup is integrated into this block in accordance with the S-function standards.

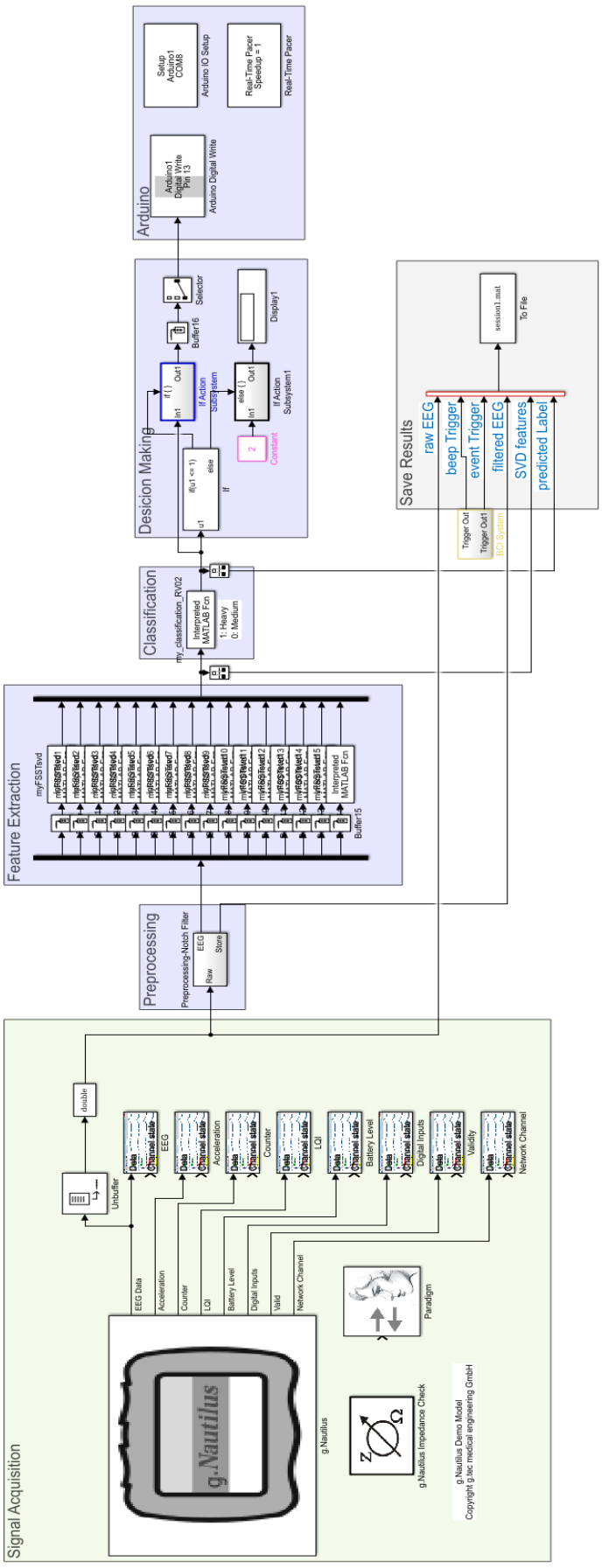

Figure 4. 11 Real-time signal processing model built using SIMULINK

4.3 Results

Research has been conducted at various stages and with different approaches to detect visual weight perception from EEG signals discriminating the tasks listed in Table 4.4 for different classes. The fundamental approach involved extracting features using S-T-F-TF and FSST-SVD feature extraction and selection methods, followed by a classification process. Accuracy, AUC, and p-values for these classification problems are presented in Table 4.5. In the studies encompassing all classification possibilities, the highest accuracy values were achieved using the kNN classification method with S-T-F-TF features, particularly during the differentiation of imagining light and heavy objects and imagining light and medium-weight objects. The accuracy level is in the range of 62-62.5%. Generally, low achievements have been observed in this part of the thesis.

Table 4.4 Tasks to be classified.

Classification Classes	Experiment
2 classes	Resting - weight imagination
2 classes	Binary combination of the weights (light- medium weight), (light-heavy), …
3 classes	Light, medium weight, heavy object
4 classes	Resting, light, medium weight, heavy object

In addition to these methods, deep learning results containing a weight dataset for classifying object weights are presented in Table 4.6. Here, a multi-class classification problem has been applied. Scalogram images and 3D cube images were provided as inputs to the deep learning algorithm. According to the results, when the scalogram image is considered as input separately for each channel (RGB image), it achieved the highest accuracy of 63.54%.

The classification results of features obtained from relative band power are presented in Table 4.7. According to this feature, the highest classification performance was achieved in the classification of light and medium-heavy objects with an accuracy rate of 52%. These accuracy rates were even higher than random selection (50% for binary, 33.3% for ternary).

Table 4.5 Classification accuracy, AUC and p-values obtained with the S-T-F-TF and FSST-SVD features used in the study.

Classification Problem	Features	p-value	Classifier	Accuracy (%)	AUC
Imagination of Light, Heavy object (2 classes)	S-T-F-TF	> 0,05	KNN	**62,1**	**0.61**
	FSST-SVD	> 0.05	KNN	54.3	0.55
Imagination of light, medium-weight object (2 classes)	S-T-F-TF	> 0.05	KNN	**62.4**	**0.62**
	FSST-SVD	> 0.05	Decision tree	54.7	0.52
Imagination of medium-weight, heavy object (2 classes)	S-T-F-TF	> 0.05	KNN	55.5	0.57
	FSST-SVD	> 0.05	KNN	55.5	0.57
Rest- Weight imagination (2 classes)	S-T-F-TF	< 0.05[1]	KNN	57.9	0.6
	FSST-SVD	> 0.05	Decision tree	53.2	0.54
Imagination of Heavy, Light, Medium-weight object (3 classes)	S-T-F-TF	< 0.05[2]	Decision tree	42.4	0.54
	FSST-SVD	> 0.05	KNN	39.0	0.54
Rest, Imagination of Heavy, Light, Medium-weight object (4 classes)	S-T-F-TF	< 0.05[3]	KNN	50.0	0.48
	FSST-SVD	< 0.05[4]	Naive Bayes	22.0	0.44

Table 4.6 Accuracy according to different input shapes for CNN.

Classification Problem	Input	Network	Accuracy (%)
*Imagination of **Heavy, Light, Medium-weight object** **(3 classes)***	Stacked EEG	GoogLeNet	33.15
	RGB image	GoogLeNet	63.54
	3D cube	CCNN	43.08

Table 4.7 Mean accuracy of 30 subjects' relative power features for subbands.

Classes/Subbands	RDelta	RTheta	RAlpha	RBeta	RGamma
Multiclass	34%	34%	**35%**	32%	34%
Light vs Heavy	49%	47%	49%	**50%**	49%
Light vs Medium weight	**52%**	48%b	51%	47%	50%
Medium weight vs Heavy	49%	48%	**51%**	49%	48%

The second-order statistical features calculated from the matrix obtained through the GLCM method were classified using the kNN classifier, and the results are presented in Table 4.8. When objects of light and medium weight were classified, the highest accuracy of 53.1% was achieved. The results are comparable to the outcomes of relative

[1] Except for the skewness method, other methods have statistically significant for both classes.
[2] The average rank in the imagination of light and medium-weight objects showed statistical differences for PSD, alpha band power, beta frequency band power, energy and the logarithmic Energy Entropy, whereas imagination of light and heavy objects have statistically significance for DWT and skewness.
[3] The resting group has statistically significant difference from the other groups.
[4] The resting group has statistically significant difference from the other groups.

band power. In the imagination section, when only signals from the imagination phase were utilized, it was observed that the classification performance remained at a low level. To overcome the challenges of low accuracy levels, the utilization of actual movement data in the training set proves to be a valuable advantage compared to relying solely on the imagination section.

Table 4.8 Accuracy of classification of second-order statistical features

Classes/Features	**FSST + GLCM**
Multiclass	36.7%
Light vs Heavy	50.9%
Light vs Medium weight	53.1%
Medium weight vs Heavy	52.7%

In Table 4.9 the results when we only used signals from the imagination phase of the imagery session are reported. The classification performance was assessed using six different machine learning algorithms: SVM with Gaussian kernel, SVM with quadratic kernel, KNN, LDA, Fine Tree, and Naive Bayes. Accuracy and f-measure values were calculated as performance metrics. The features utilized, FSST-SVD and S-T-F-TF, were presented for comparison. Three binary classification scenarios were considered: light vs heavy, light vs medium, and heavy vs medium.

Table 4.9 Classification performance of the imagery session.

Classes	**Features**	**Evaluation Metrics**	**Classifier**					
			SVMG	SVMQ	KNN	LDA	FineT	NaïveB
Light-Heavy	FSST-SVD	ACC (%)	**50**	40	50	35	50	45
		f-measure	**0.60**	0.45	0.55	0.38	0.54	0.48
	S-T-F-TF	ACC (%)	35	**50**	40	40	45	45
		f-measure	0.29	**0.66**	0.50	0.44	0.44	0.0
Light-Medium	FSST-SVD	ACC (%)	45	30	55	30	**70**	50
		f-measure	0.28	0.2	0.59	0.26	**0.62**	0.63
	S-T-F-TF	ACC (%)	50	30	45	**50**	40	55
		f-measure	0.1	0.53	0.57	**0.26**	0.2	0.0
Heavy-Medium	FSST-SVD	ACC (%)	55	35	45	40	**60**	45
		f-measure	0.26	0.13	0.44	0.29	**0.49**	0.44
	S-T-F-TF	ACC (%)	**50**	50	45	45	45	45
		f-maksure	**0.1**	0.0	0.24	0.23	0.21	0.61

According to feature comparison, the highest accuracy, reaching 70%, was achieved in distinguishing the Light-medium class using features obtained with FSST-SVD. In the classification comparison, the Fine Tree classifier yielded the highest accuracy, particularly in distinguishing between light and medium, as well as heavy and medium. However, the binary classification for light vs heavy did not surpass the chance level (0.5).

From the results, we can clearly observe that the classification performance remains low. To overcome this problem, using the actual movement session in training data has a valuable advantage in comparison with using only the signals corresponding to imagination of lifting the object. As demonstrated in Table 4.10, we got the highest accuracy with the level of 80% using FSST-SVD as a feature and SVM quadratic as a classifier to discriminate medium weight and heavy objects. The proposed method has been observed to achieve a 20% increase in accuracy in distinguishing between the light-heavy classes and separating the heavy-medium classes.

Table 4.10 Classification performance of the proposed method (imagery session + actual movement session).

Classes	**Features**	Evaluation Metrics	Classifier					
			SVMG	SVMQ	KNN	LDA	FineT	NaïveB
Light-Heavy	FSST-SVD	ACC (%)	55	55	45	52	**70**	50
		f-measure	0.64	0.45	0.5	0.46	**0.68**	0.66
	S-T-F-TF	ACC (%)	55	**65**	50	60	50	45
		f-measure	0.66	**0.46**	0.61	0.52	0.47	0.58
Light-Medium	FSST-SVD	ACC (%)	50	45	50	**55**	50	40
		f-measure	0.51	0.44	0.57	**0.53**	0.6	0.08
	S-T-F-TF	ACC (%)	50	30	45	50	40	55
		f-measure	0.46	0.24	0.54	0.36	0.42	0.23
Heavy-Medium	FSST-SVD	ACC (%)	65	**80**	50	60	65	50
		f-measure	0.52	**0.82**	0.49	0.54	0.58	0.1
	S-T-F-TF	ACC (%)	45	60	55	60	60	55
		f-measure	0.23	0.58	0.42	0.55	0.56	0.23

Findings on Real-time Tests

In the current state, the most efficient results have been obtained from offline studies, particularly with the novel method we propose. Therefore, a similar approach to this method has been employed in real-time studies, where training data were generated using pre-recorded data. Accordingly, an offline training dataset was created, taking into account the data from 31 individuals during the holding and imagining phases of movement, considering grasping the object and imagining the weight of the object. This offline training dataset was then tested on participants. Real-time signal processing was performed in segments of 500 samples (1 second), and the classification experiment setup was applied only to the 3-second signals obtained from the specified phase of lifting the object. Therefore, the classification result is generated three times based on the participants' performance during the experiment. However, only the third decision output is sent to the prosthesis motor. This output is visually presented in Figure 4.12. As there were 5 trials in one session, the classification was performed 5 times. The labels 0 and 1 on the y-axis represent the classified weight, while label 2 is used for phases other than the object-holding phase in the experiment, as there is no signal of interest for our classifier in those phases.

As seen in the Figure 4.12 our classifier model predicted correctly for each trial. However, since the third decision was used as a command to the motor, trial 3 and trial 4

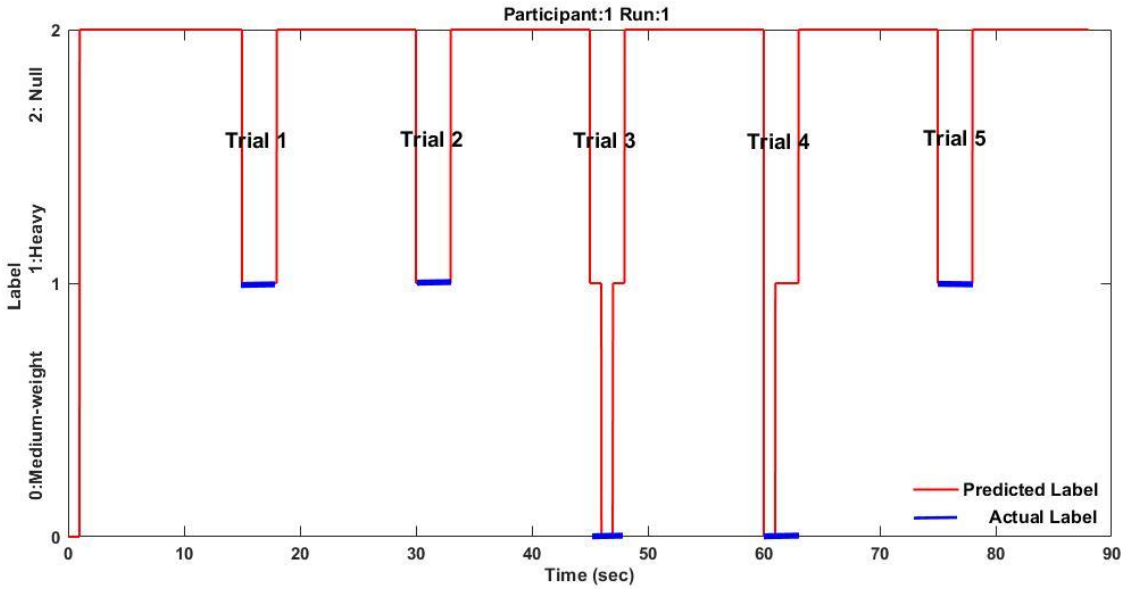

Figure 4.12 Label values predicted by the classifier recorded from participant 001's online trials

were evaluated as incorrectly classified. For this reason, the accuracy value was noted as 60%.

The classification results of these tests with 20 healthy individuals are summarized in Table 4.11. According to the results obtained, the average accuracy for all participants is 48.83%. There are instances where the classifier made correct classifications in at least one of the three decisions it produced (This situation is explained in Figure 4.12). However, since only the third decision is transmitted to the prosthetic hand's motor, the classification accuracies are calculated based on the third decision.

Table 4.11 Real-time session accuracy results

Participants	**Accuracy (%)**		
	Decision produced in 1 second	**Decision produced in 3 seconds**	**Most produced decision**
001	**80**	46.67	53.33
002	46.67	40.00	46.67
003	40	40.00	40
004	46.67	46.67	46.67
005	50	60.00	60
006	46.67	53.33	46.67
007	50	50.00	50
008	46.67	46.67	46.67
009	60	46.67	53.33
010	60	**66.67**	**73.33**
011	50	60.00	50
012	46.67	46.67	46.67
013	40	46.67	46.67
014	40	53.33	40
015	53.33	40.00	40
016	46.67	40.00	43.33
017	46.67	46.67	46.67
018	26.67	53.33	26.67
019	46.67	46.67	40
020	46.67	46.67	46.67
Average	48.50	**48.83**	47.17

4.4 Discussion and Conclusions

In this research, we introduce the use of FSST (Fourier-based Spatio-Temporal), statistical, time, frequency, and time-frequency domain features (S-T-F-TF), relative band power features, and second-order statistical features from GLCM. The purpose is to discriminate and classify the weight categories (light, heavy, medium weight) of objects to be manipulated, utilizing EEG signals. Our study is designed to discern and characterize different weights through the subject-specific imagination phase during testing, and a combination of imagination and actual movement sessions during the training of multichannel Electroencephalogram (EEG) signals to precondition muscles. Accurately estimating the weight of the object to be manipulated is crucial for pre-adjusting the prosthesis's torque prior to movement.

The experiments were conducted in two sessions: actual movement and imagery movement. The actual movement session comprised five phases: resting, holding, lifting-up, putting-down, and relaxation. The imagery movement session involved subjects performing mental imagery tasks of lifting up and putting down bottles. In this session, trials consisted of four phases: resting, visual cue, imagination, and relaxation. Each subject performed 30 imagination trials (10 for each bottle). In total, there were 924 trials for the actual movement session and 924 trials for the motor imagery session. EEG recording was conducted using 16 channels.

Our proposed method incorporates subject-specific, intertrial classification. Initially, the method constructs distinct training and test datasets for each subject to systematically investigate the impact of actual movements on evaluating the classification performance within the context of weight perception. To achieve this, the trials from the imagination phase of the imagery session for a given subject were partitioned into five-folds, with one-fold designated as the test dataset. The remaining four folds, comprising 16 trials from the subject's imagination phase and 20 trials from the lifting phases of the actual movement session, constituted the training dataset. This procedure was iteratively performed for each subject, allowing for a comprehensive examination of the method's performance across different subjects.

This study concentrated on forecasting the weights of objects categorized as light, heavy, and medium weight through the analysis of EEG signals. The results indicate that

the FSST-SVD features representing medium and heavy objects exhibited the most distinctive characteristics when compared to the other pairwise groups.

Chapter 5

Surface Electromyography Based Weight Perception During Holding Phase for Torque Control of Upper Limb Prosthesis

This chapter focuses on using the one-second holding phase signal to differentiate between light, medium, and heavy weights for torque control in an EMG-based upper limb prosthesis. Time-domain features are employed to dynamically adjust the wrist component's stiffness during this phase, emphasizing the importance of perceiving the object's weight for controlling muscle contraction intensity. The research aims to enhance upper-limb prostheses' functionality and user-friendliness, granting users more natural and intuitive control over their interactions with the environment. The study used 32 time-domain methods to extract features from one-second EMG signals. In addition to the features, empirical mode decomposition (EMD) was evaluated. Feature selection employed the analysis of variance (ANOVA) test. For binary classification, logistic regression, K-nearest neighbors (KNN), support vector machines (SVM), and XGBoost were employed with leave-one-subject-out cross-validation approach. The methodology introduced in this study has shown an impressive classification accuracy when distinguishing between light and heavy objects. Specifically, it achieved a high accuracy of 78.5% using time-domain features directly derived from EMG signals, whereas using features extracted from IMF1 (68.8%) and IMF2 (67.6%) obtained through EMD resulted in slightly lower accuracy levels. This research promises to significantly improve upper-limb prostheses, enhancing user experience and control.

5.1 Introduction

Surface electromyography (sEMG) is a non-invasive method used to capture myoelectric signals. It involves placing electrodes on the skin's surface, allowing for the measurement of neural activity in muscles without the need for surgical procedures. This

approach enhances our comprehension of muscle activity and neuromuscular control. sEMG is a safe, user-friendly, and painless technique that provides valuable information for various applications, including prosthetic system design [272]. The potential uses of sEMG encompass a wide range of applications, such as electric wheelchairs, the control of upper limb robotic arms, with a particular focus on neural prostheses [273].

Reaching and grasping, which are typical activities for human control, are widely encountered in our daily lives and function as interfaces for controlling robotic systems [133]. Ozdemir et al., proposed an approach for classifying seven different hand gestures using deep learning with spectrogram images of sEMG signals and achieved a test accuracy of 99.59% [274]. Sharmina and Raghunadhan focused on the classification of hand movements with entropy features and found that combining them with other features improved classification accuracy [275]. Overall, these papers demonstrate the potential of sEMG measurements for accurately identifying hand movements using various machine learning techniques.

Additionally, to investigate the application of sEMG for object weight classification, Maoz and Lashgari developed an automated pipeline that utilized EMG data for predicting object weight during a reach-grasp-lift task [276]. They achieved a high classification accuracy by employing dimensionality reduction and classification algorithms. Similarly, Aziz et al., employed EMG signals for weight-lifting tasks, achieving high classification accuracy through denoising and feature analysis [277]. On the other hand, Liang focused on object detection rather than classification, proposing novel methodologies to improve the accuracy and performance of object detection models using EMG data [278]. These papers collectively demonstrate the potential of EMG for object weight classification and detection tasks.

Moreover, as signal processing and machine learning techniques have progressed, a range of novel approaches has emerged for classifying sEMG signals. EMG signal processing techniques consist of three main steps: preprocessing, feature extraction, and classification. Filtering is a commonly used preprocessing method [279]. There is a wealth of information and methods in the literature related to feature extraction and classification. Phinyomark et al., highlighted challenges of feature selection in biological signal pattern recognition, present a novel approach using topological tools to address these challenges, and demonstrate its effectiveness through a case study with EMG

datasets. The approach helps identify meaningful feature groups that can be applied across different datasets for classification and analysis purposes [280]. Too J. et al., focused on the extraction of electromyography (EMG) features to improve the accuracy of classifying hand movements. Two novel EMG features, namely, enhanced wavelength (EWL) and enhanced mean absolute value (EMAV), were introduced. These features were modifications of the existing wavelength (WL) and mean absolute value (MAV) measures. The goal was to enhance the prediction accuracy for the classification of hand movements [133]. Furthermore, Samuel et al., introduced a set of new, straightforward yet highly effective time-domain features. These features involve calculating the absolute value of the mean value of the square root (MSR) and the absolute value of the summation of the square root (ASS) of the data within a defined set of analysis windows [281]. Hudgins et al., emphasized the idea of employing four distinct time-domain characteristics to decode the intention behind limb movements [282]. These features are the most widely used feature sets consist of mean absolute value, waveform length, zero crossings, and slope sign changes [283]. Additionally, in the study by Karabulut et al., the main objective was to conduct a comparative evaluation of commonly used time-domain features of EMG signals, specifically integrated EMG (IEMG), root mean square (RMS), and waveform length (WL), in the estimation of external forces applied to human hands [284]. After extracting these features, a classification process was implemented using artificial neural networks (ANN) to predict the external forces.

On the other hand, empirical mode decomposition (EMD) is an effective technique for processing EMG signals. Andrade et al., compared EMD with wavelet transform for EMG signal filtering and found that EMD successfully attenuates background activity in EMG signals [285]. Moreover, Zhang and Zhou explored the use of ensemble EMD (EEMD) for denoising surface EMG signals and demonstrated that EMD-based methods outperform traditional digital filters, especially in low signal-to-noise ratio conditions [286]. Srivastava et al., focused on the suppression of additive white Gaussian noise (AWGN) in EMG signals using EEMD and morphological filtering, reporting improved results compared to conventional EMD and EEMD approaches [287]. Overall, these papers highlight the effectiveness of EMD and its variants for processing EMG signals and reducing noise interference.

While there have been numerous studies on EMG signal processing and EMG-controlled upper limb prostheses in existing literature, there has not been sufficient

exploration of weight perception algorithms that are compatible with EMG signals. This study aims to fill this gap by focusing on the use of the holding phase (a one-second signal) to differentiate between light, heavy, and medium weights. These distinctions will be utilized in the torque control of an EMG-based upper limb prosthesis, employing time-domain features [133], [288], [289]. In this study we hypothesize that utilizing signals from holding/grasping phase (before actual lifting starts) to control the adjustment of the stiffness of the wrist component of the prosthesis, which constitutes the primary focus of this study. This hypothesis stems from the observation that lightly feeling the object's weight is essential in adjusting the intensity of muscle contraction while lifting the object. This research has the potential to improve the functionality and user-friendliness of upper-limb prostheses, granting individuals more natural and intuitive control over their interactions with their surroundings.

5.2 Materials and Methods

5.2.1 Experimental Setup and Dataset

In this work, 30 healthy volunteers have enrolled (mean age: 22 years, age range: 19–35). Subjects sat in a chair approximately 1 meter away from the computer screen and performed an actual movement session in a sequence with 30 repetitions. Trials consisted of five phases: the rest phase, holding phase, lifting phase, replacement phase and relaxation phase. In the rest phase, a red circle was presented in the middle of the plus sign for 2.5 s. The subjects fixed their eyes on the circle. In the holding phase, three visual cues representing one of the three objects with different weights were presented for 0.5 s to aid the subjects in holding for the grasping the weight for 1 s. Then, in the lifting phase, the up-arrow icon was presented for 2 s to lead the subjects in lifting the object up. In the replacement phase, the subjects replaced the object to its initial position after the appearance of the down-arrow icon. In the relaxation phase, the subjects relaxed and prepared mentally for the next trial. Each of the three weights was performed 10 times. The experimental paradigm is shown in Figure 5.1.

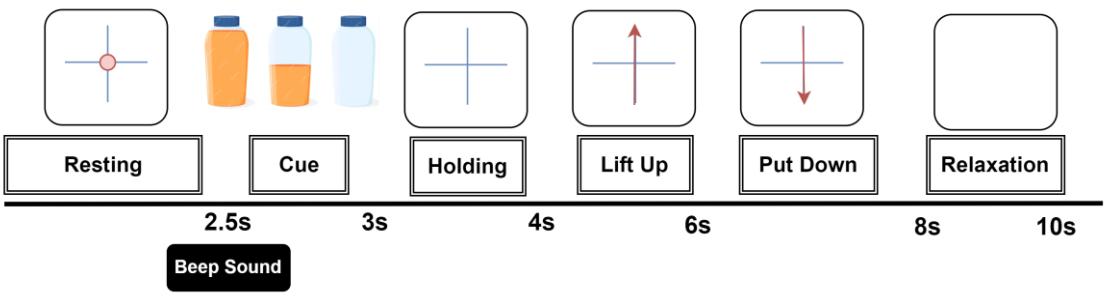

Figure 5.1 The experimental paradigm.

In the actual movement session, subjects were asked to carry out the requested task immediately after the execution cue appeared. Each of the three different weights of the objects in any given epoch was randomly selected. All the subjects were healthy with no history of neurological disease and were instructed to remain relaxed during the recordings. Except for eye blinks, they were asked to avoid eye movements, body adjustments, throat clearing, and other movements. The research was approved by the Erciyes University Ethics Committee (January 9, 2019, 2019/32), Kayseri, Turkey. [259].

In the experiment g.tec (Schiedleberg, Austria) products and PYTHON based software were used. g.USBamp bioamplifier was employed in order to record four channels located at extensor carpi radialis brevis (ECRB), extensor digitorum (ED), extensor carpi ulnaris (ECU), and flexor carpi radialis (FCR). The electrode placement of the four EMG channels on the forearm is illustrated in Figure 5.2. The sampling rate of the signal acquisition system was 512 Hz. In the system, the signals were filtered using a hardware bandpass (2-200 Hz) and a notch (50 Hz) filter.

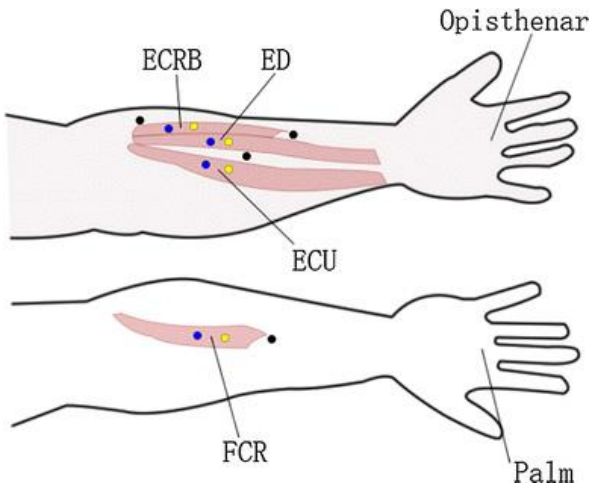

Figure 5.2 EMG electrodes' placement (ECRB: extensor carpi radialis brevis, ED: extensor digitorum, ECU: extensor carpi ulnaris, FCR: flexor carpi radialis) [290].

The data of each subject for one session has a total of 30 trial data, and each trial represents one actual movement task, belongs to one of three weight class: 10 trials light weight (25g empty bottle), 10 trials medium-weight (523g half full bottle of water) and 10 trials heavy weight (1037g full bottle of water). The grand total of trials from all subjects amounted to 900 trials for the actual movement session. The EMG signals corresponding to the 30 repetitive muscle contraction and relaxation durations of participant number 1 and the EMG signals from the 4th trial of the same subject, depicted in phases, were shown in Figure 5.3.

5.2.2 Preprocessing

Python software was used to pre-process the collected data. After the frequency analysis of the collected signals, the observed 150 Hz noise was removed using a notch filter that suppresses this frequency (fo = 150; Q = 35; BW = 2*(fo/(fs/2))/Q). When examining the signals corresponding to the fourth trial (highlighted in the red box in Fig. 3. top panel) in more detail, the time intervals corresponding to the phases of resting (phase 1), reaching for the bottle (phase 2), preparing the muscles to lift the bottle (phase 3), lifting the bottle (phase 4), holding it aloft (phase 5), lowering it (phase 6), and returning the hand to its initial position (phase 7) can be observed in Figure 5.3 bottom panel. It should be noted that, even though instructions were presented to participants with precise timing cues (such as "at this second, perform this action"), there were slight variations in the onset and offset times of these phases from person to person and even from trial to trial. Therefore, the signals of all participants were individually examined, and at least the onset timing of phase 1 was manually determined.

On the other hand, it has been assessed as more suitable to utilize signals from phase 3 (highlighted in green in Figure 5.3 bottom panel) to control the adjustment of the stiffness of the wrist component of the prosthesis, which constitutes the primary focus of this study. The general observation from both participants and the authors is that lightly feeling the object's weight is essential in adjusting the intensity of muscle contraction. In line with this observation, one-second signals were segmented for each participant and each trial and subsequently transferred into a matrix format for all four channels. Thus, feature extraction procedures have been initiated on a matrix comprising a total of 3600 rows (30x30 trials, each with four channels) and 512 columns (one-second signal sampled

at 512 Hz). In Figure 5.4, one-second signals recorded from participants 1 and 11 are displayed for three different weight conditions.

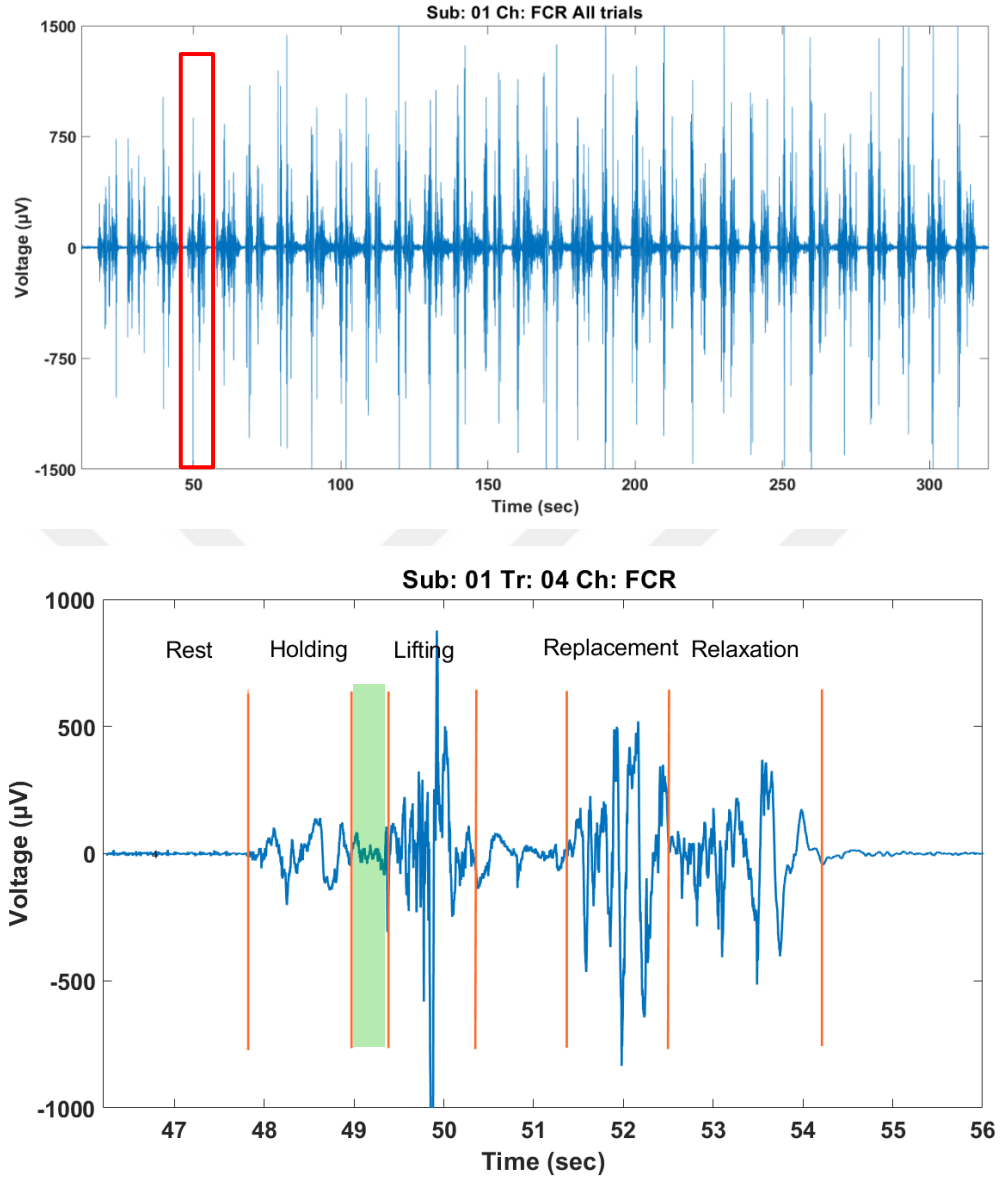

Figure 5.3 The raw EMG signals of subject number 01 that belong to the flexor carpi radialis muscle (Sub: Subject number, Tr: Trial number, Ch: Channel). The 30 repetitive muscle contraction and relaxation durations (top panel). The 4th trial of the same subject in the form of phases (bottom panel).

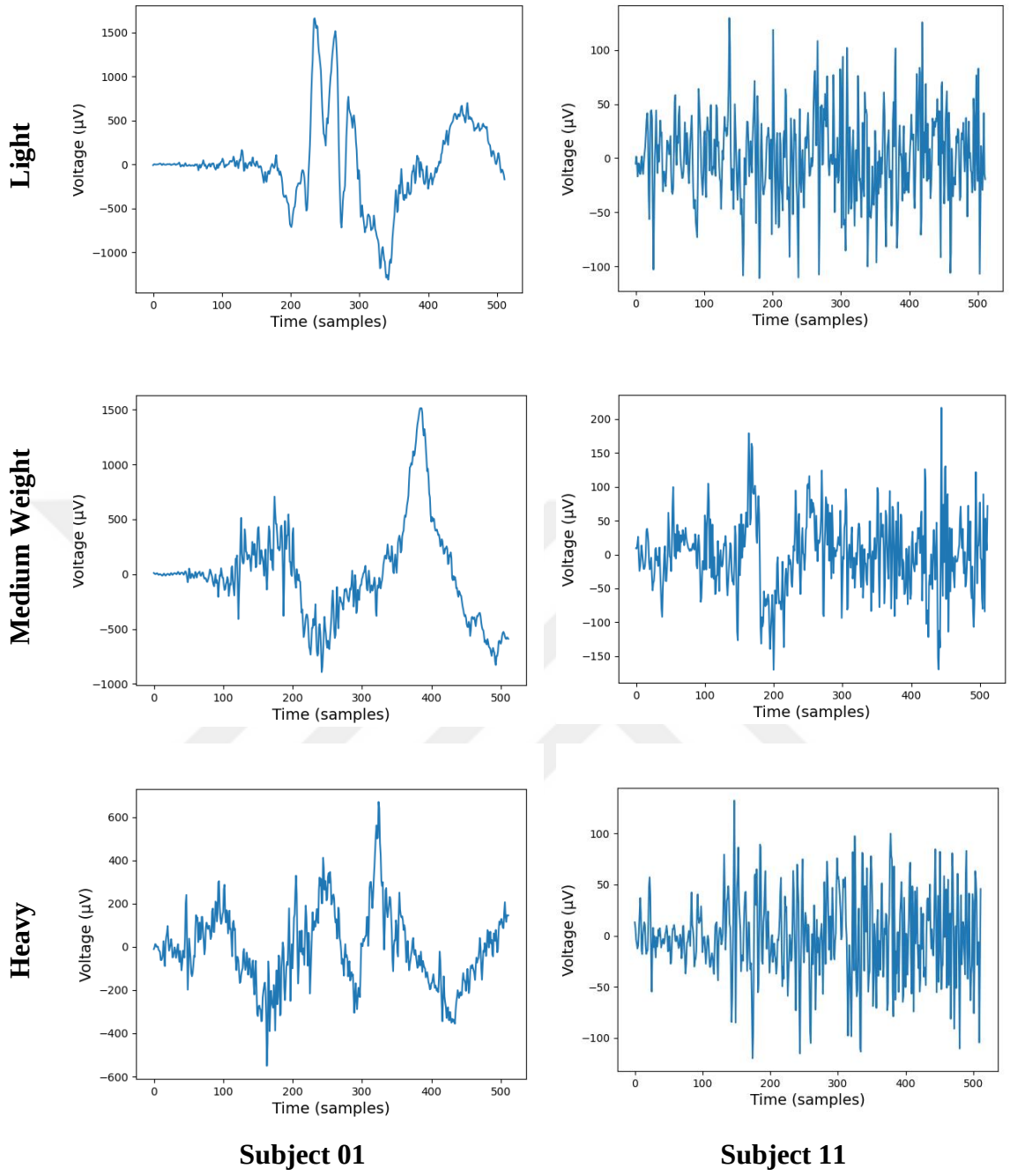

Figure 5.4 A one-second signal with three different weight conditions for Subject 01 and Subject 11.

5.2.3 Feature Extraction / Selection

The aim was to predict weight perception using EMG signals collected from the section that prepares the muscles for lifting the bottle. Therefore, we utilized phase 3 of the paradigm, which enables the decoding of weight perception during the holding of the bottle.

The names of the 32 time-domain methods used to extract features from the one-second EMG signals extracted from each trial are listed in Table 5.1. Technical/methodological details about these methods are widely available in the literature [279], [280], [291], [292], [293].

Table 5.1 Features for a single time window.

1	Maximum Fractal Length
2	Log Detector
3	Zeros Crossing
4	Interquartile Range
5	Difference Variance Value
6	Log Teager Kaiser Energy Operator
7	Enhanced Mean Absolute Value
8	Difference Absolute Standard Deviation Value
9	Slope Sign Change
10	Standard Deviation
11	Mean Absolute Deviation
12	Log Difference Absolute Mean Value
13	Mean Value of Square Root
14	Energy of Autoregressive Coefficient
15	Modified Mean Absolute Value
16	Waveform Length
17	Average Amplitude Change
18	Mean Absolute Value
19	Coefficient of Variation
20	Difference Absolute Mean Value
21	Log Difference Absolute Standard Deviation Value
22	Absolute Value of Summation of Square Root
23	Modified Mean Absolute Value 2
24	Root Mean Square
25	Integrated EMG
26	Kurtosis
27	Temporal Moment (Order = 3)
28	Cardinality (Threshold = 0.01)
29	Absolute Value of Summation of *exp* Root
30	V-Order (Order = 2)
31	Log Coefficient of Variation
32	Enhanced Wavelength

As a result of using the methods listed in Table 5.1, a feature matrix was created by combining the 32 features extracted for each trial. The matrix was reshaped as 900 × 128 (32 features, each with four channels) in size. Each attribute was normalized to each participant. Instead of global normalization, participant-based normalization was performed. During normalization, the minimum value was set to zero, the maximum value was equal to one, and the values were adjusted to increase linearly. The last column of this matrix was added as the label for each trial: light (1), heavy (2), and medium-heavy (3).

In scikit-learn library, analysis of variance (ANOVA) test was used for the feature selection. Thus, a structure that combines attributes and labels and allows the use of various machine-learning methods was obtained. Additionally, for a single channel, matrices consisting of features were prepared for the channel selection.

In addition to the features indicated in Table 5.1, empirical mode decomposition (EMD) was evaluated in this study. EMD is a signal processing technique used to analyze and decompose nonstationary time-series data. Huang et al., introduced this method in the late 1990s to adaptively decompose signals into a set of intrinsic mode functions (IMFs) [294].

The basic idea behind EMD is to decompose a signal into components with well-defined instantaneous frequencies. Unlike the traditional Fourier-based methods, EMD does not assume that the signal is composed of a fixed set of sinusoidal components with constant frequencies. Instead, it aims to extract components directly from the data by identifying and separating oscillatory modes. This decomposition can help extract useful information from EMG signals [295], [296], [297]. The obtained intrinsic mode functions (IMFs) from Channel FCR for one second of the first trial of participant number 01 can be seen in Figure 5.5. After extracting the IMFs using the EMD method, the feature extraction methods listed in Table 5.1 were applied to IMF1 and IMF2, resulting in a new feature matrix.

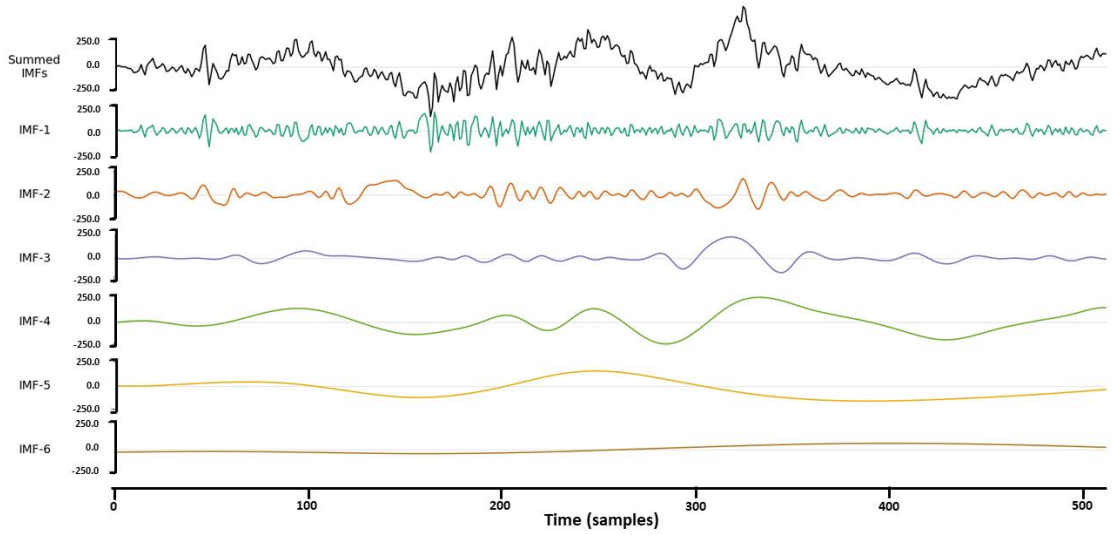

Figure 5.5 The obtained IMFs from Channel FCR for the one second of the first trial of participant number 01.

5.2.4 Classification

The classification performances of different machine learning approaches were analyzed using features obtained from EMG signals. Tests were conducted using logistic regression, K-nearest neighbors (KNN), support vector machines (SVM), and XGBoost for binary classification. Observations were made to determine which method yielded higher accuracy compared to the others. Subsequently, it was observed that all approaches produced similar results, but logistic regression yielded approximately 1-2% higher classification accuracy compared to the others. Therefore, it was decided to report the results of this method in the interest of simplicity, as it provided consistency across numerous trials with varying feature sets and classification types. At this point, it should be noted that in this part of the study, an approach was demonstrated where all channels and all features were examined for binary classification. Additionally, an approach was presented where individual channels were considered, and analyses were conducted using reduced or selected features.

Leave-one-subject-out cross-validation (LOSOCV) classification was used in machine learning studies. Additionally, the classification was repeated three times, and the average accuracy values were included in the tables. The aim of this study was to understand which channel or channels, and how many features, resulted in higher

accuracy in binary classification. Similar classification experiments were repeated with the selected features as well.

5.3 Results

The performance of machine learning approaches was examined on the 32 features listed in Table 5.1 Features for a single time window.. Additionally, for binary comparisons (1 vs. 2, 1 vs. 3, and 2 vs. 3) made from these features, the ANOVA feature selection and reduction method were applied using the "SelectKBest" class from the scikit-learn library in Python to obtain different numbers of features, and new feature matrices were obtained by combining these selected features.

The results of the LOSOCV method used in classification can be seen in Figure 5.6 for each participant in the experiment. In Figure 5.6, the results obtained by directly applying the features listed in Table 5.1 to the EMG signals, forming the feature matrix (EMG) and providing it as input to the classifier, are shown. Additionally, the results acquired by applying the features from Table 5.1 on IMF1 and IMF2 generated from the EMD method and providing the resulting feature matrix as input to the classifier are also displayed. When binary classification is performed based on three classes (light, heavy, medium-weight), the results are visualized in Figure 5.6 as follows: (a) light vs. heavy, (b) light vs. medium-weight, and (c) heavy vs. medium-weight. The figure reveals discernible variations in classification accuracy among participants. Notably, subject 16 consistently demonstrates lower accuracy results. Conversely, subjects 14, 17, 18, 25, and 30 consistently achieve accuracy rates ranging between 75 and 100% in light and heavy object weight classification.

A closer examination of the feature methods used reveals in Figure 5.7 that the average accuracy (Figure 5.7(a)) and f-measure (Figure 5.7(b)) values for the 30 participants are presented on a per-channel basis when employing the feature matrix generated by directly applying the features listed in Table 5.1 to the EMG signals. As seen in Figure 5.7, the highest accuracy value was achieved by directly applying the features from all channels to the EMG signals. When channels were evaluated individually, Channel 2 exhibited the highest accuracy with 75% accuracy when classifying light and heavy object weight.

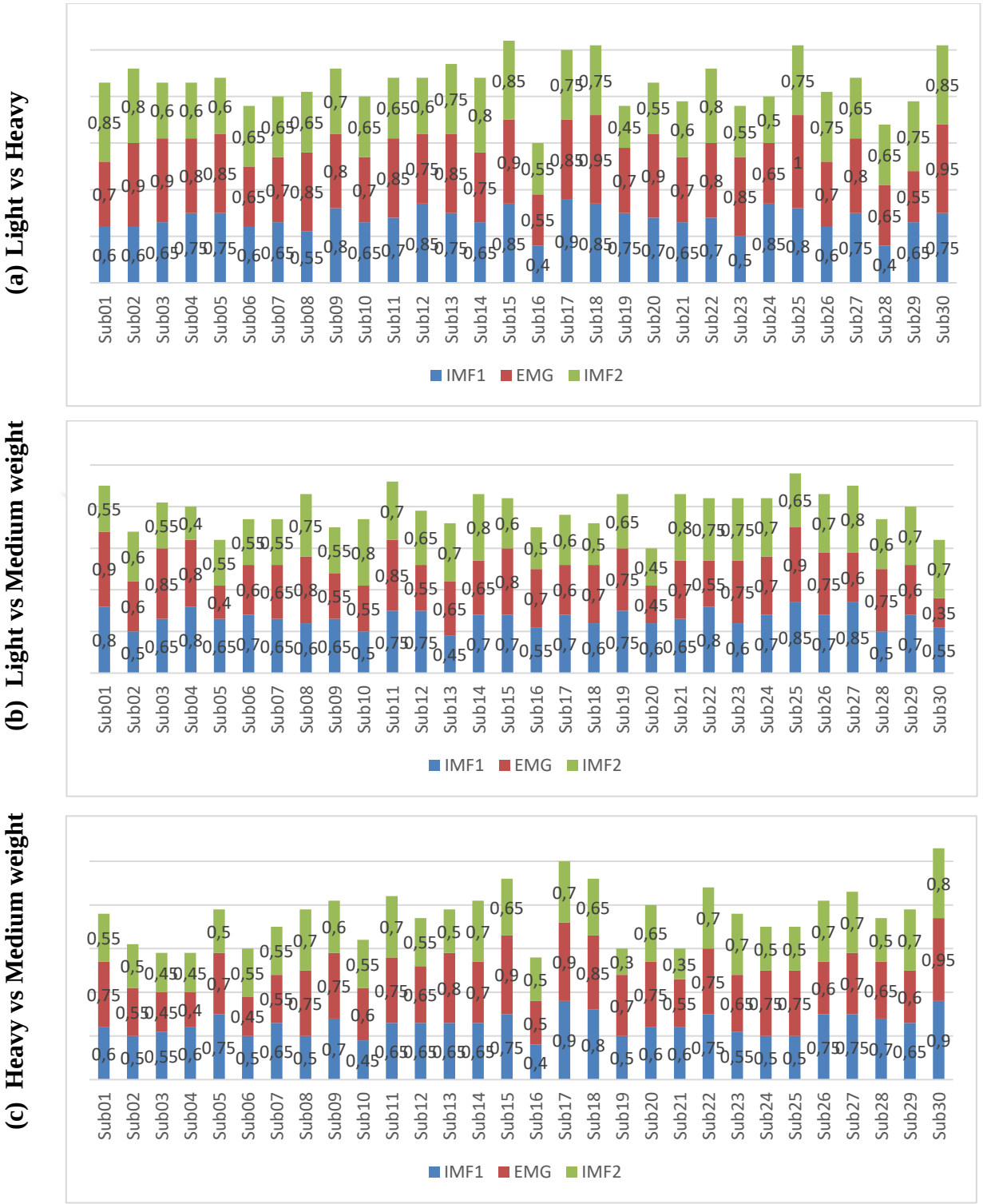

Figure 5.6 The accuracy results (out of one) of LOSOCV classification for features versus subject ID (SubX). (a) Classification accuracies of class light and class heavy, (b) classification accuracies of class light and medium weight, (c) classification accuracies of class heavy and class medium weight.

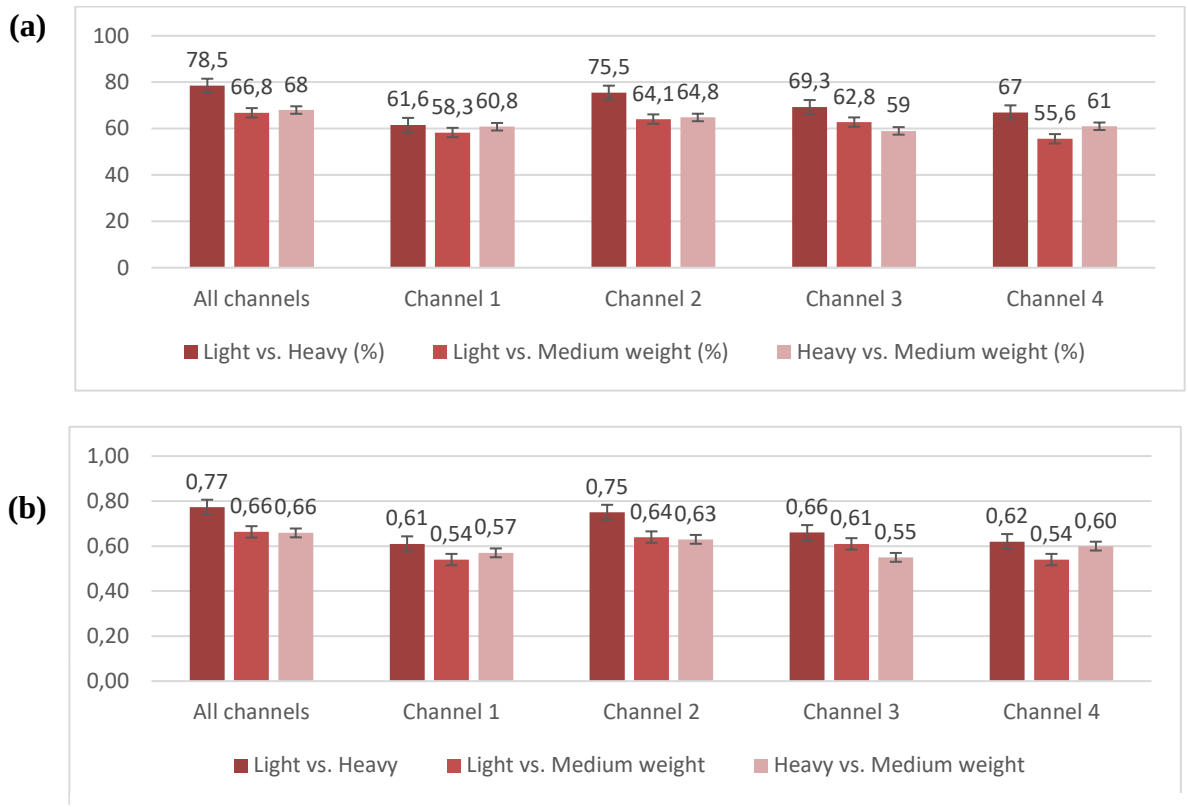

Figure 5.7 Classification results for the features in Table 1 when applied to EMG signals. (a) Accuracy (%), (b) f-measure out of one.

In Figure 5.8 and Figure 5.9, the accuracy and f-measure values obtained by using the feature matrix generated by sequentially applying the features listed in Table 5.1 on IMF1 and IMF2 obtained from the EMD method are presented as the average of 30 individuals. The highest accuracy obtained from IMF1 shown Figure 5.8, using features from all channels, is 68.8%, which is for classifying the weights of light and heavy objects. When examined individually by channels, Channel 2 yielded the highest accuracy. The lowest accuracy, on the other hand, comes from Channel 1 and Channel 4 with a value of 53.3%.

Similar observations can also be made for Figure 5.9. When examining the figure, the highest accuracy, once again, is achieved for the classification of the weights of light and heavy objects, with an accuracy of 67.6%, when using features from all channels. When individually examining the channels in a similar manner for Figure 5.9, Channel 2 provides the highest accuracy, with an accuracy value of 64.5% whereas the lowest accuracy comes from Channel 1, with an accuracy of 54%.

(a)

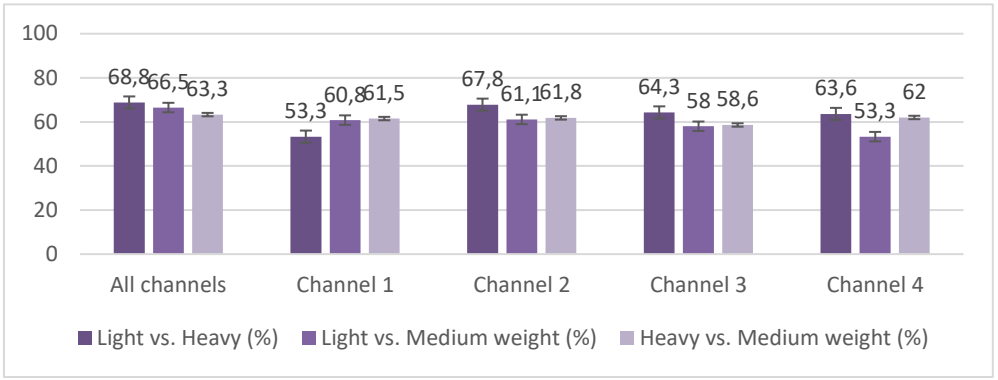

(b)

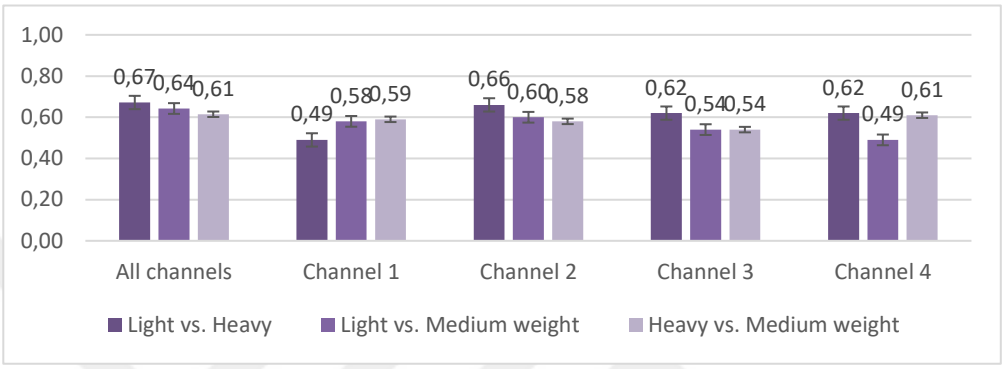

Figure 5.8 Classification results for the features in Table 1 when applied to IMF1. (a) Accuracy (%), (b) f-measure out of one.

(a)

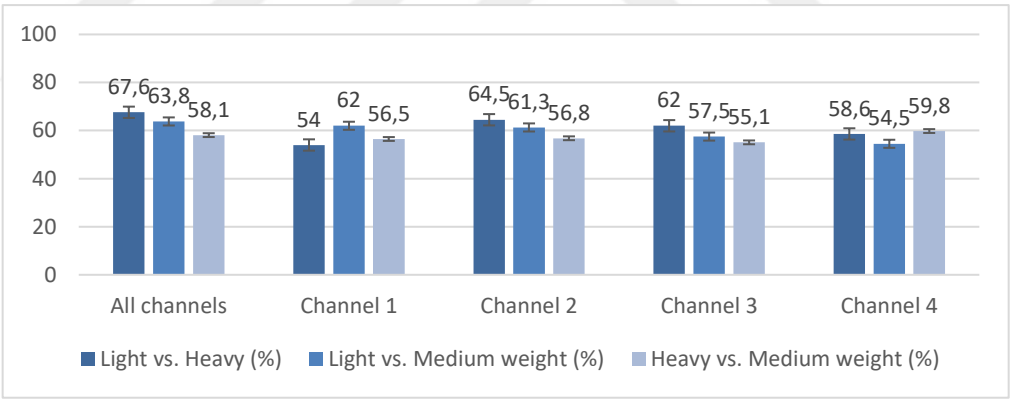

(b)

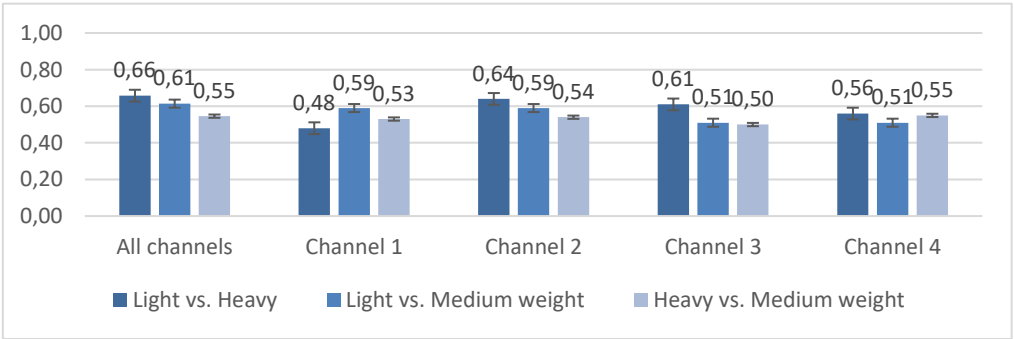

Figure 5.9 Classification results for the features in Table 1 when applied to IMF2. (a) Accuracy (%), (b) f-measure out of one.

In addition to the results reported here, it has been observed that the accuracies can be improved to the 1% level using the feature selection approach. In other words, by utilizing signals from all channels, an accuracy of 79.5% was achieved in binary classification (for distinguishing between light and heavy objects).

5.4 Discussion

In this paper, we introduce Empirical Mode Decomposition (EMD) and 32 commonly used time-domain features for discriminating and classifying the weight of objects (light, heavy, medium weight) to be carried using EMG signals. Our study aims to identify and characterize different weights through the holding phase of multichannel EMG signals to precondition muscles. Properly estimating the weight of the object to be carried is crucial for adjusting the prosthesis's torque before movement. We conducted experiments, during which the participants were instructed to rest, reach for and hold a bottle, prepare their muscles to lift the bottle, lift it, hold it at a higher position, lower it, and return their hand to the initial position. To address variations in muscle strength among participants, we recorded EMG signals from 30 participants. Each phase was repeated 30 times, resulting in a total of 900 trials across three weight classes. We utilized four EMG channels distributed across the forearm and extracted 32 features from both the Intrinsic Mode Functions (IMFs) obtained through EMD and the raw EMG signal. Additionally, we selected specific channels for single-channel analysis. Our proposed method incorporates EMD as a feature, and for the first time in EMG signal processing literature, explores the problem of weight perception during the holding phase. The effect of EMD is compared with several popular feature extraction approaches listed in Table 5.1. Our primary focus in this research was to propose the optimal electrode-feature combination for distinguishing the weight of objects during the holding phase (muscle preparation for lifting). We believe that this can facilitate the use of an easily and quickly controllable upper limb prosthesis for patients. This classification scheme is crucial because it can be utilized in real-time to adjust the torque of the prosthesis based on the weight of the object being carried.

The study illustrates noticeable differences in the classification accuracy among the participants. These findings are supported by the fact that EMG data is specific to each subject. It is worth mentioning that Participant 16 consistently exhibits lower accuracy results. One possible explanation for this phenomenon is that it may imply a potential

case of muscle fatigue. Factors such as genetics, dietary habits, and physical activity could be considered as potential contributors for this participant. This inference is also supported by the study conducted by A.K. Mukhopadhyay and S. Samui [298].

This study focused on predicting the weights of light, heavy, and medium weight object using EMG signals. According to our findings, when all channels were used, it was determined that the features representing light and heavy objects had the most distinguishing features compared to the other pairwise groups. The outcomes of this study are in line with earlier research by Cisotto et al., in which they used both EEG (Electroencephalography) and EMG (Electromyography) to classify WAY-EEG-GAL dataset. [122], [254]. In their study, they focused on classifying two out of three available classes, specifically the most extreme weights, which were 165 grams and 660 grams. Despite having imbalanced classes with an imbalance ratio of 0.81 between the number of trials in the two classes, they chose to evaluate their results in terms of accuracy. They achieved a maximum accuracy of 94% when considering only the Brachioradial muscle data. When we conduct our analysis using all available muscles but restrict it to the data from only the 12 subjects, we achieve an accuracy rate of 89.5%. As a result, despite exclusively utilizing EMG data, we managed to attain similar outcomes. However, Lashgari and Maoz used only EMG to classify the WAY-EEG-GAL dataset [254], [276]. They used multichannel classification with 3 classes (165, 330 and 660 gr). They developed an automated feature-extraction directly from the (filtered) raw EMG time-domain signal. They achieved high classification accuracy in terms of f1-score 88.2±3.5%. They performed a classification process using features obtained from all phases of reaching, grasping, and lifting recorded signals in the signal processing step. Nevertheless, our findings have contributed to the literature by focusing solely on the grasping phase and determining whether EMG signals were preconditioned based on the target weight.

The direct application of commonly used feature extraction methods to EMG signals has been compared with their application to IMF1 and IMF2 obtained from EMD. According to this comparison, the classification accuracy of common features directly obtained from EMG signals is 78.5%, whereas the classification accuracy of features obtained from IMF1 and IMF2 is 68.8% and 67.6%, respectively. The fact that the IMFs are sorted by frequency and that IMF1, which has a higher frequency, performs better than IMF2, which has a lower frequency, might be explained by the high-frequency

characteristics of the EMG. In this case, we can observe that the low frequency (IMF2) is relatively weak in representing EMG signals. There is a study in the literature regarding the use of EMD for EMG signals. Aziz et al., proposed a methodology for load classification using sEMG signals, achieving a classification accuracy of 99% for a three-class problem [277]. However, the results of this study diverge from our research, indicating an alternative approach to utilizing EMD for signal denoising. While they reconstructed the signal using selected IMFs, we, on the other hand, employed the IMFs as individual signals.

Furthermore, it is noteworthy that various muscles exhibit distinct performances in terms of class differentiation, particularly in distinguishing between light and heavy objects. For example, the classification accuracies are ranked as follows, from highest to lowest: Channel 2 (extensor carpi radialis brevis (ECRB)) at 75.5%, Channel 3 (extensor digitorum (ED)) at 69.3%, Channel 4 (extensor carpi ulnaris (ECU)) at 67%, and Channel 1 (flexor carpi radialis (FCR)) at 61%. To state it another way, the muscles that provide the highest classification accuracy can be regarded as the most informative for distinguishing between two weights. In particular, when all muscles were used, they achieved the highest accuracy in classifying the weights. Cisotto et al., presented findings that suggest considering a greater number of muscles leads to enhanced accuracy [122].

The upper limb prosthesis can be used more effectively if torque control can be adjusted when the object is visually perceived. Therefore, we introduced that the selected signal area during the holding phase has the potential to provide informative features for recognizing object weight perception. The classification accuracy of the common features extracted from the EMG signal, used to classify light and heavy object weights, showed high success rates through the application of machine learning approaches.

Additionally, we made a contribution to the literature on the use of the EMD method for representing EMG signals with its IMFs. Although the classification accuracies of the IMFs from the EMG signals remain low, they offer valuable accuracy in representing the EMG signals. Consequently, these findings support the notion that IMFs can be employed for data augmentation in deep learning.

While we achieved successful classification of both light and heavy weights, our study is constrained by certain limitations stemming from its offline analysis. In

subsequent research, we plan to overcome this limitation by implementing real-time classification methods that offer enhanced accuracy and robustness.

5.5 Conclusions

In this chapter, we introduced an innovative approach for weight perception using sEMG signals. Our methodology focuses on utilizing sEMG signals captured during the holding phase to differentiate between object weights. Furthermore, we explored the implementation of EMD-based feature extraction techniques. The selected feature set was then employed in logistic regression to distinguish between different binary load categories. The proposed methodology in this study achieved a classification accuracy of 78.5% for light vs. heavy load category, specifically 25g (empty bottle) and 1097g (full bottle of water). The findings of this research validate the utility of analyzing the holding phase of sEMG signals for weight perception purposes. Future studies may consider incorporating real-time analysis, which can further enhance the practicality of our proposed approach.

Chapter 6

Conclusions and Future Prospects

6.1 Discussion

In the initial phase of our project, the primary goal was to automatically determine the intention to move by using multi-channel EEG signals to transition the brain-machine interface system from sleep mode to active mode without the need for additional accessories/methodologies. An approach was developed based on Fourier-based synchrosqueezed transform (FSST) for feature extraction and singular value decomposition (SVD) for feature selection, aiming to achieve high accuracy in distinguishing and classifying rest and motor intention states using multi-channel EEG signals. This approach was compared with other machine learning approaches, including common spatial patterns (CSP), supervised CSP (SCSP), discrete wavelet transform (DWT), and autoregressive (AR), among nine other feature extraction methods. It is important to note that the experiments involved 30 participants, with data from 28 participants being used for analysis. Participants were instructed to stay still, imagine moving their limbs, or imagine opening and closing their hands during experiments with a 16-channel EEG system. The data resulted in over 1500 trials for each class.

The performance of FSST and SVD was compared with CSP, SCSP, DWT, AR, and the other mentioned feature extraction methods in terms of classification results. Additionally, distinctive electrode-feature combinations were explored for each classification scheme. The main focus of this study was to propose the best electrode-feature combination and classification methodology for distinguishing between rest and motor movement imagination states. The ultimate goal was to pave the way for the use of a self-initiated, portable, and wireless EEG-based Brain-Computer Interface (BCI) system for weight perception.

In this study, it was found that, although the classification accuracy of the S-T-F-TF method (the constituent methods of S-T-F-TF have been individually used in the

literature but not commonly combined as we did here) was comparable to FSST, the FSST method achieved the highest accuracy, ranging between 99% and 100%, and had a calculation time of 0.24 seconds with SVD, demonstrating superior noise resilience. While the SBCSP approach was more effective than CSP in the classification of motor imagery tasks, the combination of the introduced 11 features in this study (S-T-F-TF) did not perform as well as expected. The achieved high accuracies indicate the potential usefulness of this approach (feature extraction with FSST and SVD) in the field, particularly in detecting motor intention waves and transitioning brain-machine interfaces from sleep mode to active mode.

Various studies in the literature have explored different features related to motor movement. For instance, Niazi et al., detected movement-related cortical potentials (MRCP) from EEG signals in real-time for eight healthy subjects [232]. They reported a true positive rate (TPR) of 67.15% ± 7.87% for the MRCP task. Another study, Ahmadian et al., used constrained blind source extraction (CBSE) to detect readiness potentials (RP) for three healthy subjects, achieving a TPR of 75% ± 11% [233]. Jochumsen et al., investigated recognizing MRCPs during grasp tasks in five stroke patients and 15 healthy individuals using a single EEG channel [234]. They reported detecting approximately 75% of the movements accurately around 100 ms before the onset of the movement. Similarly, Xu et al., demonstrated the intentional movement detection using MRCPs, achieving a classification accuracy of 79% ± 11% in their study [235].

The results of our study affirm the significant impact of motor imagery on brain signals. However, the accuracy of predicting motor intention in our study is lower compared to some other works in the literature, such as Bai et al., who reported an accuracy rate of 75% for predicting motor intention [25]. Additionally, Niazi et al., used MRCPs to distinguish between real and imagined movements, achieving a high TPR of 82.5% ± 7.8% [240]. Nevertheless, Madhavan et al., achieved a 100% accuracy rate using a 2D-convolutional neural network (CNN) to classify focused and unfocused categories using FSSD of EEG signals [242].

Methods based on FSST allow the analysis of non-stationary signals like EEG in the time-frequency (TF) domain. Unlike STFT, FSST has the advantage of obtaining a high-resolution TF representation of non-stationary signals by minimizing unnecessary information. Therefore, the classification accuracy of FSST for distinguishing rest and

motor intention states was proposed in the initial phase of our project, along with machine learning algorithms. However, it's worth noting that FSST, when used in conjunction with machine learning algorithms, has limitations, such as the need for feature selection to extract features from the TF coefficient matrix.

In the second phase of our project, research was initiated to detect weight perception using EEG and/or EMG signals before establishing a connection between the decision information obtained from the signals and the prosthetic limb. A literature review revealed studies that employed keywords such as "Weight perception," "grab and lift (GAL)," and "EEG and EMG" in various focus areas and datasets. For example, Luciw et al., designed an experimental setup using 32 electrodes on the scalp to investigate sensation, intention, and action detection using EEG signals from individuals performing a grab and lift task [254]. The dataset, named WAY-EEG-GAL, was made publicly available for other researchers to use. Another study, Hasan et al., conducted experiments on the same dataset, exploring various preprocessing methods and deep learning approaches such as convolutional neural networks (CNN) and long short-term memory (LSTM) to determine their performance [299]. They found that a combination of a discrete wavelet transforms (DWT)-based noise removal filter, data standardization, and a CNN-based classification approach achieved a high area under the curve (AUC) value of 0.944. Additionally, Liu and Yang classified stages of hand movements using a three-branch CNN architecture on the WAY-EEG-GAL dataset [300], while Orellana et al., used DWT and empirical mode decomposition (EMD) to achieve the best classification performance (around 89%) for the six movements within the 0-4 Hz range [300].

Other research groups working on their specific datasets have also contributed to the literature. Aslam et al., conducted a study where participants applied pressures corresponding to different weight levels to their hands as a tactile stimulus, and 4-channel EEG signals were used to classify the brain's weight perception [301]. They achieved successful results using the relative power values of alpha and beta sub-bands as features and a radial basis function (RBF) kernel support vector machine (SVM) classifier. Van Polanen and Davare used 32-channel EEG signals and EMG signals from five arm and hand muscles to estimate the weight of randomly selected light or heavy objects lifted in a semi-random order [302]. Chang proposed a comprehensive study on using brain signals during a human-in-the-loop robotic system, where EEG signals were employed for a robot's grasping and lifting function [303]. In their study, Chacko et al., collected EEG

signals from a 129-channel system while participants performed the task of grasping and lifting a water-filled cup, achieving a 95% accuracy in detecting motor imagery intentions using the 8-14 Hz frequency band [304].

In addition to EEG-based studies, there are works in the literature that focus on EMG signals. Furmanek et al., provided open access to EMG signals recorded during hand and arm movements performed in a virtual reality environment [305]. Totah et al., investigated the feasibility of developing an assistive device for weight lifting based on the electromyographic signals recorded during the process of lifting various loads [306]. They extracted seven features from EMG signals and used multinomial logistic regression for classification, achieving successful results in predicting the weight carried by the participants. Shair et al., conducted an experimental study on detecting fatigue during weight lifting in workers using EMG signals [307].

Unlike the studies summarized above, this thesis focuses on the decomposition of visual perception related to weights. In our study, we aim to predict weights from the brain signals of an individual exposed to different weights and precondition the prosthetic hand system accordingly. Both offline (without a prosthesis) and with healthy individuals using a prosthesis, trials have been conducted, contributing a significant dataset and approach to the literature. In our study, a binary classification accuracy of 70-80% was achieved for weight prediction using offline EEG signals. In a machine learning study using data from the phase corresponding to the time when the weight was grasped but not lifted, EMG signals achieved approximately 85% binary and 70% ternary classification accuracy with a single channel. In the latest study, experiments were conducted with healthy individuals using prosthetics, resulting in approximately 50% classification accuracy in binary classification.

In conclusion, this thesis addresses a unique aspect by focusing on the visual perception of weights and aims to contribute valuable insights and a dataset to the literature.

6.2 Conclusions

Our main objective in the project, as can be inferred from the title, is to harness multi-channel brain signals for reducing the mental burden in individuals with amputations, particularly in the context of shoulder-controlled prosthetic hands—the

most widely used type of prosthetics. The aim is to provide users with a more natural prosthetic experience in their daily lives. To achieve the reduction of mental burden, the primary focus is on the role of visual weight perception. The idea is to utilize brain signals, expected to vary based on whether the perceived object is heavy, medium-weight, or light, to adjust the torque of the electric motor embedded in the wrist part of the prosthetic hand. Consequently, it would be possible to set higher stiffness for lifting heavy objects and lower stiffness for lifting light objects. Additionally, to support this concept, the study explores the use of electromyography (EMG) signals from the arm muscles during the moments corresponding to post-grasping and pre-lifting for adjusting the wrist stiffness.

Within this framework, complementary and interrelated activities are carried out. Initially, the collection of biosignals such as EEG and EMG from healthy participants is performed using specially designed paradigms for the given problem. Subsequently, offline and online methods are employed to analyze the signals and investigate the application of machine learning to generate decisions addressing issues in the functioning of the prosthesis. Various preprocessing, feature extraction, reduction, and classification methods have been experimented with to process the signals and determine the weight perception and amount, aiming to identify the most suitable combinations.

In the scope of the thesis, the first study aimed to process, analyse, and classify biosignals using machine learning methods. The focus was on investigating the potential of activating any prosthesis or external device from a sleep mode using motor intention waves. This offline analysis involved multi-channel EEG signals obtained from 30 healthy participants during motor intention, utilizing Fourier-based synchrosequeezing transform (FSST) for feature extraction and singular value decomposition (SVD) for dimensionality reduction. The second-order kernel Support Vector Machine (SVM) with a quadratic kernel achieved a classification accuracy of 99% for rest and movement imagination.

The discriminative power of some channels over others was observed, and the study demonstrated that using signals categorized as acceptable, rather than only clean EEG signals, did not compromise performance. The combination of FSST and SVD for feature extraction and classification, based on the cleanliness level of the signals, was applied for the first time in detecting motor intention waves from EEG signals.

Initiating the functionality of a Brain-Machine Interface (BMI) trigger is crucial. Different methods were proposed for achieving this goal. The project suggests that detecting the imagined movement of a prosthesis system through the identification of motor intention in brain signals can achieve high performance. The application of the novel FSST method in the time-frequency domain may facilitate this. These findings could potentially be applied to the developed prosthetic hand system in future work, and the approach could be tested on other publicly available datasets.

In the second phase of the project, a preparatory study was conducted before the real-time and online signal processing and classification application with the prosthesis. Offline signal processing and classification involved collecting multi-channel EEG and EMG signals simultaneously from 31 participants during grasping and lifting experiments. Different feature extraction and reduction approaches were applied, and various machine learning and deep learning methods were explored for classification in binary and ternary problems. The study included a paradigm where participants imagined the weight levels of objects seen on the screen (light, medium, and heavy) while EEG data were collected, alongside a paradigm where EEG and EMG data were collected during the guidance of actual grasping and lifting movements.

6.3 Societal Impact and Contribution to Global Sustainability

The thesis carries significant societal impact and contributes substantially to global sustainability by revolutionizing the field of upper-limb prosthetics. At the societal level, the research is poised to greatly enhance the lives of individuals with limb loss. The incorporation of neuroimaging techniques, particularly the innovative use of EEG signals, promises a breakthrough in the control mechanisms of prosthetic limbs. This not only addresses the physical challenges faced by amputees but also significantly reduces the mental burden associated with conventional mechanical prostheses, thereby improving overall well-being.

The neurofeedback system's development, enabling users to estimate the weight of grasped objects through their prosthetic limbs, signifies a major leap forward in assistive technology. By integrating user-centric visual weight perception, the project strives to

provide a more natural and intuitive control system, empowering individuals with limb loss and fostering independence.

From a global sustainability perspective, the project aligns with principles of resource efficiency and environmental responsibility. Advancements in prosthetic technology through biosignal processing and machine learning have the potential to create more sustainable and durable prosthetic devices. This, in turn, could reduce the need for frequent replacements, ultimately lessening the environmental impact associated with the production and disposal of prosthetic materials.

The commitment to innovative methodologies, such as the Fourier-based synchrosequeezing transform (FSST) and singular value decomposition (SVD) approaches, reflects a dedication to pushing the boundaries of knowledge. Disseminating these findings in high-impact journals not only contributes to academic discourse but also fosters a culture of knowledge-sharing and collaboration, vital components for addressing global challenges.

In conclusion, the societal impact of this project is profound, offering transformative possibilities for individuals with limb loss and contributing significantly to global sustainability through the development of advanced, resource-efficient prosthetic solutions. The dissemination of knowledge further positions the project as a key player in advancing technological innovation for societal well-being on a global scale.

6.4 Future Prospects

The study observed that the feature set obtained from the FSST-SVD combination, along with common spatial patterns (CSP) approaches, achieved around 70% accuracy in binary weight perception classification (e.g., distinguishing between light and heavy objects). However, the accuracy significantly dropped in ternary classification. CSP-based feature extraction yielded better results, but the lower performance in distinguishing between rest and movement imagination in EEG signals raised some concerns. Further in-depth analyses and additional experiments are planned to address these issues before publishing the study in a high-impact journal.

In conclusion, the research identified a crucial application and approach: the inclusion of EEG signals collected during actual movement in the training dataset

significantly contributes to the test performance in classifying the imagined weight perception. This observation suggests potential improvements and novel avenues for research in the field of Brain-Machine Interfaces (BMI). Additionally, a novel approach involving the adjustment of the wrist part's stiffness during the lifting process based on the perceived weight level is introduced. While the desired accuracy values have not been achieved at this stage, the significance of this study prompts a revaluation of the process from both signal processing and classification perspectives and prosthetic design. Post-project, there is ample room for further development and improvement efforts.

BIBLIOGRAPHY

[1] J. R. Wolpaw, N. Birbaumer, D. J. McFarland, G. Pfurtscheller, and T. M. Vaughan, "Brain–computer interfaces for communication and control," *Clin Neurophysiol*, vol. 113, no. 6, pp. 767–791, Jun. 2002, doi: 10.1016/S1388-2457(02)00057-3.

[2] L. F. Nicolas-Alonso and J. Gomez-Gil, "Brain computer interfaces, a review," *Sens*, vol. 12, no. 2. pp. 1211–1279, Feb. 2012. doi: 10.3390/s120201211.

[3] R. A. Ramadan and A. V. Vasilakos, "Brain computer interface: control signals review," *Neurocomputing*, vol. 223, pp. 26–44, Feb. 2017, doi: 10.1016/j.neucom.2016.10.024.

[4] S. Waldert, T. Pistohl, C. Braun, T. Ball, A. Aertsen, and C. Mehring, "A review on directional information in neural signals for brain-machine interfaces," *J Physiol Paris*, vol. 103, no. 3–5, pp. 244–254, 2009, doi: 10.1016/j.jphysparis.2009.08.007.

[5] M. W. Slutzky and R. D. Flint, "Physiological properties of brain-machine interface input signals," *J Neurophysiol*, vol. 118, no. 2. American Physiological Society, pp. 1329–1343, Aug. 14, 2017. doi: 10.1152/jn.00070.2017.

[6] M. Hauschild, G. H. Mulliken, I. Fineman, G. E. Loeb, and R. A. Andersen, "Cognitive signals for brain-machine interfaces in posterior parietal cortex include continuous 3D trajectory commands," *Proc Natl Acad Sci U S A*, vol. 109, no. 42, pp. 17075–17080, Oct. 2012, doi: 10.1073/pnas.1215092109.

[7] S. P. Kim, J. D. Simeral, L. R. Hochberg, J. P. Donoghue, and M. J. Black, "Neural control of computer cursor velocity by decoding motor cortical spiking activity in humans with tetraplegia," *J Neural Eng*, vol. 5, no. 4, pp. 455–476, 2008, doi: 10.1088/1741-2560/5/4/010.

[8] R. Abiri, S. Borhani, E. W. Sellers, Y. Jiang, and X. Zhao, "A comprehensive review of EEG-based brain-computer interface paradigms," *J Neural Eng*, vol. 16, no. 1, p. 011001, Feb. 2019, doi: 10.1088/1741-2552/AAF12E.

[9] J. Polich, "Updating P300: An integrative theory of P3a and P3b," *Clin Neurophysiol*, vol. 118, no. 10. pp. 2128–2148, 2007. doi: 10.1016/j.clinph.2007.04.019.

[10] E. Donchin and D. B. D. Smith, "The contingent negative variation and the late positive wave of the average evoked potential," *Electroencephalogr Clin Neurophysiol*, vol. 29, no. 2, pp. 201–203, Aug. 1970, doi: 10.1016/0013-4694(70)90124-0.

[11] M. Lotze and L. G. Cohen, "Volition and imagery in neurorehabilitation," *Cogn Behav Neurol*, vol. 19, no. 3, pp. 135–140, 2006, doi: 10.1097/01.wnn.0000209875.56060.06.

[12] C. Neuper, R. Scherer, S. Wriessnegger, and G. Pfurtscheller, "Motor imagery and action observation: Modulation of sensorimotor brain rhythms

during mental control of a brain-computer interface," *Clin Neurophysiol*, vol. 120, no. 2, pp. 239–247, 2009, doi: 10.1016/j.clinph.2008.11.015.

[13] G. Pfurtscheller and C. Neuper, "Motor imagery activates primary sensorimotor area in humans," *Neurosci Lett*, vol. 239, no. 2–3, pp. 65–68, Dec. 1997, doi: 10.1016/S0304-3940(97)00889-6.

[14] C. S. Nam, Y. Jeon, Y. J. Kim, I. Lee, and K. Park, "Movement imagery-related lateralization of event-related (de)synchronization (ERD/ERS): Motor-imagery duration effects," *Clin Neurophysiol*, vol. 122, no. 3, pp. 567–577, 2011, doi: 10.1016/j.clinph.2010.08.002.

[15] J. L. Contreras-Vidal, A. Presacco, H. Agashe, and A. Paek, "Restoration of whole body movement: Toward a noninvasive brain-machine interface system," *IEEE Pulse*, vol. 3, no. 1, pp. 34–37, 2012, doi: 10.1109/MPUL.2011.2175635.

[16] T. Mulder, "Motor imagery and action observation: Cognitive tools for rehabilitation," *J Neural Transm*, vol. 114, no. 10, pp. 1265–1278, 2007, doi: 10.1007/s00702-007-0763-z.

[17] M. Lotze *et al.*, "Activation of cortical and cerebellar motor areas during executed and imagined hand movements: An fMRI study," *J Cogn Neurosci*, vol. 11, no. 5, pp. 491–501, 1999, doi: 10.1162/089892999563553.

[18] G. Pfurtscheller, C. Neuper, D. Flotzinger, and M. Pregenzer, "EEG-based discrimination between imagination of right- and left-hand movement," *Electroencephalogr Clin Neurophysiol*, vol. 103, no. 6, pp. 642–651, Dec. 1997, doi: 10.1016/S0013-4694(97)00080-1.

[19] F. Babiloni *et al.*, "Linear classification of low-resolution EEG patterns produced by imagined hand movements," *IEEE Trans Rehabil Eng*, vol. 8, no. 2, pp. 186–188, 2000, doi: 10.1109/86.847810.

[20] T. Wang and B. He, "An efficient rhythmic component expression and weighting synthesis strategy for classifying motor imagery EEG in a brain-computer interface," *J Neural Eng*, vol. 1, no. 1, pp. 1–7, 2004, doi: 10.1088/1741-2560/1/1/001.

[21] A. Vallabhaneni and B. He, "Motor imagery task classification for brain computer interface applications using spatiotemporal principle component analysis," *Neurol Res*, vol. 26, no. 3, pp. 282–287, 2004, doi: 10.1179/016164104225013950.

[22] W. D. Penny, S. J. Roberts, E. A. Curran, and M. J. Stokes, "EEG-based communication: A pattern recognition approach," *IEEE Trans Rehabil Eng*, vol. 8, no. 2, pp. 214–215, Jun. 2000, doi: 10.1109/86.847820.

[23] G. Pfurtscheller, G. R. Müller-Putz, J. Pfurtscheller, and R. Rupp, "EEG-based asynchronous BCI controls functional electrical stimulation in a tetraplegic patient," *EURASIP J Appl Signal Processing*, vol. 2005, no. 19, pp. 3152–3155, 2005, doi: 10.1155/ASP.2005.3152.

[24] H. G. Tan, H. H. Zhang, C. C. Wang, C. Y. Shee, W. T. Ang, and C. T. Guan, "Arm flexion and extension exercises using a brain-computer interface and functional electrical stimulation," in *Proceedings of the 6th*

IASTED International Conference on Biomedical Engineering, 2008, pp. 322–326.

[25] O. Bai, P. Lin, S. Vorbach, J. Li, S. Furlani, and M. Hallett, "Exploration of computational methods for classification of movement intention during human voluntary movement from single trial EEG," *Clin Neurophysiol*, vol. 118, no. 12, pp. 2637–2655, Dec. 2007, doi: 10.1016/j.clinph.2007.08.025.

[26] E. López-Larraz, L. Montesano, Á. Gil-Agudo, and J. Minguez, "Continuous decoding of movement intention of upper limb self-initiated analytic movements from pre-movement EEG correlates," *J Neuroeng Rehabil*, vol. 11, no. 1, pp. 153–167, Nov. 2014, doi: 10.1186/1743-0003-11-153.

[27] B. Kim, L. Kim, Y. H. Kim, and S. K. Yoo, "Cross-association analysis of EEG and EMG signals according to movement intention state," *Cogn Syst Res*, vol. 44, pp. 1–9, Aug. 2017, doi: 10.1016/j.cogsys.2017.02.001.

[28] K. K. Ang *et al.*, "A clinical study of motor imagery-based brain-computer interface for upper limb robotic rehabilitation," in *Annu Int Conf IEEE Eng Med Biol Soc, EMBC 2009*, 2009, pp. 5981–5984. doi: 10.1109/IEMBS.2009.5335381.

[29] A. Muralidharan, J. Chae, and D. M. Taylor, "Extracting attempted hand movements from eegs in people with complete hand paralysis following stroke," *Front Neurosci*, vol. 5, no. MAR, p. 39, 2011, doi: 10.3389/fnins.2011.00039.

[30] O. Bai *et al.*, "Prediction of human voluntary movement before it occurs," *Clin Neurophysiol*, vol. 122, no. 2, pp. 364–372, Feb. 2011, doi: 10.1016/j.clinph.2010.07.010.

[31] D. Rozado, A. Duenser, and B. Howell, "Improving the performance of an EEG-based motor imagery brain computer interface using task evoked changes in pupil diameter," *PLoS One*, vol. 10, no. 3, p. e0121262, Mar. 2015, doi: 10.1371/journal.pone.0121262.

[32] R. Leeb, L. Tonin, M. Rohm, L. Desideri, T. Carlson, and J. D. R. Millán, "Towards independence: A BCI telepresence robot for people with severe motor disabilities," *Proc IEEE Int*, vol. 103, no. 6, pp. 969–982, 2015, doi: 10.1109/JPROC.2015.2419736.

[33] J. Karam, S. Al Majeed, C. N. Yalung, and L. Mirtskhulava, "Neural network for recognition of brain wave signals," *Int J Enhanc Res Sci Technol Eng*, vol. 5, no. 10, pp. 36–42, 2016.

[34] C. Guger, W. Harkam, G. Pfurtscheller, and C. Hertnaes, "Prosthetic control by an EEG-based brain-computer interface (BCI)," *AAATE 5th European Conference for the Advancement of Assistive Technology*, no. February 2016, pp. 2–7, 1999.

[35] A. Sun, B. Fan, and C. Jia, "Motor imagery EEG-based online control system for upper artificial limb," *Proceedings 2011 International Conference on Transportation, Mechanical, and Electrical Engineering, TMEE 2011*, pp. 1646–1649, 2011, doi: 10.1109/TMEE.2011.6199526.

[36] R. Roy, A. Konar, D. N. Tibarewala, and R. Janarthanan, “EEG driven model predictive position control of an artificial limb using neural net,” *2012 3rd International Conference on Computing, Communication and Networking Technologies, ICCCNT 2012*, no. July, pp. 1–9, 2012, doi: 10.1109/ICCCNT.2012.6395913.

[37] C.-C. K. L. Ming-Shaung Ju, Chih-Wei Chen, “Hand orthosis controlled using brain-computer interface,” *J Med Biol Eng*, vol. 29, pp. 234–241, 2009.

[38] E. Uyar, K. Şenli, and L. Mutlu, “Beyin dalgası kontrollü protez kol tasarımı,” *Sakarya University Journal of Science*, vol. 16, no. 3, pp. 164–169, 2012.

[39] R. Leeb, H. Sagha, R. Chavarriaga, and J. D. R. Millán, “A hybrid brain-computer interface based on the fusion of electroencephalographic and electromyographic activities,” in *J Neural Eng*, Apr. 2011. doi: 10.1088/1741-2560/8/2/025011.

[40] E. A. Kirchner, M. Tabie, and A. Seeland, “Multimodal movement prediction - towards an individual assistance of patients,” *PLoS One*, vol. 9, no. 1, p. e85060, 2014, doi: 10.1371/journal.pone.0085060.

[41] J. Rouillard, A. Duprès, F. Cabestaing, and S. Leclercq, “Hybrid BCI coupling EEG and EMG for severe motor disabilities,” *Procedia Manuf*, vol. 3, pp. 29–36, 2015, doi: 10.1016/j.promfg.2015.07.104.

[42] K. A. Carbine, “Sample size calculations in human electrophysiology (EEG and ERP) studies: A systematic review and recommendations for increased rigor,” *Int J Psychophysiol*, vol. 111, pp. 33–41, Jan. 2017, doi: 10.1016/J.IJPSYCHO.2016.06.015.

[43] J. M., Delgado, “Permanent implantation of multilead electrodes in the brain,” *Yale J Biol Med*, vol. 24, no. 5, p. 351, Apr. 1952, Accessed: Nov. 03, 2023. [Online]. Available: https://www.ncbi.nlm.nih.gov/pmc/articles/PMC2599161/

[44] A. Kübler, “The history of BCI: From a vision for the future to real support for personhood in people with locked-in syndrome,” *Neuroethics*, vol. 13, no. 2, pp. 163–180, Jul. 2020, doi: 10.1007/S12152-019-09409-4/FIGURES/11.

[45] J. R. Wolpaw *et al.*, “Brain-computer interface technology: A review of the first international meeting,” *IEEE Trans Rehabil Eng*, vol. 8, no. 2, pp. 164–173, Jun. 2000, doi: 10.1109/TRE.2000.847807.

[46] D. B. Rubin *et al.*, “Interim safety profile from the feasibility study of the BrainGate neural interface system,” *Neurology*, vol. 100, no. 11, pp. E1177–E1192, Mar. 2023, doi: 10.1212/WNL.0000000000201707.

[47] X. Mao *et al.*, “Progress in EEG-based brain robot interaction systems,” *Comput Intel Neurosc*, vol. 2017. p. 25, 2017. doi: 10.1155/2017/1742862.

[48] Z. P. Zhao *et al.*, “Modulating brain activity with invasive brain-computer interface: A narrative review,” *Brain Sci*, vol. 13, no. 1, p. 134, Jan. 2023, doi: 10.3390/BRAINSCI13010134.

[49] C. Guger, B. Z. Allison, and N. Mrachacz-Kersting, “Brain-computer interface research: A state-of-the-art summary 7,” in *Brain-Computer Interface Research*, SpringerBr., A. B. Guger C., Mrachacz-Kersting N., Ed., Springer, Cham, 2019, pp. 1–9. doi: 10.1007/978-3-030-05668-1_1.

[50] A. N. Pisarchik, V. A. Maksimenko, and A. E. Hramov, “From novel technology to novel applications: Comment on ‘An integrated brain-machine interface platform with thousands of channels’ by Elon Musk and Neuralink,” *J Med Internet Res*, vol. 21, no. 10, p. e16356, Oct. 2019, doi: 10.2196/16356.

[51] “Enabling Connection II: BCI for Assistive Communication | NeuroExplainer.” Accessed: Mar. 29, 2024. [Online]. Available: https://www.paradromics.com/blog/enabling-connection-ii-bci-for-assistive-communication

[52] L. C. Frey and M. C. Spitz, “Electroencephalography,” in *Behavioral Neurology and Neuropsychiatry*, A. C. F. C. Arciniegas DB, Ed., Cambridge University Press, 2013, pp. 442–458. doi: 10.1017/CBO9781139016919.030.

[53] M. Congedo, L. Korczowski, A. Delorme, and F. Lopes da silva, “Spatio-temporal common pattern: A companion method for ERP analysis in the time domain,” *J Neurosci Methods*, vol. 267, pp. 74–88, 2016, doi: 10.1016/j.jneumeth.2016.04.008.

[54] Q. Wu, Y. Zhang, J. Liu, J. Sun, A. Cichocki, and F. Gao, “Regularized group sparse discriminant analysis for P300-based brain-computer interface,” *Int J Neural Syst*, vol. 29, no. 6, p. 1950002, Aug. 2019, doi: 10.1142/S0129065719500023.

[55] Y. Yu *et al.*, “Toward a bybrid BCI: Self-paced operation of a P300-based speller by merging a motor imagery-based ‘brain switch’ into a P300 spelling approach,” *Int J Hum Comput Interact*, vol. 33, no. 8, pp. 623–632, Aug. 2017, doi: 10.1080/10447318.2016.1267450.

[56] S. Gao *et al.*, “An online hybrid BCI system based on SSVEP and EMG,” *J Neural Eng*, vol. 13, no. 2, p. 26020, Feb. 2016, doi: 10.1088/1741-2560/13/2/026020.

[57] Q. Wei, S. Zhu, Y. Wang, X. Gao, H. Guo, and X. Wu, “A training data-driven canonical correlation analysis algorithm for designing spatial filters to enhance performance of SSVEP-based BCIs,” *Int J Neural Syst*, vol. 30, no. 5, p. 2050020, Apr. 2020, doi: 10.1142/S0129065720500203.

[58] Z. Wang, Y. Yu, M. Xu, Y. Liu, E. Yin, and Z. Zhou, “Towards a hybrid BCI gaming paradigm based on motor imagery and SSVEP,” *Int J Hum Comput Interact*, vol. 35, no. 3, pp. 197–205, Feb. 2018, doi: 10.1080/10447318.2018.1445068.

[59] N. Birbaumer, T. Elbert, A. G. M. Canavan, and B. Rockstroh, “Slow potentials of the cerebral cortex and behavior.,” *Physiol Rev*, vol. 70, no. 1, pp. 1–41, 1990, doi: 10.1152/PHYSREV.1990.70.1.1.

[60] T. Hinterberger *et al.*, “Brain-computer communication and slow cortical potentials,” *IEEE Trans Biomed Eng*, vol. 51, no. 6, pp. 1011–1018, Jun. 2004, doi: 10.1109/TBME.2004.827067.

[61] "New Research Reveals the Body-Mind Connection — Hanna Sound Somatics." Accessed: Mar. 29, 2024. [Online]. Available: https://soundsomatics.net/blog/2023/7/26/homuculos-redefined-new-research-proves-body-mind-connection

[62] M. E. M. Mashat, C. T. Lin, and Di. Zhang, "Effects of task complexity on motor imagery-based brain-computer interface," *IEEE Trans Neural Syst Rehabil Eng*, vol. 27, no. 10, pp. 2178–2185, Oct. 2019, doi: 10.1109/TNSRE.2019.2936987.

[63] R. Dhiman, Priyanka, and J. S. Saini, "Motor imagery classification from human EEG signatures," *Int J Biomed Eng Technol*, vol. 26, no. 1, pp. 101–110, 2018, doi: 10.1504/IJBET.2018.089265.

[64] R. Scherer and C. Vidaurre, "Motor imagery-based brain-computer interfaces," in *Smart Wheelchairs and Brain-computer Interfaces: Mobile Assistive Technologies*, Elsevier, 2018, pp. 171–195. doi: 10.1016/B978-0-12-812892-3.00008-X.

[65] G. D. Schott, "Penfield's homunculus: a note on cerebral cartography," *J Neurol Neurosurg Psychiatry*, vol. 56, no. 4, pp. 329–333, 1993, doi: 10.1136/JNNP.56.4.329.

[66] W. Penfield and E. Boldrey, "Somatic motor and sensory representation in the cerebral cortex of man as studied by electrical stimulation," *Brain*, vol. 60, no. 4, pp. 389–443, Dec. 1937, doi: 10.1093/BRAIN/60.4.389.

[67] Y. Hou, L. Zhou, S. Jia, and X. Lun, "A novel approach of decoding EEG four-class motor imagery tasks via scout ESI and CNN," *J Neural Eng*, vol. 17, no. 1, p. 016048, Feb. 2020, doi: 10.1088/1741-2552/AB4AF6.

[68] A. Ameera, A. Saidatul, and Z. Ibrahim, "Analysis of EEG spectrum bands using power spectral density for pleasure and displeasure state," *IOP Conf Ser Mater Sci Eng*, vol. 557, no. 1, p. 012030, Jun. 2019, doi: 10.1088/1757-899X/557/1/012030.

[69] J. Minguillon, M. A. Lopez-Gordo, and F. Pelayo, "Trends in EEG-BCI for daily-life: Requirements for artifact removal," *Biomed Signal Process Control*, vol. 31, pp. 407–418, Jan. 2017, doi: 10.1016/J.BSPC.2016.09.005.

[70] G. Pfurtscheller and F. H. Lopes Da Silva, "Event-related EEG/MEG synchronization and desynchronization: Basic principles," *Clin Neurophysiol*, vol. 110, no. 11, pp. 1842–1857, Nov. 1999, doi: 10.1016/S1388-2457(99)00141-8.

[71] S. B. Erdoğan, E. Özsarfati, B. Dilek, K. S. Kadak, L. Hanoğlu, and A. Akin, "Classification of motor imagery and execution signals with population-level feature sets: Implications for probe design in fNIRS based BCI," *J Neural Eng*, vol. 16, no. 2, pp. 1–46, 2019, doi: 10.1088/1741-2552/aafdca.

[72] B. Graimann, J. E. Huggins, S. P. Levine, and G. Pfurtscheller, "Visualization of significant ERD/ERS patterns in multichannel EEG and ECoG data," *Clin Neurophysiol*, vol. 113, no. 1, pp. 43–47, 2002, doi: 10.1016/S1388-2457(01)00697-6.

[73] S. J. and A. Ra'ad, "Comparison of preprocessing algorithms using an affordable EEG headset," *Int J Comput Appl*, vol. 160, no. 1, pp. 25–31, 2017, doi: 10.5120/ijca2017912949.

[74] B. A. Moore and J. E. Barnett, "Niedermeyer's electroencephalography: Basic principles, clinical applications, and related fields," in *Case Studies in Clinical Psychological Science: Bridging the Gap from Science to Practice*, no. August, Oxford University Press, 2017, pp. 1–7. doi: 10.1093/MED/9780190228484.001.0001.

[75] K. K. Ang, Z. Y. Chin, H. Zhang, and C. Guan, "Filter Bank Common Spatial Pattern (FBCSP) in brain-computer interface," *Proc Int Jt Conf Neural Netw*, pp. 2390–2397, 2008, doi: 10.1109/IJCNN.2008.4634130.

[76] K. K. Ang, Z. Y. Chin, C. Wang, C. Guan, and H. Zhang, "Filter bank common spatial pattern algorithm on BCI competition IV datasets 2a and 2b," *Front Neurosci*, vol. 6, no. MAR, pp. 1–9, 2012, doi: 10.3389/fnins.2012.00039.

[77] R. Janapati, V. Dalal, and R. Sengupta, "Advances in modern EEG-BCI signal processing: A review," *Mater Today Proc*, vol. 80, pp. 2563–2566, Jan. 2023, doi: 10.1016/J.MATPR.2021.06.409.

[78] M. Hämäläinen, R. Hari, R. J. Ilmoniemi, J. Knuutila, and O. V. Lounasmaa, "Magnetoencephalography—theory, instrumentation, and applications to noninvasive studies of the working human brain," *Rev Mod Phys*, vol. 65, no. 2, p. 413, Apr. 1993, doi: 10.1103/RevModPhys.65.413.

[79] M. Kumngern, F. Khateb, T. Kulej, D. Arbet, and M. Akbari, "Fully differential fifth-order dual-notch low-pass filter for portable EEG system," *AEU - Int J Electron Commun*, vol. 146, p. 154122, Mar. 2022, doi: 10.1016/J.AEUE.2022.154122.

[80] M. Saber, "Removing powerline interference from EEG signal using optimized FIR filters," *J Artif Intell Metaheuristics*, vol. 1, no. 1, pp. 8–19, 2022, doi: 10.54216/JAIM.010101.

[81] S. Saba-Sadiya, E. Chantland, T. Alhanai, T. Liu, and M. M. Ghassemi, "Unsupervised EEG artifact detection and correction," *Front Digit Health*, vol. 2, p. 57, Jan. 2021, doi: 10.3389/FDGTH.2020.608920.

[82] A. Delorme, T. Sejnowski, and S. Makeig, "Enhanced detection of artifacts in EEG data using higher-order statistics and independent component analysis.," *Neuroimage*, vol. 34, no. 4, pp. 1443–9, Feb. 2007, doi: 10.1016/j.neuroimage.2006.11.004.

[83] J. Gao, C. Zheng, and P. Wang, "Online removal of muscle artifact from electroencephalogram signals based on canonical correlation analysis," *Clin EEG Neurosci*, vol. 41, no. 1, pp. 53–59, Jan. 2010, doi: 10.1177/155005941004100111.

[84] A. Kilicarslan, R. G. Grossman, and J. L. Contreras-Vidal, "A robust adaptive denoising framework for real-time artifact removal in scalp EEG measurements," *J Neural Eng*, vol. 13, no. 2, p. 026013, Feb. 2016, doi: 10.1088/1741-2560/13/2/026013.

[85] N. Kamal Al-Qazzaz, S. Hamid Bin Mohd Ali, S. Anom Ahmad, M. Shabiul Islam, and J. Escudero, "Automatic artifact removal in EEG of normal and demented individuals using ICA-WT during working memory tasks," *Sens (Switzerland)*, vol. 17, no. 6, p. 1326, Jun. 2017, doi: 10.3390/s17061326.

[86] H. Nolan, R. Whelan, and R. B. Reilly, "FASTER: Fully automated statistical thresholding for EEG artifact rejection," *J Neurosci Methods*, vol. 192, no. 1, pp. 152–162, Sep. 2010, doi: 10.1016/j.jneumeth.2010.07.015.

[87] W. De Clercq, A. Vergult, B. Vanrumste, W. Van Paesschen, and S. Van Huffel, "Canonical correlation analysis applied to remove muscle artifacts from the electroencephalogram," *IEEE Trans Biomed Eng*, vol. 53, no. 12, pp. 2583–2587, Dec. 2006, doi: 10.1109/TBME.2006.879459.

[88] C.-Y. Chang, S.-H. Hsu, L. Pion-Tonachini, and T.-P. Jung, "Evaluation of artifact subspace reconstruction for automatic artifact components removal in multi-channel EEG recordings," *IEEE Trans Biomed Eng*, vol. 67, no. 4, pp. 1114–1121, Apr. 2020, doi: 10.1109/TBME.2019.2930186.

[89] S. Blum, N. S. J. Jacobsen, M. G. Bleichner, and S. Debener, "A Riemannian modification of artifact subspace reconstruction for EEG artifact handling," *Front Hum Neurosci*, vol. 13, p. 141, Apr. 2019, doi: 10.3389/fnhum.2019.00141.

[90] F. Yger, M. Berar, and F. Lotte, "Riemannian approaches in brain-computer interfaces: A review," *IEEE Trans Neural Syst Rehabil Eng*, vol. 25, no. 10, pp. 1753–1762, Oct. 2017, doi: 10.1109/TNSRE.2016.2627016.

[91] A. Barachant, S. Bonnet, M. Congedo, and C. Jutten, "Multiclass brain-computer interface classification by Riemannian geometry," *IEEE Trans Biomed Eng*, vol. 59, no. 4, pp. 920–928, Apr. 2012, doi: 10.1109/TBME.2011.2172210.

[92] T. Uehara, T. Tanaka, and S. Fiori, "Robust averaging of covariance matrices by Riemannian geometry for motor imagery brain–computer interfacing," in *Advances in Cognitive Neurodynamics (V)*, R. Wang and X. Pan, Eds., Springer, Singapore, 2016, pp. 347–353. doi: 10.1007/978-981-10-0207-6_48.

[93] M. Congedo, A. Barachant, and R. Bhatia, "Riemannian geometry for EEG-based brain-computer interfaces; a primer and a review," *Brain-Comput Interfaces*, vol. 4, no. 3, pp. 155–174, Jul. 2017, doi: 10.1080/2326263X.2017.1297192.

[94] B. Jagadish and P. Rajalakshmi, "A novel feature extraction framework for four class motor imagery classification using log determinant regularized riemannian manifold," *Annu Int Conf IEEE Eng Med Biol Soc, EMBS*, pp. 6754–6757, 2019, doi: 10.1109/EMBC.2019.8857393.

[95] P. Gaur, R. B. Pachori, H. Wang, and G. Prasad, "A multi-class EEG-based BCI classification using multivariate empirical mode decomposition based filtering and Riemannian geometry," *Expert Syst Appl*, vol. 95, pp. 201–211, Apr. 2018, doi: 10.1016/j.eswa.2017.11.007.

[96] B. Blankertz, R. Tomioka, S. Lemm, M. Kawanabe, and K. R. Müller, "Optimizing spatial filters for robust EEG single-trial analysis," *IEEE*

Signal Process Mag, vol. 25, no. 1, pp. 41–56, 2008, doi: 10.1109/MSP.2008.4408441.

[97] H. Ramoser, J. Müller-gerking, and G. Pfurtscheller, "Optimal spatial filtering of single trial EEG during imagined hand movement," *IEEE Trans Rehabil Eng*, vol. 8, no. 4, pp. 441–446, 2000.

[98] S. Lemm, B. Blankertz, G. Curio, and K. R. Müller, "Spatio-spectral filters for improving the classification of single trial EEG," *IEEE Trans Biomed Eng*, vol. 52, no. 9, pp. 1541–1548, 2005, doi: 10.1109/TBME.2005.851521.

[99] M. Jochumsen, I. K. Niazi, N. Mrachacz-Kersting, N. Jiang, D. Farina, and K. Dremstrup, "Comparison of spatial filters and features for the detection and classification of movement-related cortical potentials in healthy individuals and stroke patients," *J Neural Eng*, vol. 12, no. 5, p. 56003, 2015, doi: 10.1088/1741-2560/12/5/056003.

[100] S. Raghu *et al.*, "Cross-database evaluation of EEG based epileptic seizures detection driven by adaptive median feature baseline correction," *Clin Neurophysiol*, vol. 131, no. 7, pp. 1567–1578, Jul. 2020, doi: 10.1016/J.CLINPH.2020.03.033.

[101] M. Gyurkovics, G. M. Clements, K. A. Low, M. Fabiani, and G. Gratton, "The impact of 1/f activity and baseline correction on the results and interpretation of time-frequency analyses of EEG/MEG data: A cautionary tale," *Neuroimage*, vol. 237, p. 118192, Aug. 2021, doi: 10.1016/J.NEUROIMAGE.2021.118192.

[102] S. K. Veeramalla and T. V. K. H. Rao, "Resampling schemes within a particle filter framework for brain source localisation," *Int J Biomed Eng Technol*, vol. 40, no. 1, pp. 18–38, 2022, doi: 10.1504/IJBET.2022.125100.

[103] P. K. Saha, M. A. Rahman, and M. N. Mollah, "Frequency domain approach in CSP based feature extraction for EEG signal classification," in *2nd Int Conf Electr Comput Commun Eng, ECCE 2019*, Institute of Electrical and Electronics Engineers Inc., Apr. 2019, pp. 7–9. doi: 10.1109/ECACE.2019.8679463.

[104] P. Ozel, A. Akan, and B. Yilmaz, "Synchrosqueezing transform based feature extraction from EEG signals for emotional state prediction," *Biomed Signal Process Control*, vol. 52, pp. 152–161, 2019, doi: 10.1016/j.bspc.2019.04.023.

[105] R. V. Wankar, P. Shah, and R. Sutar, "Feature extraction and selection methods for motor imagery EEG signals: A review," *Proceedings of 2017 International Conference on Intelligent Computing and Control, I2C2 2017*, vol. 2018-Janua, pp. 1–9, 2018, doi: 10.1109/I2C2.2017.8321831.

[106] R. Chatterjee, T. Bandyopadhyay, D. K. Sanyal, and D. Guha, "Comparative analysis of feature extraction techniques in motor imagery EEG signal classification," *Smart Innov Syst Technol*, vol. 79, 2018, doi: 10.1007/978-981-10-5828-8_8.

[107] A. Singh *et al.*, "A comprehensive review on critical issues and possible solutions of motor imagery-based electroencephalography brain-computer

interface," *Sens 2021, Vol. 21, Page 2*m*173*, vol. 21, no. 6, p. 2173, Mar. 2021, doi: 10.3390/S21062173.

[108] S. B. Lee, H. J. Kim, H. Kim, J. H. Jeong, S. W. Lee, and D. J. Ki, "Comparative analysis of features extracted from EEG spatial, spectral and temporal domains for binary and multiclass motor imagery classification," *Inf Sci (N Y)*, vol. 502, pp. 190–200, Oct. 2019, doi: 10.1016/j.ins.2019.06.008.

[109] S. A. Park, H. J. Hwang, J. H. Lim, J. H. Choi, H. K. Jung, and C. H. Im, "Evaluation of feature extraction methods for EEG-based brain-computer interfaces in terms of robustness to slight changes in electrode locations," *Med Biol Eng Comput*, vol. 51, no. 5, pp. 571–579, 2013, doi: 10.1007/s11517-012-1026-1.

[110] M. Tavakolan, Z. Frehlick, X. Yong, and C. Menon, "Classifying three imaginary states of the same upper extremity using time-domain features," *PLoS One*, vol. 12, no. 3, pp. 1–18, Mar. 2017, doi: 10.1371/journal.pone.0174161.

[111] M. Hamedi, S. H. Salleh, A. M. Noor, and I. Mohammad-Rezazadeh, "Neural network-based three-class motor imagery classification using time-domain features for BCI applications," in *IEEE TENSYMP 2014 - 2014 IEEE Region 10 Symposium*, Institute of Electrical and Electronics Engineers Inc., Jul. 2014, pp. 204–207. doi: 10.1109/TENCONSPRING.2014.6863026.

[112] O. W. Samuel, Y. Geng, X. Li, and G. Li, "Towards efficient decoding of multiple classes of motor imagery limb movements based on EEG spectral and time domain descriptors," *J Med Syst*, vol. 41, no. 12, p. 194, Dec. 2017, doi: 10.1007/S10916-017-0843-Z.

[113] P. Ofner, A. Schwarz, J. Pereira, and G. R. Müller-Putz, "Upper limb movements can be decoded from the time-domain of low-frequency EEG," *PLoS One*, vol. 12, no. 8, Aug. 2017, doi: 10.1371/journal.pone.0182578.

[114] P. T. von Hippel, "Mean, median, and skew: Correcting a textbook rule," *J stat educ*, vol. 13, no. 2, pp. 965–971, 2005, doi: 10.1080/10691898.2005.11910556.

[115] K. P. Balanda and H. L. MacGillivray, "Kurtosis: A critical review," *Am Stat*, vol. 42, no. 2, p. 111, May 1988, doi: 10.2307/2684482.

[116] S. Aydın, H. M. Saraoğlu, and S. Kara, "Log energy entropy-Based EEG classification with multilayer neural networks in seizure," *Ann Biomed Eng*, vol. 37, no. 12, pp. 2626–2630, 2009, doi: 10.1007/s10439-009-9795-x.

[117] G. Roy, A. K. Bhoi, and S. Bhaumik, "A comparative approach for MI-based EEG signals classification using energy, power and entropy," *IRBM*, vol. 43, no. 5, pp. 434–446, Oct. 2022, doi: 10.1016/J.IRBM.2021.02.008.

[118] K. K. Parhi and M. Ayinala, "Low-complexity welch power spectral density computation," *IEEE Trans Circuits Syst I: Regul Pap*, vol. 61, no. 1, pp. 172–182, Jan. 2014, doi: 10.1109/TCSI.2013.2264711.

[119] G. Roy, A. K. Bhoi, S. Das, and S. Bhaumik, "Cross-correlated spectral entropy-based classification of EEG motor imagery signal for triggering

lower limb exoskeleton," *Signal Image Video Process*, vol. 16, no. 7, pp. 1831–1839, Oct. 2022, doi: 10.1007/S11760-022-02142-1/METRICS.

[120] R. Zhang *et al.*, "Predicting inter-session performance of SMR-based brain–computer interface using the spectral entropy of resting-state EEG," *Brain Topogr*, vol. 28, no. 5, pp. 680–690, Sep. 2015, doi: 10.1007/S10548-015-0429-3/METRICS.

[121] A. F. C. Infantosi and A. M. F. L. Miranda de Sá, "A coherence-based technique for separating phase-locked from non-phase-locked power spectrum estimates during intermittent stimulation," *J Neurosci Methods*, vol. 156, no. 1–2, pp. 267–274, Sep. 2006, doi: 10.1016/j.jneumeth.2006.01.012.

[122] G. Cisotto, A. V. Guglielmi, L. Badia, and A. Zanella, "Classification of grasping tasks based on EEG-EMG coherence," in *2018 IEEE 20th International Conference on e-Health Networking, Applications and Services, Healthcom 2018*, Institute of Electrical and Electronics Engineers Inc., Nov. 2018, pp. 1–6. doi: 10.1109/HealthCom.2018.8531140.

[123] L. Leocani, C. Toro, P. Manganotti, P. Zhuang, and M. Hallett, "Event-related coherence and event-related desynchronization/synchronization in the 10 Hz and 20 Hz EEG during self- paced movements," *Electroencephalogr Clin Neurophysiol*, vol. 104, no. 3, pp. 199–206, May 1997, doi: 10.1016/S0168-5597(96)96051-7.

[124] D. Gwon and M. Ahn, "Alpha and high gamma phase amplitude coupling during motor imagery and weighted cross-frequency coupling to extract discriminative cross-frequency patterns," *Neuroimage*, vol. 240, p. 118403, Oct. 2021, doi: 10.1016/J.NEUROIMAGE.2021.118403.

[125] W. Wang, "Brain network features based on theta-gamma cross-frequency coupling connections in EEG for emotion recognition," *Neurosci Lett*, vol. 761, p. 136106, Sep. 2021, doi: 10.1016/J.NEULET.2021.136106.

[126] K. Kostoglou and G. R. Müller-Putz, "Using linear parameter varying autoregressive models to measure cross frequency couplings in EEG signals," *Front Hum Neurosci*, vol. 16, p. 915815, Sep. 2022, doi: 10.3389/FNHUM.2022.915815/BIBTEX.

[127] S. I. Dimitriadis and A. D. Marimpis, "Enhancing performance and bit rates in a brain–computer interface system with phase-to-amplitude cross-frequency coupling: Evidences from traditional c-VEP, fast c-VEP, and SSVEP designs," *Front Neuroinform*, vol. 12, p. 310299, May 2018, doi: 10.3389/FNINF.2018.00019/BIBTEX.

[128] N. Feng, F. Hu, H. Wang, and M. A. Gouda, "Decoding of voluntary and involuntary upper-limb motor imagery based on graph fourier transform and cross-frequency coupling coefficients," *J Neural Eng*, vol. 17, no. 5, p. 056043, Oct. 2020, doi: 10.1088/1741-2552/ABC024.

[129] M. Ahn, H. Cho, S. Ahn, and S. C. Jun, "High theta and low alpha powers may be indicative of BCI-illiteracy in motor imagery," *PLoS One*, vol. 8, no. 11, 2013, doi: 10.1371/journal.pone.0080886.

[130] Y. Ma, L. Zheng, Z. Yi, Y. Xiao, C. Wang, and X. Wu, "Short-time Fourier transform covariance and selection, a feature extraction method for binary

motor imagery classification," in *2021 IEEE International Conference on Real-Time Computing and Robotics, RCAR 2021*, Xining, China: Institute of Electrical and Electronics Engineers Inc., Jul. 2021, pp. 1316–1322. doi: 10.1109/RCAR52367.2021.9517461.

[131] Z. Wang, L. Cao, Z. Zhang, X. Gong, Y. Sun, and H. Wang, "Short time Fourier transformation and deep neural networks for motor imagery brain computer interface recognition," *Concurr Comput*, vol. 30, no. 23, p. e4413, Dec. 2018, doi: 10.1002/cpe.4413.

[132] H. Hindarto, A. Muntasa, and S. Sumarno, "Feature extraction electroencephalogram (EEG) using wavelet transform for cursor movement," *IOP Conf. Ser.: Mater. Sci. Eng.*, vol. 434, p. 012261, 2018, doi: 10.1088/1757-899X/434/1/012261.

[133] J. Too, A. R. Abdullah, and N. M. Saad, "Classification of hand movements based on discrete wavelet transform and enhanced feature extraction," *Int J Adv Comput Sci Appl*, vol. 10, no. 6, pp. 83–89, 2019, doi: 10.14569/ijacsa.2019.0100612.

[134] A. Y. Goharrizi and N. Sepehri, "Application of fast Fourier and wavelet transforms towards actuator leakage diagnosis: A comparative study," *Int J Fluid Power*, vol. 14, no. 2, pp. 39–51, 2013.

[135] "Classify time series using wavelet analysis and deep learning - MATLAB & Simulink example - MathWorks United Kingdom." Accessed: Jun. 14, 2021. [Online]. Available: https://uk.mathworks.com/help/wavelet/ug/classify-time-series-using-wavelet-analysis-and-deep-learning.html?s_eid=PSM_15028

[136] G. Ruffini *et al.*, "Deep learning with EEG spectrograms in rapid eye movement behavior disorder," *Front Neurol*, vol. 10, no. JUL, p. 806, 2019, doi: 10.3389/FNEUR.2019.00806.

[137] L. Yuan and J. Cao, "Patients' EEG data analysis via spectrogram image with a convolution neural network," *Smart Innov Syst Technol*, vol. 72, pp. 13–21, 2017, doi: 10.1007/978-3-319-59421-7_2.

[138] S. Ali, M. J. Ferdous, E. Hamid, and K. I. Molla, "Time-frequency coherence of multichannel EEG signals : synchrosqueezing transform based analysis," *Int j comput sci trends technol*, vol. 4, no. 3, pp. 40–48, 2016, [Online]. Available: http://www.ijcstjournal.org/volume-4/issue-3/IJCST-V4I3P8.pdf

[139] S. Mamli and H. Kalbkhani, "Gray-level co-occurrence matrix of Fourier synchro-squeezed transform for epileptic seizure detection," *Biocybern Biomed Eng*, vol. 39, no. 1, pp. 87–99, Jan. 2019, doi: 10.1016/J.BBE.2018.10.006.

[140] L. Thomas and A. K. Johnson, "Synchrosqueezing transform and its applications: A review," *Int Res J Eng Technol*, vol. 6, no. 1, pp. 1536–1541, 2019, Accessed: Dec. 23, 2020. [Online]. Available: www.irjet.net

[141] D. Degirmenci, M. Yalcin, M. A. Ozdemir, and A. Akan, "Synchrosqueezing transform in biomedical applications: A mini review," in *TIPTEKNO 2020 - Tip Teknolojileri Kongresi - 2020 Medical*

Technologies Congress, TIPTEKNO 2020, 2020, pp. 1–5. doi: 10.1109/TIPTEKNO50054.2020.9299225.

[142] J. P. Amezquita-Sanchez and H. Adeli, "Synchrosqueezed wavelet transform-fractality model for locating, detecting, and quantifying damage in smart highrise building structures," *Smart Mater Struct*, vol. 24, no. 6, p. 065034, May 2015, doi: 10.1088/0964-1726/24/6/065034.

[143] N. Karakullukcu and B. Yilmaz, "Detection of movement intention in EEG-based brain-computer interfaces using Fourier-based synchrosqueezing transform," *Int J Neural Syst*, vol. 32, no. 1, p. 2150059, Jan. 2022, doi: 10.1142/S0129065721500593.

[144] G. Sierningstrasse and E. Tel, "Common spatial patterns BCI," *Europe*, no. 43, pp. 1–20, 2010, doi: 10.2495/SC130541.

[145] H. Kang, Y. Nam, and S. Choi, "Composite common spatial pattern for subject-to-subject transfer," *IEEE Signal Process Lett*, vol. 16, no. 8, pp. 683–686, 2009, doi: 10.1109/LSP.2009.2022557.

[146] M. Mousavi and V. R. De Sa, "Temporally adaptive common spatial patterns with deep convolutional neural networks," in *Annu Int Conf IEEE Eng Med Biol Soc, EMBS*, Institute of Electrical and Electronics Engineers Inc., Jul. 2019, pp. 4533–4536. doi: 10.1109/EMBC.2019.8857423.

[147] H. Lu, K. N. Plataniotis, and A. N. Venetsanopoulos, "Regularized common spatial patterns with generic learning for EEG signal classification," *Annu Int Conf IEEE Eng Med Biol Soc, EMBC 2009*, pp. 6599–6602, 2009, doi: 10.1109/IEMBS.2009.5332554.

[148] L. Zhang, G. Liu, and Y. Wu, "Wavelet and common spatial pattern for EEG signal feature extraction and classification," *2010 International Conference on Computer, Mechatronics, Control and Electronic Engineering, CMCE 2010*, vol. 5, no. 4, pp. 243–246, 2010, doi: 10.1109/CMCE.2010.5609989.

[149] J. Khan, M. H. Bhatti, U. G. Khan, and R. Iqbal, "Multiclass EEG motor-imagery classification with sub-band common spatial patterns," *EURASIP J Wirel Commun Netw*, vol. 2019, no. 1, pp. 1–9, Dec. 2019, doi: 10.1186/S13638-019-1497-Y/TABLES/2.

[150] F. Lotte and C. Guan, "Regularizing common spatial patterns to improve BCI designs: Unified theory and new algorithms," *IEEE Trans Biomed Eng*, vol. 58, no. 2, pp. 355–362, 2011, doi: 10.1109/TBME.2010.2082539.

[151] J. Wang, Z. Feng, and N. Lu, "Feature extraction by common spatial pattern in frequency domain for motor imagery tasks classification," *Proceedings of the 29th Chinese Control and Decision Conference, CCDC 2017*, pp. 5883–5888, 2017, doi: 10.1109/CCDC.2017.7978220.

[152] Ö. Aydemir, "Common spatial pattern-based feature extraction from the best time segment of BCI data," *Tur J Electr Eng Comput Sci*, vol. 24, no. 5, pp. 3976–3986, 2016, doi: 10.3906/elk-1502-162.

[153] F. Jamaloo and M. Mikaeili, "Discriminative common spatial pattern sub-bands weighting based on distinction sensitive learning vector quantization

method in motor imagery based brain-computer interface," *J Med Signals Sens*, vol. 5, no. 3, pp. 156–161, 2015, doi: 10.4103/2228-7477.161482.

[154] E. Eilbeigi and S. K. Setarehdan, "Detecting intention to execute the next movement while performing current movement from EEG using global optimal constrained ICA," *Comput Biol Med*, vol. 99, pp. 63–75, Aug. 2018, doi: 10.1016/j.compbiomed.2018.05.024.

[155] B. Yılmaz, S. Korkmaz, D. Betül, and E. Güngör, "Like / dislike analysis using EEG : Determination of most discriminative channels and frequencies," *Comput Methods Programs Biomed*, vol. 113, no. 2, pp. 705–713, 2013, doi: 10.1016/j.cmpb.2013.11.010.

[156] S. Hou and Z. Wang, "Weighted channel dropout for regularization of deep convolutional neural network," *AAAI Conf Artif Intell*, vol. 33, no. 01, pp. 8425–8432, Jul. 2019, doi: 10.1609/AAAI.V33I01.33018425.

[157] M. Arvaneh, S. Member, C. Guan, K. K. Ang, and C. Quek, "Optimizing the channel selection and classification accuracy in EEG-based BCI," *IEEE Trans Biomed Eng*, vol. 58, no. 6, pp. 1865–1873, 2012.

[158] A. Zaitcev, G. Cook, W. Liu, M. Paley, and E. Milne, "Source localization for brain-computer interfaces," in *Intell Syst Ref Libr*, vol. 74, Springer Science and Business Media Deutschland GmbH, 2015, pp. 125–153. doi: 10.1007/978-3-319-10978-7_5/COVER.

[159] S. Saha *et al.*, "Wavelet entropy-based inter-subject associative cortical source localization for sensorimotor BCI," *Front Neuroinform*, vol. 13, p. 429736, Jul. 2019, doi: 10.3389/FNINF.2019.00047/BIBTEX.

[160] X. Peng, J. Liu, Y. Huang, Y. Mao, and D. Li, "Classification of lower limb motor imagery based on iterative EEG source localization and feature fusion," *Neural Comput Appl*, vol. 35, no. 19, pp. 13711–13724, Jul. 2023, doi: 10.1007/S00521-021-06761-6/FIGURES/17.

[161] T. Frikha *et al.*, "Source localization of EEG brainwaves activities via mother wavelets families for SWT decomposition," *J Healthc Eng*, vol. 2021, p. 11, 2021, doi: 10.1155/2021/9938646.

[162] E. Guttmann-Flury, X. Sheng, and X. Zhu, "Channel selection from source localization: A review of four EEG-based brain–computer interfaces paradigms," *Behav Res Methods*, vol. 55, no. 4, pp. 1980–2003, Jul. 2022, doi: 10.3758/S13428-022-01897-2.

[163] P. Arpaia, F. Donnarumma, A. Esposito, and M. Parvis, "Channel selection for optimal EEG measurement in motor imagery-based brain-computer interfaces," *Int J Neural Syst*, vol. 31, no. 3, p. 2150003, 2021, doi: 10.1142/S0129065721500039.

[164] J. León, J. Ortega, and A. Ortiz, "Convolutional neural networks and feature selection for BCI with multiresolution analysis," *Lecture Notes in Computer Science (including subseries Lecture Notes in Artificial Intelligence and Lecture Notes in Bioinformatics)*, vol. 11506 LNCS, pp. 883–894, 2019, doi: 10.1007/978-3-030-20521-8_72/COVER.

[165] A. Al-Nafjan, “Feature selection of EEG signals in neuromarketing,” *PeerJ Comput Sci*, vol. 8, p. e944, Apr. 2022, doi: 10.7717/PEERJ-CS.944/SUPP-1.

[166] T. Thenmozhi and R. Helen, “Feature selection using extreme gradient boosting bayesian optimization to upgrade the classification performance of motor imagery signals for BCI,” *J Neurosci Methods*, vol. 366, p. 109425, Jan. 2022, doi: 10.1016/J.JNEUMETH.2021.109425.

[167] D. J. McFarland and J. R. Wolpaw, “Sensorimotor rhythm-based brain-computer interface (BCI): Feature selection by regression improves performance,” *IEEE Trans Neural Syst Rehabil Eng*, vol. 13, no. 3, pp. 372–379, Sep. 2005, doi: 10.1109/TNSRE.2005.848627.

[168] Z. Yin, Y. Wang, L. Liu, W. Zhang, and J. Zhang, “Cross-subject EEG feature selection for emotion recognition using transfer recursive feature elimination,” *Front Neurorobot*, vol. 11, no. APR, p. 249397, Apr. 2017, doi: 10.3389/FNBOT.2017.00019/BIBTEX.

[169] E. Gysels, P. Renevey, and P. Celka, “SVM-based recursive feature elimination to compare phase synchronization computed from broadband and narrowband EEG signals in Brain–Computer Interfaces,” *Signal Process*, vol. 85, no. 11, pp. 2178–2189, Nov. 2005, doi: 10.1016/J.SIGPRO.2005.07.008.

[170] K. K. Ang, Z. Y. Chin, H. Zhang, and C. Guan, “Mutual information-based selection of optimal spatial–temporal patterns for single-trial EEG-based BCIs,” *Pattern Recognit*, vol. 45, no. 6, pp. 2137–2144, Jun. 2012, doi: 10.1016/J.PATCOG.2011.04.018.

[171] S. Bekiryazici, A. Demir, and G. Yilmaz, “Feature selection and analysis EEG signals with sequential forward selection algorithm and different classifiers,” in *2020 28th Signal Processing and Communications Applications Conference, SIU 2020 - Proceedings*, Institute of Electrical and Electronics Engineers Inc., Oct. 2020, pp. 1–4. doi: 10.1109/SIU49456.2020.9302482.

[172] M. Radman, A. Chaibakhsh, N. Nariman-Zadeh, and H. He, “Generalized sequential forward selection method for channel selection in EEG signals for classification of left or right hand movement in BCI,” in *2019 9th International Conference on Computer and Knowledge Engineering, ICCKE 2019*, Institute of Electrical and Electronics Engineers Inc., Oct. 2019, pp. 137–142. doi: 10.1109/ICCKE48569.2019.8965159.

[173] J. A. O’Reilly and W. Chanmittakul, “L1 regularization-based selection of EEG spectral power and ECG features for classification of cognitive state,” in *Proceeding of the 2021 9th International Electrical Engineering Congress, iEECON 2021*, Institute of Electrical and Electronics Engineers Inc., Mar. 2021, pp. 365–368. doi: 10.1109/IEECON51072.2021.9440359.

[174] K. Djelloul and A. N. Belkacem, “EEG classification-based comparison study of motor-imagery brain-computer interface,” in *Proceedings - 2021 IEEE International Conference on Recent Advances in Mathematics and Informatics, ICRAMI 2021*, Institute of Electrical and Electronics Engineers Inc., 2021, pp. 1–16. doi: 10.1109/ICRAMI52622.2021.9585902.

[175] A. Al-Saegh, S. A. Dawwd, and J. M. Abdul-Jabbar, “Deep learning for motor imagery EEG-based classification: A review,” *Biomed Signal Process Control*, vol. 63. Elsevier Ltd, pp. 1746–8094, Jan. 01, 2021. doi: 10.1016/j.bspc.2020.102172.

[176] S. R. Sreeja, J. Rabha, K. Y. Nagarjuna, D. Samanta, P. Mitra, and M. Sarma, “Motor imagery EEG signal processing and classification using machine learning approach,” *Proceedings - 2017 International Conference on New Trends in Computing Sciences, ICTCS 2017*, vol. 2018-Janua, pp. 61–66, 2017, doi: 10.1109/ICTCS.2017.15.

[177] F. Lotte, M. Congedo, A. Lécuyer, F. Lamarche, and B. Arnaldi, “A review of classification algorithms for EEG-based brain-computer interfaces,” *J Neural Eng*, vol. 4, no. 2, pp. R1–R13, Jun. 2007, doi: 10.1088/1741-2560/4/2/R01.

[178] R. Fu, Y. Tian, T. Bao, Z. Meng, and P. Shi, “Improvement motor imagery EEG classification based on regularized linear discriminant analysis,” *J Med Syst*, vol. 43, no. 6, pp. 1–13, Jun. 2019, doi: 10.1007/S10916-019-1270-0/METRICS.

[179] E. Hortal, A. Ubeda, E. Ianez, D. Planelles, and J. M. Azorin, “Online classification of two mental tasks using a SVM-based BCI system,” in *Int IEEE/EMBS Conf Neural Eng, NER*, 2013. doi: 10.1109/NER.2013.6696181.

[180] R. Chatterjee and T. Bandyopadhyay, “EEG based motor imagery classification using SVM and MLP,” *Int Conf Comput Intell Netw*, vol. 2016-Janua, pp. 84–89, 2016, doi: 10.1109/CINE.2016.22.

[181] M. J. Antony *et al.*, “Classification of EEG using adaptive SVM classifier with CSP and online recursive independent component analysis,” *Sens*, vol. 22, no. 19, p. 7596, Oct. 2022, doi: 10.3390/S22197596.

[182] K. M. R. Alam, N. Siddique, and H. Adeli, “A dynamic ensemble learning algorithm for neural networks,” *Neural Comput Appl*, vol. 32, no. 12, pp. 8675–8690, Jun. 2020, doi: 10.1007/s00521-019-04359-7.

[183] M. Mohammadpour, M. K. Ghorbanian, and S. Mozaffari, “Comparison of EEG signal features and ensemble learning methods for motor imagery classification,” *2016 8th International Conference on Information and Knowledge Technology, IKT 2016*, pp. 288–292, 2016, doi: 10.1109/IKT.2016.7777767.

[184] D. Diáz-Vico *et al.*, “Deep support vector neural networks,” *Integr Comput Aided Eng*, vol. 27, no. 4, pp. 389–402, Jan. 2020, doi: 10.3233/ICA-200635.

[185] S. H. Ling, H. Makgawinata, F. H. Monsivais, A. Dos Santos Goncalves Lourenco, J. Lyu, and R. Chai, “Classification of EEG motor imagery tasks using convolution neural networks,” *Conf Proc IEEE Eng Med Biol Soc*, vol. 2019, pp. 758–761, 2019, doi: 10.1109/EMBC.2019.8857933.

[186] M. K. Alom and S. M. R. Islam, “Classification for the P300-based brain computer interface (BCI),” in *2020 2nd International Conference on Advanced Information and Communication Technology, ICAICT 2020*,

Institute of Electrical and Electronics Engineers Inc., Nov. 2020, pp. 387–391. doi: 10.1109/ICAICT51780.2020.9333481.

[187] X. Tang, T. Wang, Y. Du, and Y. Dai, “Motor imagery EEG recognition with KNN-based smooth auto-encoder,” *Artif Intell Med*, vol. 101, p. 101747, Nov. 2019, doi: 10.1016/J.ARTMED.2019.101747.

[188] M. N. A. H. Sha’abani, N. Fuad, N. Jamal, and M. F. Ismail, “kNN and SVM classification for EEG: A review,” in *Lect Notes Electr Eng*, Springer, 2020, pp. 555–565. doi: 10.1007/978-981-15-2317-5_47/COVER.

[189] A. Subasi and S. Mian Qaisar, “The ensemble machine learning-based classification of motor imagery tasks in brain-computer interface,” *J Healthc Eng*, vol. 2021, p. 12, 2021, doi: 10.1155/2021/1970769.

[190] P. N. Paranjape, M. M. Dhabu, P. S. Deshpande, and A. M. Kekre, “Cross-correlation aided ensemble of classifiers for BCI oriented EEG study,” *IEEE Access*, vol. 7, pp. 11985–11996, 2019, doi: 10.1109/ACCESS.2019.2892492.

[191] L. Zhang, D. Wen, C. Li, and R. Zhu, “Ensemble classifier based on optimized extreme learning machine for motor imagery classification,” *J Neural Eng*, vol. 17, no. 2, p. 026004, Mar. 2020, doi: 10.1088/1741-2552/AB7264.

[192] D. Pawar and S. Dhage, “EEG-based covert speech decoding using random rotation extreme learning machine ensemble for intuitive BCI communication,” *Biomed Signal Process Control*, vol. 80, p. 104379, Feb. 2023, doi: 10.1016/J.BSPC.2022.104379.

[193] C. Nasa, “Evaluation of different classification techniques for WEB data,” *Int J Comput Appl*, vol. 52, no. 9, 2012.

[194] Y. Li, G. Zhou, D. Graham, and A. Holtzhauer, “Towards an EEG-based brain-computer interface for online robot control,” *Multimed Tools Appl*, vol. 75, no. 13, pp. 7999–8017, Jul. 2016, doi: 10.1007/s11042-015-2717-z.

[195] B. Hamadicharef, “AUC confidence bounds for performance evaluation of brain-computer interface,” in *Proceedings - 2010 3rd International Conference on Biomedical Engineering and Informatics, BMEI 2010*, 2010, pp. 1988–1991. doi: 10.1109/BMEI.2010.5639671.

[196] N. E. Binti Md Isa, A. Amir, M. Z. Ilyas, and M. S. Razalli, “Motor imagery classification in brain computer interface (BCI) based on EEG signal by using machine learning technique,” *Bulletin of Electrical Engineering and Informatics*, vol. 8, no. 1, pp. 269–275, Mar. 2019, doi: 10.11591/EEI.V8I1.1402.

[197] E. Bojorges-Valdez, J. C. Echeverría, and O. Yanez-Suarez, “Evaluation of the continuous detection of mental calculation episodes as a BCI control input,” *Comput Biol Med*, vol. 64, pp. 155–162, Sep. 2015, doi: 10.1016/J.COMPBIOMED.2015.06.014.

[198] M. Billinger *et al.*, “Is it significant? Guidelines for reporting BCI performance,” in *Towards Practical Brain-Computer Interfaces*, Springer,

Berlin, Heidelberg, 2012, pp. 333–354. doi: 10.1007/978-3-642-29746-5_17.

[199] M. N. Alam, M. I. Ibrahimy, and S. M. A. Motakabber, “Feature extraction of EEG signal by power spectral density for motor imagery based BCI,” in *Proceedings of the 8th International Conference on Computer and Communication Engineering, ICCCE 2021*, Institute of Electrical and Electronics Engineers Inc., Jun. 2021, pp. 234–237. doi: 10.1109/ICCCE50029.2021.9467141.

[200] A. Schlögl, F. Lee, H. Bischof, and G. Pfurtscheller, “Characterization of four-class motor imagery EEG data for the BCI-competition 2005,” *J Neural Eng*, vol. 2, no. 4, p. L14, Aug. 2005, doi: 10.1088/1741-2560/2/4/L02.

[201] S. Sadeghi and A. Maleki, “Accurate estimation of information transfer rate based on symbol occurrence probability in brain-computer interfaces,” *Biomed Signal Process Control*, vol. 54, p. 101607, Sep. 2019, doi: 10.1016/J.BSPC.2019.101607.

[202] R. Zhang *et al.*, “The effect of stimulus number on the recognition accuracy and information transfer rate of SSVEP–BCI in augmented reality,” *J Neural Eng*, vol. 19, no. 3, p. 036010, May 2022, doi: 10.1088/1741-2552/AC6AE5.

[203] D. J. McFarland, W. A. Sarnacki, and J. R. Wolpaw, “Brain–computer interface (BCI) operation: optimizing information transfer rates,” *Biol Psychol*, vol. 63, no. 3, pp. 237–251, Jul. 2003, doi: 10.1016/S0301-0511(03)00073-5.

[204] A. Burns, H. Adeli, and J. A. Buford, “Brain-computer interface after nervous system injury,” *Neuroscientist*, vol. 20, no. 6. SAGE Publications Inc., pp. 639–651, Dec. 20, 2014. doi: 10.1177/1073858414549015.

[205] A. Ortiz-Rosario and H. Adeli, “Brain-computer interface technologies: From signal to action,” *Rev Neurosci*, vol. 24, no. 5, pp. 537–552, Oct. 2013, doi: 10.1515/revneuro-2013-0032.

[206] F. Stojic and T. Chau, “Nonspecific visuospatial imagery as a novel mental task for online EEG-based BCI control,” *Int J Neural Syst*, vol. 30, no. 6, p. 2050026, Jun. 2020, doi: 10.1142/S0129065720500264.

[207] J. J *et al.*, “Optimization of Model Training Based on Iterative Minimum Covariance Determinant In Motor-Imagery BCI,” *Int J Neural Syst*, vol. 31, no. 7, p. 2150030, Jul. 2021, doi: 10.1142/S0129065721500301.

[208] C. Ieracitano, F. C. Morabito, A. Hussain, and N. Mammone, “A hybrid-domain deep learning-based BCI for discriminating hand motion planning from EEG sources,” *Int J Neural Syst*, vol. 31, no. 9, p. 2150038, Aug. 2021, doi: 10.1142/S0129065721500386.

[209] H. Sun, J. Jin, R. Xu, and A. Cichocki, “Feature selection combining filter and wrapper methods for motor-imagery based brain–computer interfaces,” *Int J Neural Syst*, vol. 31, no. 9, p. 2150040, Aug. 2021, doi: 10.1142/S0129065721500404.

[210] A. Ortiz-Rosario, I. Berrios-Torres, H. Adeli, and J. A. Buford, “Combined corticospinal and reticulospinal effects on upper limb muscles,” *Neurosci Lett*, vol. 561, p. 30, Feb. 2014, doi: 10.1016/J.NEULET.2013.12.043.

[211] SH. George, MH. Rafiei, L. Gauthier, A. Borstad, JA. Buford, and H. Adeli, “Computer-aided prediction of extent of motor recovery following constraint-induced movement therapy in chronic stroke,” *Behav Brain Res*, vol. 329, pp. 191–199, Jun. 2017, doi: 10.1016/J.BBR.2017.03.012.

[212] A. Burns and H. Adeli, “Wearable technology for patients with brain and spinal cord injuries,” *Rev Neurosci*, vol. 28, no. 8, pp. 913–920, Nov. 2017, doi: 10.1515/REVNEURO-2017-0035.

[213] Y. Mao, J. Jin, R. Xu, S. Li, Y. Miao, and A. Cichocki, “The influence of visual attention on the performance of a novel tactile P300 brain-computer interface with cheeks-stim paradigm,” *Int J Neural Syst*, vol. 31, no. 4, Apr. 2021, doi: 10.1142/S0129065721500040.

[214] A. Lozano *et al.*, “Neurolight: A deep learning neural interface for cortical visual prostheses,” *Int J Neural Syst*, vol. 30, no. 9, Sep. 2020, doi: 10.1142/S0129065720500458.

[215] M. K. Andrade *et al.*, “An EEG brain-computer interface to classify motor imagery signals,” in *Biomed Signal Process*, G. Naik, Ed., Springer, Singapore, 2020, pp. 83–98. doi: 10.1007/978-981-13-9097-5_5.

[216] E. López-Larraz, L. Montesano, Á. Gil-Agudo, and J. Minguez, “Continuous decoding of movement intention of upper limb self-initiated analytic movements from pre-movement EEG correlates,” *J Neuroeng Rehabil*, vol. 11, no. 1, pp. 1–15, 2014, doi: 10.1186/1743-0003-11-153.

[217] D. Zapała *et al.*, “The effects of handedness on sensorimotor rhythm desynchronization and motor-imagery BCI control,” *Sci Rep*, vol. 10, no. 1, Dec. 2020, doi: 10.1038/s41598-020-59222-w.

[218] S. Meignen, T. Oberlin, and D. H. Pham, “Synchrosqueezing transforms: From low- to high-frequency modulations and perspectives,” *Comptes Rendus Physique*, vol. 20, no. 5. Elsevier Masson SAS, pp. 449–460, Jul. 01, 2019. doi: 10.1016/j.crhy.2019.07.001.

[219] I. Daubechies and S. Maes, “A nonlinear squeezing of the continuous wavelet transform based on auditory nerve models,” in *Wavelets in Medicine and Biology*, CRC Press, 1996, pp. 527–546. doi: 10.1201/9780203734032-20.

[220] J. P. Amezquita-Sanchez and H. Adeli, “Synchrosqueezed wavelet transform-fractality model for locating, detecting, and quantifying damage in smart highrise building structures,” *Smart Mater Struct*, vol. 24, no. 6, p. 065034, May 2015, doi: 10.1088/0964-1726/24/6/065034.

[221] C. A. Perez-Ramirez, J. P. Amezquita-Sanchez, H. Adeli, M. Valtierra-Rodriguez, D. Camarena-Martinez, and R. J. Romero-Troncoso, “New methodology for modal parameters identification of smart civil structures using ambient vibrations and synchrosqueezed wavelet transform,” *Eng Appl Artif Intell*, vol. 48, pp. 1–12, Feb. 2016, doi: 10.1016/J.ENGAPPAI.2015.10.005.

[222] Z. Li, H. S. Park, and H. Adeli, “New method for modal identification of super high-rise building structures using discretized synchrosqueezed wavelet and Hilbert transforms,” *Struct Des Tall Build*, vol. 26, no. 3, p. e1312, Feb. 2017, doi: 10.1002/TAL.1312.

[223] A. Mert and A. Akan, “Emotion recognition based on time–frequency distribution of EEG signals using multivariate synchrosqueezing transform,” *Digit Signal Process*, vol. 81, pp. 106–115, Oct. 2018, doi: 10.1016/j.dsp.2018.07.003.

[224] H. T. Wu, Y. H. Chan, Y. T. Lin, and Y. H. Yeh, “Using synchrosqueezing transform to discover breathing dynamics from ECG signals,” *Appl Comput Harmon Anal*, vol. 36, no. 2, pp. 354–359, Mar. 2014, doi: 10.1016/j.acha.2013.07.003.

[225] C. L. Herry, M. Frasch, A. J. E. Seely, and H. T. Wu, “Heart beat classification from single-lead ECG using the synchrosqueezing transform,” *Physiol Meas*, vol. 38, no. 2, pp. 171–187, Feb. 2017, doi: 10.1088/1361-6579/aa5070.

[226] g.tec, “g.tec medical engineering.” Accessed: Sep. 22, 2019. [Online]. Available: http://www.gtec.at/Products/Electrodes-and-Sensors/g.SAHARA-Specs-Features

[227] I. Daubechies, J. Lu, and H.-T. Wu, “Synchrosqueezed wavelet transforms: An empirical mode decomposition-like tool,” *Appl Comput Harmon Anal*, vol. 30, pp. 243–261, 2011, doi: 10.1016/j.acha.2010.08.002.

[228] S. T. Veena and M. N. Sumaiya, “Human emotion classification using EEG signals by multivariate synchrosqueezing transform,” *Learning and Analytics in Intelligent Systems* vol. 6, pp. 179–204, 2020, doi: 10.1007/978-3-030-35139-7_9.

[229] S. Aydın, H. M. Saraoğlu, and S. Kara, “Log energy entropy-Based EEG classification with multilayer neural networks in seizure,” *Ann Biomed Eng*, vol. 37, no. 12, pp. 2626–2630, 2009, doi: 10.1007/s10439-009-9795-x.

[230] F. Lotte, M. Congedo, A. Lécuyer, F. Lamarche, and B. Arnaldi, “A review of classification algorithms for EEG-based brain-computer interfaces,” *J Neural Eng*, vol. 4, no. 2, pp. R1–R13, 2007, doi: 10.1088/1741-2560/4/2/R01.

[231] MathWorks, “Choose classifier options - MATLAB & Simulink,” 2019. Accessed: Dec. 18, 2019. [Online]. Available: https://www.mathworks.com/help/stats/choose-a-classifier.html

[232] I. K. Niazi, N. Mrachacz-Kersting, N. Jiang, K. Dremstrup, and D. Farina, “Peripheral electrical stimulation triggered by self-paced detection of motor intention enhances motor evoked potentials,” *IEEE Trans Neural Syst Rehabil Eng*, vol. 20, no. 4, pp. 595–604, 2012, doi: 10.1109/TNSRE.2012.2194309.

[233] P. Ahmadian, S. Sanei, L. Ascari, L. Gonzalez-Villanueva, and M. Alessandra Umilta, “Constrained blind source extraction of readiness potentials from EEG,” *IEEE Trans Neural Syst Rehabil Eng*, vol. 21, no. 4, pp. 567–575, 2013, doi: 10.1109/TNSRE.2012.2227278.

[234] M. Jochumsen, I. Khan Niazi, D. Taylor, D. Farina, and K. Dremstrup, “Detecting and classifying movement-related cortical potentials associated with hand movements in healthy subjects and stroke patients from single-electrode, single-trial EEG,” *J Neural Eng*, vol. 12, no. 5, p. 56013, 2015, doi: 10.1088/1741-2560/12/5/056013.

[235] R. Xu, N. Jiang, C. Lin, N. Mrachacz-Kersting, K. Dremstrup, and D. Farina, “Enhanced low-latency detection of motor intention from EEG for closed-loop brain-computer interface applications,” *IEEE Trans Biomed Eng*, vol. 61, no. 2, pp. 288–296, 2014, doi: 10.1109/TBME.2013.2294203.

[236] S. Aliakbaryhosseinabadi, N. Jiang, A. Vuckovic, K. Dremstrup, D. Farina, and N. Mrachacz-Kersting, “Detection of movement intention from single-trial movement-related cortical potentials using random and non-random paradigms,” *Brain-Comput Interfaces*, vol. 2, no. 1, pp. 29–39, 2015, doi: 10.1080/2326263X.2015.1053301.

[237] K. Wang, M. Xu, Y. Wang, S. Zhang, L. Chen, and D. Ming, “Enhance decoding of pre-movement EEG patterns for brain-computer interfaces,” *J Neural Eng*, vol. 17, no. 1, 2020, doi: 10.1088/1741-2552/ab598f.

[238] G. Rodríguez-Bermúdez, P. J. García-Laencina, and J. Roca-Dorda, “Efficient automatic selection and combination of eeg features in least squares classifiers for motor imagery brain-computer interfaces,” *Int J Neural Syst*, vol. 23, no. 4, 2013, doi: 10.1142/S0129065713500159.

[239] P. Ahmadian, S. Sanei, L. Ascari, L. Gonzalez-Villanueva, and M. Alessandra Umilta, “Constrained blind source extraction of readiness potentials from EEG,” *IEEE Trans Neural Syst Rehabil Eng*, vol. 21, no. 4, pp. 567–575, 2013, doi: 10.1109/TNSRE.2012.2227278.

[240] I. K. Niazi, N. Jiang, O. Tiberghien, J. F. Nielsen, K. Dremstrup, and D. Farina, “Detection of movement intention from single-trial movement-related cortical potentials,” *J Neural Eng*, vol. 8, no. 6, 2011, doi: 10.1088/1741-2560/8/6/066009.

[241] N. Jiang, L. Gizzi, N. Mrachacz-kersting, K. Dremstrup, and D. Farina, “A brain – computer interface for single-trial detection of gait initiation from movement related cortical potentials,” *Clin Neurophysiol*, vol. 126, no. 1, pp. 154–159, 2015, doi: 10.1016/j.clinph.2014.05.003.

[242] S. Madhavan, R. K. Tripathy, and R. B. Pachori, “Time-frequency domain deep convolutional neural network for the classification of focal and non-focal EEG signals,” *IEEE Sens J*, vol. 20, no. 6, pp. 3078–3086, 2020, doi: 10.1109/JSEN.2019.2956072.

[243] M. H. Rafiei and H. Adeli, “A new neural dynamic classification algorithm,” *IEEE Trans Neural Netw Learn Syst*, vol. 28, no. 12, pp. 3074–3083, Dec. 2017, doi: 10.1109/TNNLS.2017.2682102.

[244] D. R. Pereira, M. A. Piteri, A. N. Souza, J. P. Papa, and H. Adeli, “FEMa: a finite element machine for fast learning,” *Neural Comput Appl*, vol. 32, no. 10, pp. 6393–6404, May 2020, doi: 10.1007/s00521-019-04146-4.

[245] J. Zhang, M. Xiao, L. Gao, and S. Chu, “Probability and interval hybrid reliability analysis based on adaptive local approximation of projection

outlines using support vector machine," *Comput-Aided Civ Infrastruct Eng*, vol. 34, no. 11, pp. 991–1009, Nov. 2019, doi: 10.1111/MICE.12480.

[246] R. Sánchez-Reolid, A. Martínez-Rodrigo, MT. López, and A. Fernández-Caballero, "Deep support vector machines for the identification of stress condition from electrodermal activity," *Int J Neural Syst*, vol. 30, no. 7, Jul. 2020, doi: 10.1142/S0129065720500318.

[247] R. N. Scott and P. A. Parker, "Myoelectric prostheses: state of the art," *J Med Eng Technol*, vol. 12, no. 4, pp. 143–151, 1988, doi: 10.3109/03091908809030173.

[248] A. Fougner, O. Stavdahl, P. J. Kyberd, Y. G. Losier, and P. A. Parker, "Control of upper limb prostheses: Terminology and proportional myoelectric control a review," *IEEE Trans Neural Syst Rehabil Eng*, vol. 20, no. 5, pp. 663–677, 2012, doi: 10.1109/TNSRE.2012.2196711.

[249] S. Chaudhary, S. Taran, V. Bajaj, and A. Sengur, "Convolutional neural network-based approach towards motor imagery tasks EEG signals classification," *IEEE Sens J*, vol. 19, no. 12, pp. 4494–4500, Jun. 2019, doi: 10.1109/JSEN.2019.2899645.

[250] D. Zapała *et al.*, "The effects of handedness on sensorimotor rhythm desynchronization and motor-imagery BCI control," *Sci Rep*, vol. 10, no. 1, pp. 1–11, Feb. 2020, doi: 10.1038/s41598-020-59222-w.

[251] N. Karakullukcu and B. Yilmaz, "Discrimination of rest, motor imagery and movement for brain-computer interface applications," in *2018 Medical Technologies National Congress (TIPTEKNO), Magusa*, 2018, pp. 1-4. doi: 10.1109/TIPTEKNO.2018.8597152.

[252] M. I. Singh and M. Singh, "Development of a real time emotion classifier based on evoked EEG," *Biocybern Biomed Eng*, vol. 37, no. 3, pp. 498–509, Jan. 2017, doi: 10.1016/J.BBE.2017.05.004.

[253] R. K. Tripathy and U. Rajendra Acharya, "Use of features from RR-time series and EEG signals for automated classification of sleep stages in deep neural network framework," *Biocybern Biomed Eng*, vol. 38, no. 4, pp. 890–902, Jan. 2018, doi: 10.1016/J.BBE.2018.05.005.

[254] M. D. Luciw, E. Jarocka, and B. B. Edin, "Multi-channel EEG recordings during 3,936 grasp and lift trials with varying weight and friction," *Sci Data*, vol. 1, pp. 1–11, 2014, doi: 10.1038/sdata.2014.47.

[255] S. Zhang, Z. Zhu, B. Zhang, B. Feng, T. Yu, and Z. Li, "The CSP-based new features plus non-convex log sparse feature selection for motor imagery EEG classification," *Sens*, vol. 20, no. 17, p. 4749, Aug. 2020, doi: 10.3390/S20174749.

[256] N. Yu, R. Yang, and M. Huang, "Deep Common Spatial Pattern based Motor Imagery Classification with Improved Objective Function," *International Journal of Network Dynamics and Intelligence*, pp. 73–84, Dec. 2022, doi: 10.53941/ijndi0101007.

[257] L. Thomas and A. K. Johnson, "Synchrosqueezing transform and its applications: A review," *Int Res J Eng Technol*, vol. 6, no. 1, pp. 1536–1541, 2019, Accessed: Aug. 25, 2021. [Online]. Available: www.irjet.net

[258] O. K. Cura and A. Akan, “Classification of epileptic EEG signals using synchrosqueezing transform and machine learning,” *Int J Neural Syst*, vol. 31, no. 5, May 2021, doi: 10.1142/S0129065721500052.

[259] H. Sugata, M. Hirata, T. Yanagisawa, K. Matsushita, S. Yorifuji, and T. Yoshimine, “Common neural correlates of real and imagined movements contributing to the performance of brain–machine interfaces,” *Sci Rep*, vol. 6, no. 1, pp. 1–11, Apr. 2016, doi: 10.1038/srep24663.

[260] T. Trakoolwilaiwan, B. Behboodi, J. Lee, K. Kim, and J.-W. Choi, “Convolutional neural network for high-accuracy functional near-infrared spectroscopy in a brain–computer interface: three-class classification of rest, right-, and left-hand motor execution,” *Neurophotonics*, vol. 5, no. 01, p. 1, Sep. 2017, doi: 10.1117/1.nph.5.1.011008.

[261] L. Jinbo and S. Shiliang, “Energy feature extraction of EEG signals and a case study,” in *Proc Int Jt Conf Neural Netw*, 2008, pp. 2366–2370. doi: 10.1109/IJCNN.2008.4634126.

[262] P. Gonzalez-Navarro, Y. M. Marghi, B. Azari, M. Akcakaya, and D. Erdogmus, “An event-driven AR-process model for EEG-based BCIs with rapid trial sequences,” *IEEE Trans Neural Syst Rehabil Eng*, vol. 27, no. 5, pp. 798–804, 2019, doi: 10.1109/TNSRE.2019.2903840.

[263] J. Luo, W. He, and C. Yang, “Combined perception, control, and learning for teleoperation: key technologies, applications, and challenges,” *Cogn Comput Syst*, vol. 2, no. 2, pp. 33–43, Jun. 2020, doi: 10.1049/CCS.2020.0005.

[264] Ü. Budak, A. Sengur, and M. Aslan, “Airport detection in remote sensing images using gray level co-occurrence matrix and artificial neural network,” in *International Artificial Intelligence and Data Processing Symposium (IDAP’16)*, 2016, pp. 108–112. [Online]. Available: https://www.researchgate.net/publication/322064068

[265] A. Caliskan and B. Ergen, “GRI seviye eş-oluşum matrisi tabanli avuç içi tanima sistemi,” in *2014 22nd Signal Processing and Communications Applications Conference, SIU 2014 - Proceedings*, IEEE Computer Society, 2014, pp. 826–829. doi: 10.1109/SIU.2014.6830357.

[266] R. M. Haralick, I. Dinstein, and K. Shanmugam, “Textural features for image classification,” *IEEE Trans Syst Man Cybern*, vol. SMC-3, no. 6, pp. 610–621, 1973, doi: 10.1109/TSMC.1973.4309314.

[267] R. Mane *et al.*, “Prognostic and monitory EEG-biomarkers for BCI upper-limb stroke rehabilitation,” *IEEE Trans Neural Syst Rehabil Eng*, vol. 27, no. 8, pp. 1654–1664, Aug. 2019, doi: 10.1109/TNSRE.2019.2924742.

[268] A. Mansoor, M. W. Usman, N. Jamil, and M. A. Naeem, “Deep learning algorithm for brain-computer interface,” *Sci Program*, vol. 2020, p. 12, 2020, doi: 10.1155/2020/5762149.

[269] J. Fregoso, C. I. Gonzalez, and G. E. Martinez, “Optimization of convolutional neural networks architectures using PSO for sign language recognition,” *Axioms 2021, Vol. 10, Page 139*, vol. 10, no. 3, p. 139, Jun. 2021, doi: 10.3390/AXIOMS10030139.

[270] Ö. Türk, "EEG işaretlerinden epilepsi türlerinin sınıflandırılmasında skalogram tabanlı derin öğrenme yaklaşımı," Dicle Üniversitesi, Fen Bilimleri Enstitüsü, Diyarbakır, 2019. Accessed: Nov. 24, 2022. [Online]. Available: http://acikerisim.dicle.edu.tr/xmlui/handle/11468/5116

[271] Y. Yang, Q. Wu, Y. Fu, and X. Chen, *Continuous convolutional neural network with 3D input for EEG-based emotion recognition*, vol. 11307 LNCS. Springer International Publishing, 2018. doi: 10.1007/978-3-030-04239-4_39.

[272] M. B. I. Reaz, M. S. Hussain, and F. Mohd-Yasin, "Techniques of EMG signal analysis: detection, processing, classification and applications," *Biol Proced Online*, vol. 8, no. 1, p. 11, Mar. 2006, doi: 10.1251/BPO115.

[273] A. T. Poyil, V. Steuber, and F. Amirabdollahian, "Adaptive robot mediated upper limb training using electromyogram-based muscle fatigue indicators," *PLoS One*, vol. 15, no. 5, p. e0233545, May 2020, doi: 10.1371/JOURNAL.PONE.0233545.

[274] M. A. Ozdemir, D. H. Kisa, O. Guren, A. Onan, and A. Akan, "EMG based hand gesture recognition using deep learning," in *TIPTEKNO 2020 - Tip Teknolojileri Kongresi - 2020 Medical Technologies Congress, TIPTEKNO 2020*, Antalya, Turkey: Institute of Electrical and Electronics Engineers Inc., Nov. 2020, pp. 1–4. doi: 10.1109/TIPTEKNO50054.2020.9299264.

[275] C. H. Shameem Sharmina and R. Reghunadhan, "Electromyography-based detection of human hand movement gestures," in *Advances in Machine Learning and Computational Intelligence*, Springer, Singapore, 2021, pp. 729–735. doi: 10.1007/978-981-15-5243-4_69.

[276] U. Maoz and E. Lashgari, "Dimensionality reduction for classification of object weight from electromyography," *PLoS One*, vol. 16, no. 8 August, p. 0255926, Aug. 2021, doi: 10.1371/JOURNAL.PONE.0255926.

[277] S. Aziz, M. U. Khan, F. Aamir, and M. A. Javid, "Electromyography (EMG) data-driven load classification using empirical mode decomposition and feature analysis," in *Proceedings - 2019 International Conference on Frontiers of Information Technology, FIT 2019*, Institute of Electrical and Electronics Engineers Inc., Dec. 2019, pp. 272–277. doi: 10.1109/FIT47737.2019.00058.

[278] Z. Liang, "A new knowledge distillation method for object detection based on EMD," *J Phys Conf Ser*, vol. 2083, no. 4, p. 042028, Nov. 2021, doi: 10.1088/1742-6596/2083/4/042028.

[279] A. Phinyomark, R. N. Khushaba, and E. Scheme, "Feature extraction and selection for myoelectric control based on wearable EMG sensors," *Sens (Switzerland)*, vol. 18, no. 5, p. 1615, May 2018, doi: 10.3390/s18051615.

[280] A. Phinyomark, R. N. Khushaba, E. Ibáñez-Marcelo, A. Patania, E. Scheme, and G. Petri, "Navigating features: A topologically informed chart of electromyographic features space," *J R Soc Interface*, vol. 14, no. 137, p. 20170734., Dec. 2017, doi: 10.1098/rsif.2017.0734.

[281] O. W. Samuel *et al.*, "Pattern recognition of electromyography signals based on novel time domain features for amputees' limb motion classification,"

Comput Electr Eng, vol. 67, pp. 646–655, Apr. 2018, doi: 10.1016/J.COMPELECENG.2017.04.003.

[282] B. Hudgins, P. Parker, and R. N. Scott, "A new strategy for multifunction myoelectric control," *IEEE Trans Biomed Eng*, vol. 40, no. 1, pp. 82–94, 1993, doi: 10.1109/10.204774.

[283] O. W. Samuel *et al.*, "Intelligent EMG pattern recognition control method for upper-limb multifunctional prostheses: Advances, current challenges, and future prospects," *IEEE Access*, vol. 7, pp. 10150–10165, 2019, doi: 10.1109/ACCESS.2019.2891350.

[284] D. Karabulut, F. Ortes, Y. Z. Arslan, and M. A. Adli, "Comparative evaluation of EMG signal features for myoelectric controlled human arm prosthetics," *Biocybern Biomed Eng*, vol. 37, no. 2, pp. 326–335, Jan. 2017, doi: 10.1016/J.BBE.2017.03.001.

[285] A. O. Andrade, S. Nasuto, P. Kyberd, C. M. Sweeney-Reed, and F. R. Van Kanijn, "EMG signal filtering based on Empirical Mode Decomposition," *Biomed Signal Process Control*, vol. 1, no. 1, pp. 44–55, Jan. 2006, doi: 10.1016/J.BSPC.2006.03.003.

[286] X. Zhang and P. Zhou, "Filtering of surface EMG using ensemble empirical mode decomposition.," *Med Eng Phys*, vol. 35, no. 4, pp. 537–542, Apr. 2013, doi: 10.1016/J.MEDENGPHY.2012.10.009.

[287] A. Srivastava, V. Bhateja, D. K. Tiwari, and D. Anand, "AWGN suppression algorithm in EMG signals using ensemble empirical mode decomposition," *Adv Intell Syst Comput*, vol. 673, pp. 515–524, 2018, doi: 10.1007/978-981-10-7245-1_50.

[288] S. M. Khan, A. A. Khan, and O. Farooq, "Selection of features and classifiers for EMG-EEG-Based upper limb assistive devices - A review," *IEEE Rev Biomed Eng*, vol. 13, pp. 248–260, 2020, doi: 10.1109/RBME.2019.2950897.

[289] A. Phinyomark, P. Phukpattaranont, and C. Limsakul, "Feature reduction and selection for EMG signal classification," *Expert Syst Appl*, vol. 39, no. 8, pp. 7420–7431, Jun. 2012, doi: 10.1016/J.ESWA.2012.01.102.

[290] Y. Chen, Z. Yang, H. Gong, and S. Wang, "Recognition of sketching from surface electromyography," *Neural Comput Appl*, vol. 30, no. 9, pp. 2725–2737, Nov. 2018, doi: 10.1007/S00521-017-2857-3/METRICS.

[291] J. Too, A. R. Abdullah, and N. M. Saad, "Classification of hand movements based on discrete wavelet transform and enhanced feature extraction," *Int J Adv Comput Sci Appl*, vol. 10, no. 6, pp. 83–89, 2019, doi: 10.14569/ijacsa.2019.0100612.

[292] J. Too, A. R. Abdullah, N. M. Saad, and W. Tee, "EMG feature selection and classification using a Pbest-guide binary particle swarm optimization," *Comput*, vol. 7, no. 1, p. 12, 2019, doi: 10.3390/computation7010012.

[293] D. C. Toledo-Pérez, J. Rodríguez-Reséndiz, R. A. Gómez-Loenzo, and J. C. Jauregui-Correa, "Support Vector Machine-based EMG signal classification techniques: A review," *Appl Sci (Switzerland)*, vol. 9, no. 20. MDPI AG, p. 4402, Oct. 01, 2019. doi: 10.3390/app9204402.

[294] A. Vijayvargiya, V. Gupta, R. Kumar, N. Dey, and J. M. R. S. Tavares, "A hybrid WD-EEMD sEMG feature extraction technique for lower limb activity recognition," *IEEE Sens J*, vol. 21, no. 18, pp. 20431–20439, Sep. 2021, doi: 10.1109/JSEN.2021.3095594.

[295] S. Aziz, M. U. Khan, F. Aamir, and M. A. Javid, "Electromyography (EMG) data-driven load classification using empirical mode decomposition and feature analysis," in *Proceedings - 2019 International Conference on Frontiers of Information Technology, FIT 2019*, Institute of Electrical and Electronics Engineers Inc., Dec. 2019, pp. 272–277. doi: 10.1109/FIT47737.2019.00058.

[296] G. R. Naik, S. E. Selvan, and H. T. Nguyen, "Single-channel EMG classification with ensemble-empirical-mode-decomposition-based ICA for diagnosing neuromuscular disorders," *IEEE Trans Neural Syst Rehabil Eng*, vol. 24, no. 7, pp. 734–743, Jul. 2016, doi: 10.1109/TNSRE.2015.2454503.

[297] C. Sapsanis, G. Georgoulas, A. Tzes, and D. Lymberopoulos, "Improving EMG based classification of basic hand movements using EMD," in *Annu Int Conf IEEE Eng Med Biol Soc, EMBS*, 2013, pp. 5754–5757. doi: 10.1109/EMBC.2013.6610858.

[298] A. K. Mukhopadhyay and S. Samui, "An experimental study on upper limb position invariant EMG signal classification based on deep neural network," *Biomed Signal Process Control*, vol. 55, p. 101669, Jan. 2020, doi: 10.1016/j.bspc.2019.101669.

[299] M. K. Hasan, S. R. Wahid, F. Rahman, S. K. Maliha, and S. B. Rahman, "Grasp-and-lift detection from EEG signal using convolutional neural network," in *2018 Int Conf Adv Electr Electron*, Institute of Electrical and Electronics Engineers Inc., 2022, pp. 1–6. doi: 10.1109/ICAEEE54957.2022.9836375.

[300] T. Liu and D. Yang, "A three-branch 3D convolutional neural network for EEG-based different hand movement stages classification," *Sci Rep*, vol. 11, no. 1, pp. 1–13, May 2021, doi: 10.1038/s41598-021-89414-x.

[301] M. Aslam, F. Rajbdad, and O. M. Soysal, "Weight perception analysis using electroencephalographic signals: Full/regular papers, CSCI-ISPC," in *Proceedings - 2021 International Conference on Computational Science and Computational Intelligence, CSCI 2021*, Institute of Electrical and Electronics Engineers Inc., 2021, pp. 1678–1683. doi: 10.1109/CSCI54926.2021.00319.

[302] V. van Polanen and M. Davare, "Sensorimotor memory biases weight perception during object lifting," *Front Hum Neurosci*, vol. 9, no. DEC, p. 700, Dec. 2015, doi: 10.3389/FNHUM.2015.00700.

[303] Y. Chang, "Architecture design for performing grasp-andlift tasks in brain-machine-interface-based human-in-the-loop robotic system," *IET Cyber-Phys Syst: Theory Appl*, vol. 4, no. 3, pp. 198–203, Sep. 2019, doi: 10.1049/iet-cps.2018.5066.

[304] S. G. Chacko, P. Tayade, S. Kaur, and R. Sharma, "Creation of a high-resolution EEG based brain computer interface for classifying motor imagery of daily life activities," in *7th Int Winter Conf Brain-Comput*

Interface, BCI 2019, Institute of Electrical and Electronics Engineers Inc., Feb. 2019, pp. 1–5. doi: 10.1109/IWW-BCI.2019.8737258.

[305] M. P. Furmanek, M. Mangalam, M. Yarossi, K. Lockwood, and E. Tunik, "A kinematic and EMG dataset of online adjustment of reach-to-grasp movements to visual perturbations," *Scientific Data 2022 9:1*, vol. 9, no. 1, pp. 1–18, Jan. 2022, doi: 10.1038/s41597-021-01107-2.

[306] D. Totah, L. Ojeda, D. D. Johnson, D. Gates, E. M. Provost, and K. Barton, "Low-back electromyography (EMG) data-driven load classification for dynamic lifting tasks," *PLoS One*, vol. 13, no. 2, p. e0192938, Feb. 2018, doi: 10.1371/JOURNAL.PONE.0192938.

[307] E. F. Shair, S. A. Ahmad, M. H. Marhaban, S. B. M. Tamrin, and A. R. Abdullah, "EMG processing-based measures of fatigue assessment during manual lifting," *Biomed Res Int*, vol. 2017, p. 3937254, 2017, doi: 10.1155/2017/3937254.

CURRICULUM VITAE

2011-2016 B.Sc., Biomedical Engineering,

Erciyes University, Kayseri, TÜRKİYE

2011-2017 B.Sc., Mechatronics Engineering,

Erciyes University, Kayseri, TÜRKİYE

2017- 2024 Ph.D., Electrical and Computer Engineering,

Abdullah Gül University, Kayseri, TÜRKİYE

SELECTED PUBLICATIONS AND PRESENTATIONS

J1) Karakullukcu, N., & Yilmaz, B. (2022). Detection of Movement Intention in EEG-Based Brain-Computer Interfaces Using Fourier-Based Synchrosqueezing Transform. International Journal of Neural Systems, 32(1), 2150059. https://doi.org/10.1142/S0129065721500593

J2) Karakullukcu, N., Altindis, F., & Yilmaz. B. Object Weight Perception in Motor Imagery Using FourierBased Synchrosqueezing Transform and Regularized Common Spatial Patterns. Accepted by IEEE Access– submitted on 07 Feb 2024.

J3) Karakullukcu, N., & Yilmaz. B. Surface Electromyography Based Weight Perception During Holding Phase for Torque Control of Upper Limb Prosthesis. Under review by the Neural Computing & Applications Journal – submitted on 16 November 2023.

P1) Yilmaz, B., Ünal, R., Karakullukcu, N., Khosrowshah, M., Altindis, F. (2022). Kontrol edilebilir bir yapay el sistemi. International Patent Application No. PCT/TR2022/050183.

C1) N. Öztürk & B. Yilmaz, "Discrimination of Rest, Motor Imagery and Movement for Brain-Computer Interface Applications," 2018 Medical Technologies National Congress (TIPTEKNO), Magusa, 2018, pp. 1-4, doi: 10.1109/TIPTEKNO.2018.8597152.

C2) N. Öztürk, B. Yilmaz, and A. Y. Önver, "Real-Time Robotic Car Control Using Brainwaves and Head Movement," 2018 Medical Technologies National Congress (TIPTEKNO), Magusa, 2018, pp. 1-4, doi: 10.1109/TIPTEKNO.2018.8596956.